

**FACULTY  
OF MATHEMATICS  
AND PHYSICS**  
Charles University

**MASTER THESIS**

Karel Maděra

**Accelerating cross-correlation with  
GPUs**

Department of Distributed and Dependable Systems

Supervisor of the master thesis: doc. RNDr. Martin Kruliš, Ph.D

Study programme: Computer Science

Study branch: ISS

Prague 2022



I declare that I carried out this master thesis independently, and only with the cited sources, literature and other professional sources. It has not been used to obtain another or the same degree.

I understand that my work relates to the rights and obligations under the Act No. 121/2000 Sb., the Copyright Act, as amended, in particular the fact that the Charles University has the right to conclude a license agreement on the use of this work as a school work pursuant to Section 60 subsection 1 of the Copyright Act.

In ..... date .....

Author's signature



I would like to give thanks to my thesis supervisor doc. RNDr. Martin Kruliš, Ph.D for his unending patience and constructive criticism, which were both crucial for the creation of this thesis. I would like to thank my parents for their support throughout my studies. Finally I would like to give thanks to all those I have met throughout my journey at the Faculty of Mathematics and Physics.



Title: Accelerating cross-correlation with GPUs

Author: Karel Maděra

Department: Department of Distributed and Dependable Systems

Supervisor: doc. RNDr. Martin Kruliš, Ph.D, Department of Distributed and Dependable Systems

Abstract: Cross-correlation is a commonly used tool in the field of signal processing, with applications in pattern recognition, particle physics, electron tomography, and many other areas. For many of these applications, it is often the limiting factor on system performance due to its computational complexity. In this thesis, we analyze the cross-correlation algorithm and its optimization and parallelization possibilities. We then implement several optimizations of the definition-based algorithm, mainly focused on parallelization using the Graphical processing unit (GPU). Even though the definition-based algorithm provides many possibilities for parallelization, the implementation needs to solve several problems, such as the algorithm's low arithmetic intensity. Furthermore, the problems differ between computation types, which include cross-correlating a pair of inputs, one input with many other inputs, or many inputs with many other inputs. Lastly, we compare the optimizations of the definition-based algorithm with the asymptotically faster and commonly used algorithm based on the Fast Fourier Transform. Depending on the total size of the data, we achieve parity between the two algorithms for matrix sizes ranging from 60x60 to 150x150, allowing performance improvements for systems using matrices smaller than these sizes.

Keywords: cross-correlation GPU parallelization optimization





# Contents

<b>Introduction</b>	<b>3</b>
<b>1 Cross-correlation</b>	<b>5</b>
1.1 Definition . . . . .	5
1.2 Computation using discrete Fourier Transform . . . . .	6
1.3 Definition based optimizations . . . . .	8
1.3.1 Data parallelism . . . . .	8
1.3.2 Forms of cross-correlation . . . . .	8
1.4 Post-processing . . . . .	9
<b>2 GPU</b>	<b>11</b>
2.1 Fundamentals . . . . .	11
2.2 CUDA Programming model . . . . .	11
2.2.1 Running the device code . . . . .	12
2.2.2 Thread hierarchy . . . . .	13
2.2.3 Thread cooperation . . . . .	13
2.2.4 Cooperative groups . . . . .	15
2.2.5 Memory hierarchy . . . . .	16
2.2.6 Hardware details . . . . .	17
2.2.7 Versioning . . . . .	18
2.3 Code optimizations . . . . .	19
2.3.1 Occupancy . . . . .	20
2.3.2 Pipeline saturation . . . . .	20
2.3.3 Global memory access . . . . .	21
2.3.4 Shared memory access . . . . .	21
2.3.5 General recommendations . . . . .	22
<b>3 Implementation</b>	<b>25</b>
3.1 Parallelization . . . . .	25
3.1.1 Two matrices . . . . .	26
3.1.2 Many matrices . . . . .	27
3.2 Data reuse . . . . .	29
3.2.1 Overlap . . . . .	29
3.2.2 Row group and column group . . . . .	30
3.2.3 Workers . . . . .	32
3.2.4 List of implementations . . . . .	32
3.3 Basic algorithm . . . . .	33
3.4 Warp shuffle algorithm family . . . . .	35
3.4.1 Algorithm steps . . . . .	36
3.4.2 Work distribution . . . . .	38
3.4.3 Utilizing multiple right matrices . . . . .	42
3.4.4 Multiple rows from the right matrix . . . . .	45
3.4.5 Multiple left matrices . . . . .	47
3.4.6 Multiple rows from both matrices . . . . .	49
3.4.7 Summary . . . . .	50

3.5	Warp per shift algorithm family . . . . .	52
3.5.1	Base implementation . . . . .	53
3.5.2	Simplified indexing . . . . .	54
3.5.3	Shared memory . . . . .	57
3.5.4	Shared memory with multiple right matrices . . . . .	61
3.5.5	Shared memory with single column group per block . . . . .	62
3.5.6	Work distribution . . . . .	63
3.6	Further increasing worker size . . . . .	64
3.6.1	Summary . . . . .	64
<b>4</b>	<b>Results</b>	<b>67</b>
4.1	Experiments . . . . .	67
4.1.1	Code instrumentation . . . . .	67
4.1.2	Experiment setup . . . . .	68
4.1.3	Result validation . . . . .	69
4.2	Comparing definition-based algorithms . . . . .	69
4.2.1	Warp shuffle optimizations with the one-to-one input . . . . .	70
4.2.2	Warp shuffle optimizations with the one-to-many input . . . . .	71
4.2.3	Warp shuffle optimizations with the n-to-mn input . . . . .	73
4.2.4	Warp shuffle optimizations with the n-to-m input . . . . .	75
4.2.5	Warp per shift optimizations with the one-to-one inputs . . . . .	77
4.2.6	Comparison with Basic algorithm . . . . .	78
4.3	Comparison with existing implementations . . . . .	80
4.3.1	FFT-based implementation . . . . .	80
4.3.2	SciPy . . . . .	84
4.3.3	Matlab . . . . .	85
	<b>Conclusion</b>	<b>89</b>
4.4	Future work . . . . .	90
	<b>Bibliography</b>	<b>91</b>
<b>A</b>	<b>Local array optimization</b>	<b>95</b>
A.1	Advanced optimizations and local arrays . . . . .	95
<b>B</b>	<b>Attachments</b>	<b>99</b>

# Introduction

The field of signal processing is present everywhere in today's world. From image processing through seismology to particle physics, the need to analyze, modify or synthesize signals such as sound, images, and other scientific measurements is shared across many fields. One of the commonly used algorithms in signal processing is cross-correlation, which will be the subject of this thesis. The aim is to analyze, implement and evaluate possible methods of optimization and parallelization of the definition-based cross-correlation algorithm. The implementations will then be further compared to the generally used implementation based on the Fast Fourier transform.

## Motivation

Cross-correlation is one of the key operations in both analog and digital signal processing. It is widely used in image analysis, pattern recognition, image segmentation, particle physics, electron tomography, and many other fields [5]. For many of these applications, the computation time of cross-correlation is often the limiting factor in the data processing pipeline. The amount of input data combined with the computational complexity makes simple sequential CPU-based implementations and even more advanced parallel CPU-based implementations inadequate.

Algorithms based on the definition of cross-correlation or on the Fast Fourier transform (FFT) can take advantage of the inherent high degree of data parallelism in the definition of cross-correlation or FFT, respectively. This parallelism allows them to utilize the high throughput and large amounts of computational power provided by the massively parallel systems in the form of Graphical processing units (GPU).

This thesis is a continuation of the thesis "Employing GPU to Process Data from Electron Microscope" [1], which uses both a basic definition-based cross-correlation algorithm and one based on FFT. The aim is to compare the asymptotically faster FFT-based algorithm with the asymptotically slower definition-based algorithm and provide an optimized implementation of the definition-based algorithm, which, for the input sizes used by the original thesis, should be faster than the FFT-based implementation.

## Objective

This thesis aims to analyze the possibilities for optimization and parallelization of the definition-based algorithm and provide detailed measurements and comparisons with the FFT-based algorithm for a range of input forms and sizes. The optimizations and parallelization of the definition-based algorithm will utilize capabilities provided by the CUDA platform.

The main contributions of this thesis are:

- a family of optimized definition-based implementations utilizing the CUDA platform,

- comparison of the definition-based implementations with one based on the Fast Fourier Transform,
- measurements of the behavior of these implementations and its dependence on input size and type.

## **Thesis outline**

The contents of this thesis are ordered as follows:

- description of cross-correlation algorithm;
- introduction to computations utilizing GPU hardware and the CUDA platform;
- analysis of the optimizations of the definition-based algorithm, focused on parallelization using the CUDA platform,
- measurement of the behavior of both the optimized definition-based algorithm and the algorithm based on the Fast Fourier transform.

# 1. Cross-correlation

In this chapter, we define cross-correlation and describe algorithms for its computation. We first define one-dimensional cross-correlation, extending it into multiple dimensions and introducing circular cross-correlation. We then illustrate how circular cross-correlation is used to compute cross-correlation using discrete Fourier transform. Lastly we list the possibilities for optimization and parallelization of cross-correlation, with real-world usage examples of where these optimizations can be utilized.

## 1.1 Definition

Cross-correlation, also known as sliding dot product or sliding inner-product, is a function describing similarity of two series or two functions based on their relative displacement [19]. Cross-correlation of functions  $f, g : \mathbb{C} \rightarrow \mathbb{R}$ , denoted as  $f \star g$ , is defined by the following formula:

$$(f \star g)(\tau) = \int_{-\infty}^{\infty} \overline{f(t)}g(t + \tau) dt,$$

where  $\overline{f(t)}$  denotes the complex conjugate of  $f(t)$  and  $\tau$  is the displacement of the two functions  $f$  and  $g$ . In simpler words, the value  $(f \star g)(\tau)$  tells us how similar the function  $f$  is to  $g$  when  $g$  is shifted by  $\tau$ , with a higher value representing higher similarity. Figure 1.1 shows the cross-correlation of two example functions.

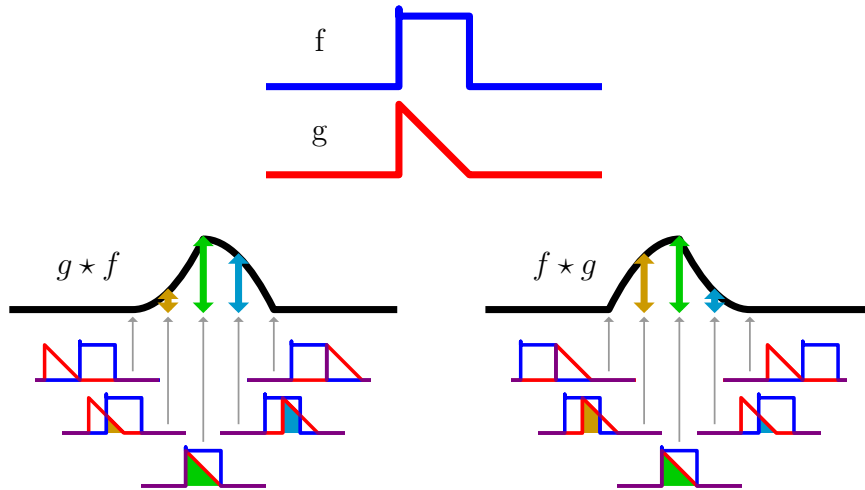


Figure 1.1: Cross-correlation of two functions. [18]

For two discrete functions, as will be used in our case, cross-correlation of functions  $f, g : \mathbb{Z} \rightarrow \mathbb{R}$  is defined by the following formula:

$$(f \star g)[m] = \sum_{i=-\infty}^{\infty} \overline{f[i]}g[i + m],$$

This definition of cross-correlation can be extended for use in two dimensions, as is required, for example, in image processing. For two discrete functions  $f, g : \mathbb{Z}^2 \rightarrow \mathbb{R}$ , cross-correlation is defined as:

$$(f \star g)[m, n] = \sum_{i=-\infty}^{\infty} \sum_{j=-\infty}^{\infty} \overline{f[m, n]} g[m + i, n + j],$$

Even though cross-correlation is defined on the whole  $\mathbb{Z}$  for one dimension and  $\mathbb{Z}^2$  for two dimensions, most use cases of cross-correlation work only on finite inputs, such as image processing working on finite images. The only values we are interested in are those where the two images overlap, which restricts the computation to  $(w_1 + w_2 - 1) * (h_1 + h_2 - 1)$  resulting values, where  $w_i$  denotes width of the image  $i$  and  $h_i$  denotes the height of the image  $i$ .

This limits the part of the output we are interested in and leads us to the time complexity of the definition based algorithm, or *naive* algorithm as it is called in the code attached to this thesis. For each of the  $(w_1 + w_2 - 1) * (h_1 + h_2 - 1)$  output values, we need to multiply the overlapping pixel values and sum up all the multiplication results. There will be at most  $\min(w_1, w_2) * \min(h_1, h_2)$  overlapping pixels. For simplicity, let us work with two images of size  $w_i * h_i$ . Then the time complexity of the definition based algorithm is  $((2 * w_i - 1) * (2 * h_i - 1) * (w_i * h_i))$ , which gives us asymptotic complexity of  $\mathcal{O}(w_i^2 * h_i^2)$ .

## 1.2 Computation using discrete Fourier Transform

In this section, we describe an algorithm which uses the discrete Fourier transform to compute the cross-correlation of two finite two-dimensional series. The asymptotic complexity of this algorithm will be  $\mathcal{O}(w_i * h_i * \log_2(w_i * h_i))$ , where  $w_i$  is the width of each series and  $h_i$  the height of each series. This improves on the asymptotic complexity  $\mathcal{O}(w_i^2 * h_i^2)$  of the definition based algorithm described in the previous section 1.1.

Discrete Fourier transform can only be used to compute a special type of cross-correlation, the so called *circular* cross-correlation. For a finite series  $N \in \mathbb{N}$ ,  $\{x\}_n = x_0, x_1, \dots, x_{N-1}$ ,  $\{y\}_n = y_0, y_1, \dots, y_{N-1}$ , circular cross-correlation is defined as:

$$(x \star_N y)_m = \sum_{i=0}^{N-1} \overline{x_m} y_{(m+i) \bmod N},$$

where  $\overline{x_m}$  denotes the complex conjugate of  $x_m$ .

Based on the Cross-Correlation Theorem [17], circular cross-correlation  $(x \star_N y)_m$  can be computed using discrete Fourier Transform according to the following formula:

$$(x \star_N y)_m = \mathbb{F}^{-1}(\overline{\mathbb{F}(x)} * \mathbb{F}(y))$$

where  $\mathbb{F}(x)$  and  $\mathbb{F}(y)$  denote discrete Fourier Transform of series  $x$  and  $y$  respectively,  $\overline{\mathbb{F}(x)}$  denotes the complex conjugate of the discrete Fourier Transform,  $*$  denotes element-wise multiplication of two series and  $\mathbb{F}^{-1}$  denotes inverse discrete Fourier Transform.

As described by Bali [1], to compute non-circular (linear) cross-correlation of non-periodic series of size  $N$ , we pad both series with  $N$  zeros to the size  $2N$ , as

can be see in Figure 1.2. The results of circular cross-correlation are then the results of linear cross-correlation, only circularly shifted by  $N - 1$  places to the left with one additional 0 value at index  $N$ .

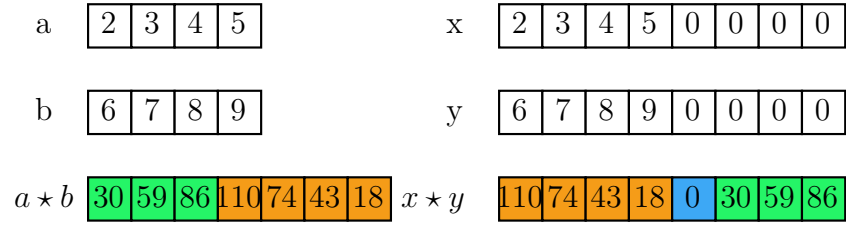


Figure 1.2: Comparison of linear and circular cross-correlation [1].

This process can be expanded into two dimensions, where the matrices are padded with  $N$  rows and  $N$  columns of zeros before being passed through 2D discrete Fourier transform. Here the circular shift of the results can be inverted by swapping the quadrants of the results while discarding row  $N$  and column  $N$ , which will be filled with zeros [1], as shown by Figure 1.3.

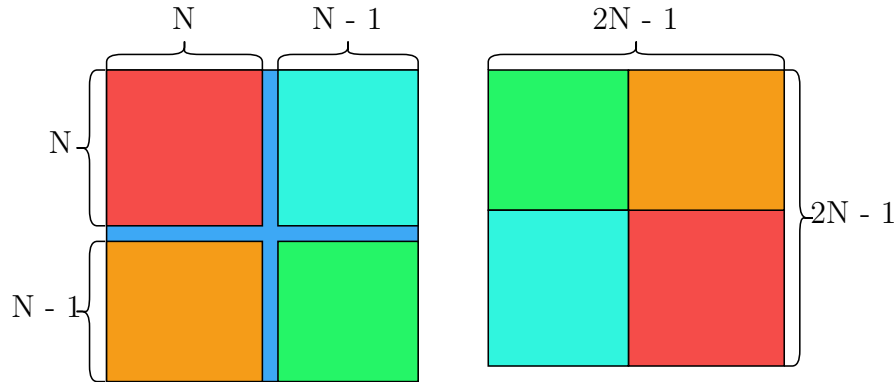


Figure 1.3: Result quadrant swap.

Based on this description, we can deduce the time complexity of the algorithm. For two matrices  $a, b \in \mathbb{R}^{h \times w}$ , the steps of the algorithm are:

1. Padding  $a_p, b_p \in \mathbb{R}^{2h \times 2w}$  of  $a$  and  $b$  with  $h$  rows and  $w$  columns of zeros in  $\mathcal{O}(h * w)$ ;
2. Discrete Fourier Transform  $A, B \in \mathbb{C}^{2h \times 2w}$  of  $a_p$  and  $b_p$  in  $\mathcal{O}(h * w * \log_2(h * w))$ ;
3. Element-wise multiplication, also known as the Hadamard product,  $C \in \mathbb{C}^{2h \times 2w} : C = \overline{A} \circ B$ , where  $\overline{A}$  the denotes complex conjugate of  $A$ , in  $\mathcal{O}(w_i * h_i)$ ;
4. Inverse Discrete Fourier Transform  $c \in \mathbb{R}^{2h \times 2w}$  of  $C$  in  $\mathcal{O}(h * w * \log_2(h * w))$ ;
5. Quadrant swap in  $\mathcal{O}(h * w)$

Put together, the steps described above give us an algorithm with asymptotic time complexity of  $\mathcal{O}(h * w * \log_2(h * w))$ .

## 1.3 Definition based optimizations

In the original thesis by Bali [1], and in the field of image processing in general, 2D version of cross-correlation is mostly used to find a grayscale image or a piece of a grayscale image represented as an integer or floating point matrix in another image, also represented as such a matrix. This can be done to, for example, find the displacement of a certain point of interest between images taken at different times, as is done in Bali [1] and Zhang et al. [22].

This thesis will implement cross-correlation of integer and floating point matrices, which encompasses the usage in the previously mentioned works. These implementations will be optimized to take advantage of different forms of cross-correlation input, such as the cross-correlation of one matrix with many other matrices, different sizes of input matrices etc.

### 1.3.1 Data parallelism

The definition based algorithm for computing cross-correlation is highly data parallel. Not only can every element in the result matrix be computed independently, but also the computation of each element can be parallelized with a simple reduction of the final results.

When using the definition based algorithm, each element of the resulting matrix corresponds to an overlap of the two cross-correlated matrices. Every two overlapping elements of the two input matrices are multiplied and the results of these multiplications are then summed up to get the final value for the given overlap.

For each overlap, there is  $h_o * w_o$  multiplications, where  $h_o$  and  $w_o$  describe the number of rows and columns that overlap. The following formula describes the total number of multiplications for all overlaps:

$$(h * (h + 1) - 1) * (w * (w + 1) - 1)$$

All these multiplications can be done independently in parallel. Afterwards, each overlap has to compute a sum of the  $h_o * w_o$  intermediate results to produce the final result.

### 1.3.2 Forms of cross-correlation

In works using cross-correlation, there are several forms of computation which allow for different types of optimizations, such as data caching and reuse, batching, and precomputing. These forms differ in the number of inputs and in the way cross-correlation is computed between the inputs. The four basic forms are, as shown in Figure 1.4:

1. one left input with one right input, in the rest of the thesis referred to as *one-to-one* and depicted in Figure 1.4a;
2. one left input with many right inputs, referred to as *one-to-many* and depicted in Figure 1.4b;



3.  $n$  left inputs, each cross-correlated with  $m$  **different** right inputs, referred to as  $n$ -to- $mn$  and depicted in Figure 1.4c (used by Bali [1], Zhang et al. [22], Kapinchev et al. [5]);
4.  $n$  left inputs, each cross-correlated with all  $m$  right inputs, referred to as  $n$ -to- $m$  and depicted in Figure 1.4d (used by Clark et al. [3]).

While each pair of input matrices can always be computed independently, the *one-to-many*, *n-to-mn* and *n-to-m* types allow for the reuse of the left input matrix data for computation with multiple right input matrices. Additionally, the *n-to-m* makes it possible to reuse data from the right matrix for computation with multiple left input matrices.

For the same size of input data, i.e.  $x$  left input matrices and  $y$  right input matrices, the *n-to-m* requires computation of  $x * y$  pairs of matrices, compared to the *n-to-mn* type which results in only  $y$  pairs. The increased level of parallelism and increased arithmetic intensity allow for additional optimizations of the *n-to-m* computation type compared to the *n-to-mn* type. The *one-to-one* and *one-to-many* types are described separately, as compared to the general *n-to-mn* or *n-to-m* implementation, their implementations can more aggressively cache and reuse the left input matrix .

Implementations of the two simpler types *one-to-one* and *one-to-many* can be used to implement either *n-to-m* or *n-to-mn* by running the simpler type of cross-correlation multiple times, possibly in parallel. Inversely, any implementation of either *n-to-m* or *n-to-mn* can be used to implement the two simpler types. Another type which we could consider is the computation of a large number of pairs, which can be implemented by *n-to-mn* with  $m$  equal to one. The large number of pairs type is not discussed further as it does not provide any additional opportunity for optimization compared to running the *one-to-one* several times in parallel.

## 1.4 Post-processing

In most use cases, the cross-correlation itself is not the final output, but the results are used for further processing. It is often used to find the position of a smaller signal in a larger signal, for example in the field of Digital image processing for template matching, image alignment etc. In these applications, the only information of interest is the maximum value in the result matrix.

In Digital Image correlation, we are also interested in finding the maximum, but this time with a subpixel precision. This requires us to find the maximum value and use the results in an area around it to interpolate a function [22] [1].

In the field of Seismology, cross-correlation is used for picking, ambient noise monitoring, waveform comparison, and signal, event and pattern detection [15].

In optical coherence tomography, the whole result the of cross-correlation is summed up to compute the intensity of each pixel [5].

Although post-processing is often also a good candidate for optimization and parallelization, it is outside the scope of this thesis. The cross-correlation results will be taken as they are and validated against a preexisting cross-correlation implementations.

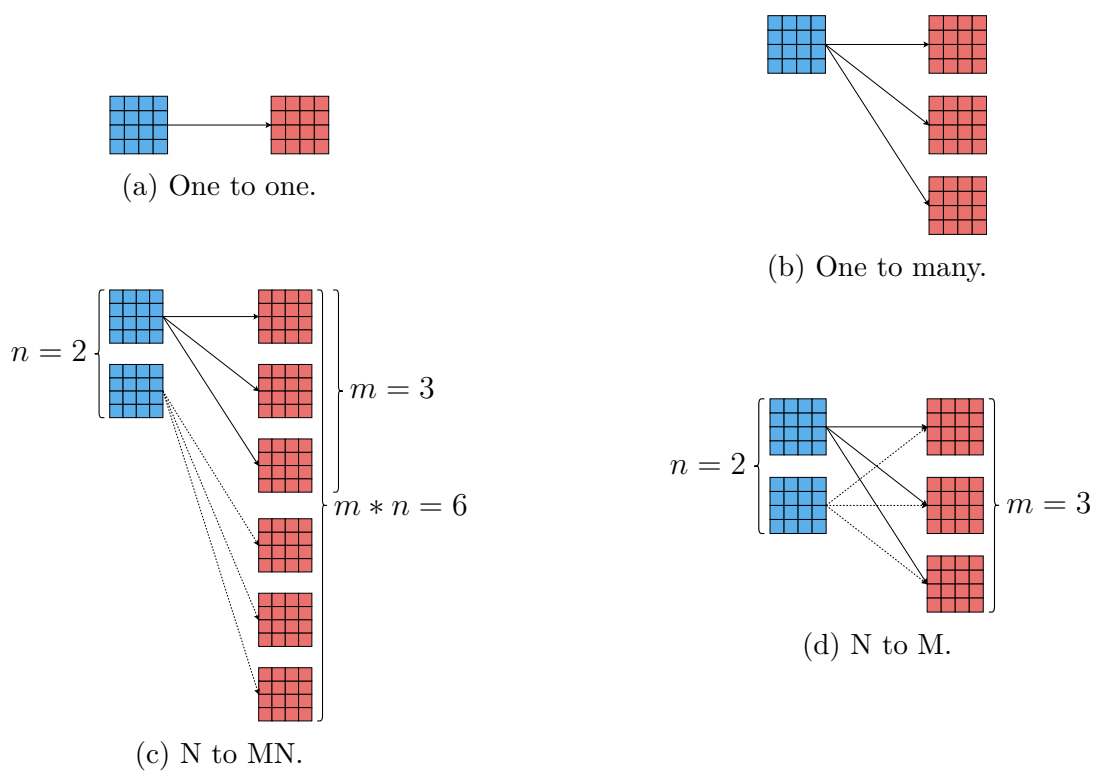


Figure 1.4: Forms of cross-correlation.

## 2. GPU

This chapter describes the graphics processing unit (GPU) hardware and its primary advantages and disadvantages compared to the Central processing unit (CPU). Next, we introduce Compute Unified Device Architecture, better known by its acronym CUDA, a "general purpose parallel computing platform and programming model" [11], which will be used in this thesis. Lastly, we list several key points which need to be addressed for optimal code performance, mainly in CUDA, but also applicable when working with GPUs of other vendors or when using GPUs for graphics.

### 2.1 Fundamentals

The graphics processing unit (GPU) is optimized for the throughput of a single stream of instructions working on many streams of data. This allows GPU hardware design to make trade-offs not available for Central processing unit (CPU) hardware. CPUs are optimized to process a single stream of instructions working on a single stream of data as fast as possible. This goal requires CPU design to minimize instruction latency, which is achieved using branch predictions, multiple levels of caching, and other such mechanisms. On the other hand, the single stream of instructions is executed many times in parallel in a GPU, allowing the GPU hardware to hide high latency operations by switching to other threads instead of optimizing for lower latency of each instruction. Furthermore, the thread switching is made instantaneous by keeping the execution context, such as registers, of all threads resident at all times. Compare this with CPU context switching, where the state of all registers has to be offloaded into memory and the state of another thread loaded from memory each time a CPU switches threads.

Another defining characteristic of the GPU hardware is separate memory space. Code running on the GPU device cannot directly access the same memory as code running on the CPU. Instead, all data processed on the GPU must first be moved across the bus connecting the GPU to the host system, most commonly a PCIe bus. Similar to the GPU execution units, the separate GPU device memory is optimized for high throughput at the cost of higher latency compared to the host memory. The device memory is further optimized for specific access patterns by groups of threads running on the GPU, with the Nvidia GPU version of the optimization described in Section 2.3.3.

### 2.2 CUDA Programming model

Compute Unified Device Architecture, better known by its acronym CUDA, is a "general purpose parallel computing platform and programming model" [11], which allows simplified utilization of NVIDIA Graphics processing units (GPU) for solving complex computational problems.

CUDA distinguishes two parts of the system running two types of code. First is the *host* code running on the host part of the system. This is a standard C++ program running on the CPU, accessing system memory and calling the operating

system, as any other standard C++ program would. The second part is the *device* code, running on a device or multiple devices. Each device corresponds to a single GPU <sup>1</sup>.

Both parts of the code are programmed in the same language, CUDA C++, an extension of the C++ language. This extension places some restrictions on the device code, while some parts of the language are only usable in the device code. One of the important things CUDA C++ introduces are the *function execution space specifiers*. These specifiers are attributes added to a function declaration that specify if the given function is part of the host code, device code or if it should be compiled both for host and device code. The available *function execution space specifiers* are:

- `__global__`, which declares the function as being a kernel, callable from host code and executed on the device,
- `__device__`, which declares the function as executed on the device, callable by another device or global function,
- `__host__`, which declares the function as executed on the host, callable from the host only.

Without any specifiers, a function is compiled as part of the host code. **Kernel** is a function with the `__global__` specifier, which is callable from the host code but is executed on a device. Kernels serve as entry points that the host code uses to offload computation to the device. Kernel invocation is asynchronous, where the function call to the kernel in host code does not wait for the kernel on the device to finish but returns immediately after the kernel is submitted.

When invoking a kernel, the host code specifies the number of threads that are to run the device code. A basic description of how the device code is run on the GPU is provided in Section 2.2.1. A detailed description of the abstraction defining the behavior of the device code called the SIMT execution model is given in Section 2.2.6.

## 2.2.1 Running the device code

The device code, written in CUDA C++ as a part of a *global* or a *device* function, describes the behavior of a single thread running on the device. Compared to the host code running on the CPU, the device code is always run by many threads simultaneously. On the surface, the device code is very similar to the host code written for the CPU and will most likely work correctly if written as if for the CPU. The number of threads running the device code is determined by the arguments provided to the *kernel* function. The threads are hierarchically grouped on several levels. These groups define scheduling behavior, access to different kinds of memory, and primitives for cooperation.

To maximize performance, one must structure the code and the overall algorithm according to details provided in Section 2.2.6.

---

<sup>1</sup>Since Compute Capability 8.0 Ampere, a device can represent a GPU slice.

## 2.2.2 Thread hierarchy

Threads on the device are grouped into Cooperative Thread Arrays (CTA), also known as thread blocks. Thread blocks can be one-dimensional, two-dimensional, or three-dimensional, which provides an easy way to distribute work when processing arrays, matrices, or volumes. Thread blocks are further organized into a one-dimensional, two-dimensional, or three-dimensional grid, as shown in Figure 2.1. When launching a kernel, we specify the thread block size and the grid size, which combined give us the number of threads executing the given kernel.

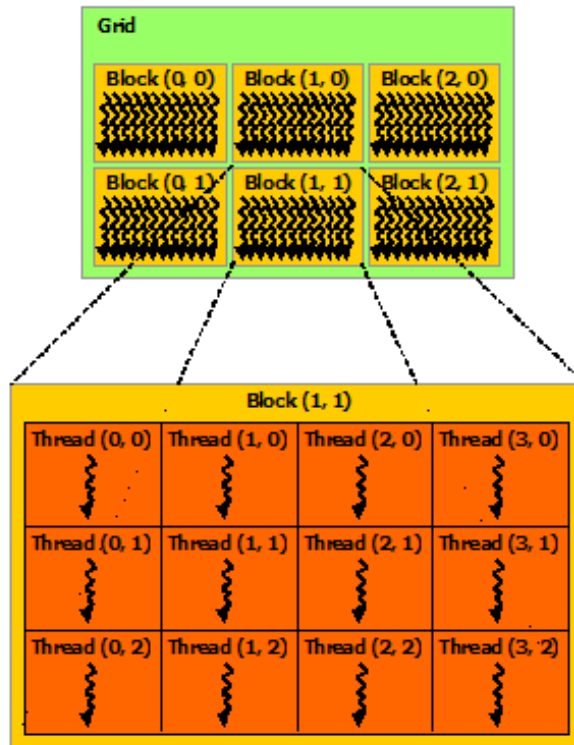


Figure 2.1: Thread hierarchy [11].

Each thread is assigned an index, accessible through `threadIdx` built-in variable. Each thread can also access the index of the thread block it is part of through `blockIdx`, the block size through `blockDim` and the grid size through `gridDim`. All of these variables are three-dimensional vectors, with dimensions unused during kernel launch set to zero for indices and one for dimensions. Using these built-in variables, we can distribute work between threads, most often assigning each thread a part of the input to process.

Due to hardware details described in Section 2.2.6, every 32 threads of a thread block are grouped into a *warp*. Warps are used for scheduling and close cooperation of threads.

## 2.2.3 Thread cooperation

CUDA provides several mechanisms for thread cooperation. Threads can cooperate on the following levels of thread hierarchy, with increasing levels of speed and capability:

- grid level,
- thread block level,
- warp level.

The rest of this subsection describes the older API using intrinsic functions. The newer Cooperative Groups API, a superset of the older API, is described in Subsection 2.2.4.

### Grid level

On the grid level, the only available tools for cooperation are atomic operations on the global memory. These operations can be used to perform read-modify-write on a 32-bit or 64-bit word in global memory without introducing race conditions.

### Thread block level

On a thread block level, threads can use two mechanisms for cooperation:

- shared memory,
- synchronization barrier.

As per the CUDA C++ programming guide: "the shared memory is expected to be a low-latency memory near each processor core (much like an L1 cache) and `__syncthreads()` is expected to be lightweight" [11].

Shared memory is a small memory close to the execution cores, described in more detail in Section 2.2.5. Each thread block receives a slice of shared memory accessible only from the threads of the given thread block. Shared memory can be used as software managed cache or to share results between threads of the thread block.

To synchronize threads of a single thread block, for example, to communicate through shared memory, we use synchronization barrier `__syncthreads()`. All threads in the block must execute the call to `__syncthreads()` before any of the threads can proceed beyond the call to `__syncthreads()`. The `__syncthreads()` function also serves as memory barrier.

### Warp level

Threads of the warp, or lanes as they are referred to in the documentation, can utilize intrinsic functions to exchange data without the use of shared memory and perform simple hardware accelerated operations.

For data exchange between lanes of a warp, the CUDA framework provides the following warp shuffle functions: `__shfl_sync`, `__shfl_up_sync`, `__shfl_down_sync`, `__shfl_xor_sync`. These functions differ in how they interpret the provided index, either using it directly as lane index, adding or subtracting from the current lane index, or executing *xor* with the current lane index. The data exchange does not have to span the whole warp. Shuffle operations allow the warp to be subdivided into groups with a width of a power of 2. These operations can be used for

different data exchange patterns, such as the obvious shuffle up or down, data rotation across lanes, broadcast of a value from a single lane, etc.

Warps can perform the following types of operations:

- vote operations (`--any_sync`, `--all_sync`, `--ballot_sync`) determine if any or all threads provided non-zero value or return a mask of threads which provided non-zero value respectively;
- match operations (`--match_any_sync`, `--match_all_sync`) return a mask of threads that provided the same value or determine if all threads provided the same value;
- reduce operations (`--reduce_[op]_sync`) execute one of the following operations on values provided: *add*, *max*, *min*, *and*, *or*, *xor*.

The API described in this subsection forms the basis of the thread cooperation in CUDA. Most of this API has been available since the early versions of CUDA. Subsection 2.2.4 will describe the newer Cooperative groups API, which builds on top of and extends the API described in this subsection.

## 2.2.4 Cooperative groups

Cooperative Groups API, introduced with CUDA 9, is an extension to the CUDA programming model for organizing groups of communicating threads [11]. The API introduces data types representing groups of cooperating threads, be it a warp, a part of a warp, a thread block, a grid, or even a multigrid<sup>2</sup>.

The API distinguishes two types of groups. First are the *implicit groups*, which are present implicitly in each CUDA kernel. These are:

- thread block,
- grid,
- multigrid.

The API provides functions to create objects representing the implicit groups. The other type is the *explicit groups*, which must be explicitly created from one of the implicit groups. The two explicit groups are:

- thread block tile,
- coalesced group.

Both of these groups represent a warp or a subwarp size grouping of threads. Thread block tile can be created from a thread block or from another thread block tile, representing a warp or a part of a warp of size of a power of 2. The warp level operations described in Section 2.2.3 are available as methods on the object representing this group, with mask and width arguments of the built-in functions implicitly derived from the properties of the group.

---

<sup>2</sup>Multigrid represents multiple grids each running on a separate device.

Coalesced group contains threads of a warp that are currently active, i.e., not masked.

Creating an object representing an implicit group is a collective operation in which all threads of the group must participate. Creating the object in a conditional branch may lead to deadlocks or data corruption. It may also introduce unnecessary synchronization points, limiting concurrency. Similar to the implicit group object creation, partitioning groups is a collective operation that all threads of the parent group must execute and may introduce synchronization points. Therefore, it is recommended to create objects representing implicit groups and do all partitioning at the start of the kernel and pass *const* references throughout the code [11].

## 2.2.5 Memory hierarchy

Each CUDA device has its own DRAM memory, so-called *device memory* or *VRAM*, which is separate from the host system memory and the *device memory* of all other devices. Physically, *device memory* can be seen on most GPU boards as DRAM chips separate from the main silicon chip.

Data transferred between the host and device memory has to cross over the PCI-e bus, either explicitly by calls to *cudaMemcpy* in the host code or by mapping parts of host memory to the *device memory* address space using the *Unified Memory* system, which then handles the data transfers in the background automatically.

From the point of view of a CUDA thread, several types of memory are available, as can be seen in Figure 2.2. For this thesis, the main types are:

- global memory,
- shared memory,
- registers,
- local memory.

**Global memory** is part of the device memory. It is shared by all threads of a grid, and as such, any access which could lead to a race condition must be synchronized using atomic operations, as described in Section 2.2.3. Global memory is allocated by the host code using the `cudaMalloc` family of functions. When the host code transfers data to the device using `cudaMemcpy` or any other means, global memory is the part of device memory this data will be transferred to. The pointers returned by `cudaMalloc` and possibly used in `cudaMemcpy` are then passed as arguments to the kernel. The device code can then use these to access the global memory.

**Shared memory**, as mentioned in the section 2.2.3, is expected to be a low-latency memory near each processor core (much like an L1 cache). The relation with the L1 cache can be seen in the fact that each kernel can configure the proportion between hardware allocated to the L1 cache and to Shared memory, which means these memories share the same underlying hardware. Shared memory can be allocated either dynamically by declaring an array type variable





Figure 2.2: Memory types on a CUDA device.

with the memory space specifier `__shared__` and providing the size to be allocated during kernel launch, or statically by defining the variable with a static size.

**Registers** are the fastest memory available for the device code. Compared to CPUs, GPUs provide a large number of registers. For all recent GPU generations, the register file provides 65536 32bit registers. All variables used by the kernel code are stored in registers. If a kernel requires more registers than available, the data is *spilled* into Local memory.

**Local memory** is part of device memory private for each thread, allocated automatically based on the requirements of the CUDA compiler. This type of memory is used for register spilling, arrays with non-constant indexing, and large structures or arrays which would consume too much register space.

## 2.2.6 Hardware details

The abstraction defining the behavior of the device code is called the Single Instruction, Multiple Threads (SIMT) execution model. In this execution model, threads on the device are split into groups of 32, called *warps*. Each warp of threads is scheduled together, starting at the same program address and executing in lockstep.<sup>3</sup>

If branching occurs, as shown in Figure 2.3, any branch taken by at least a single thread of a warp is executed by the whole warp, masking out any threads that did not take the given branch. When masked, the thread does not execute

<sup>3</sup>Since Compute Capability 7.0 Volta, threads of a warp can be scheduled more independently and do not execute strictly in lockstep [10].

any reads or writes but still has to continue execution with other threads in the warp. This is most apparent in loops, where a single thread of a warp executing the loop a thousand times will result in the whole warp executing the loop a thousand times, even if other threads are masked and do nothing for most of the loops. This cuts the theoretical throughput by a factor of 32, as only one of the 32 threads does useful work.

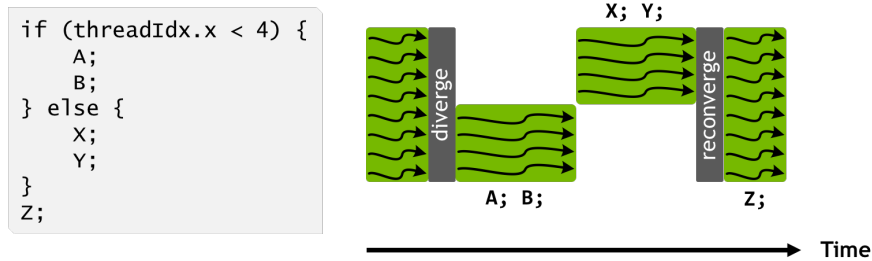


Figure 2.3: Branching in device code [11].

On the other side of the spectrum, the SIMT execution model can be compared to the Single Instruction, Multiple Data (SIMD) execution model, where the number of elements processed by a single instruction is directly exposed in the user code. This can be compared to the SIMT model, where the user code itself describes the behavior of a single thread, and the grouping of threads is abstracted by the platform.

To maximize performance, one must keep in mind the SIMT model, grouping into warps, thread divergence when branching, coalesced memory accesses, etc.

NVIDIA GPUs are built around an array of *Streaming Multiprocessors* (SM). SM of a GPU is similar to a core of a multicore CPU. Each SM has separate execution units, schedulers, register file, shared memory, and L1 cache. An example of an SM is shown in Figure 2.4. Each SM can have multiple schedulers, each scheduling up to one warp per cycle.

Each thread block is assigned to a single SM exclusively, and each SM can run multiple thread blocks at once. Warps of all thread blocks resident on the given SM are scheduled regardless of the thread block the warps belong to.

## 2.2.7 Versioning

When working with CUDA, there are two main parts of the platform which are versioned separately:

- CUDA Toolkit,
- GPU Compute Capability.

The CUDA toolkit represents the software development part of the CUDA platform, encompassing the CUDA runtime library, the *nvcc* compiler, and other tools for software development.

GPU Compute Capability (CC) represents the features provided by the hardware. These features include the number of registers, memory sizes, set of instructions, etc. Generally, each consumer GPU generation corresponds to a new CC, such as GTX 1000 cards corresponding to CC 6.0 Pascal and RTX 3000 cards



Figure 2.4: Streaming multiprocessor [10].

corresponding to CC 8.0 Ampere. An example of an exception to this rule is CC 7.0 Volta which has enterprise cards. With each release of new Compute Capability cards, there is generally an accompanying CUDA Toolkit release providing access to the new features provided by the hardware.

Compute Capabilities are backwards compatible, so code created for an older generation of cards can be run on newer cards, even though it may not take advantage of new hardware features and may be inefficient on the newer cards.

## 2.3 Code optimizations

This section introduces basic principles for producing performant CUDA code. The observations and recommendations provided in this section are based on the principles and properties described in the previous section 2.2.

### 2.3.1 Occupancy

The GPU design prioritizes high instruction throughput of many concurrent threads over single thread performance at the cost of high latency of each instruction. To hide the high latency between dependent instructions, each scheduler keeps a pool of warps between which it switches, possibly on each instruction. Warps in a scheduler pool are called *active* warps. Each cycle, there may be multiple warps that have instructions ready to be executed. Such warps are called *eligible* warps. Each cycle, a warp scheduler can select one of the *eligible* warps as *issued* warp, issuing its instruction to be executed.

For optimal performance, we want to have enough active warps so that there is at least one eligible warp each cycle to enable the GPU to hide the high latency of each instruction. As described in Section 2.2.6, the number of warps resident on an SM depends on the number and size of thread blocks resident on an SM.

The number of thread blocks assigned to an SM is limited by three factors:

- hardware limit,
- register usage,
- shared memory usage.

The hardware limit differs but is either 16 or 32 for all currently supported Compute Capabilities.

To enable execution context switching with no cost, the whole execution context (program counters, registers, etc.) for all warps is kept on the SM for the whole lifetime of each warp.

The number of registers used by all warps of all blocks which reside on the given SM must be smaller than or equal to the number of registers in the register file. For example, for an SM with 65536 registers, and code using 64 registers per thread and 512 threads in a block, there can only be two blocks resident on the SM, as  $2 * 512 * 64 = 65536$ . If the code requires a single additional register, only a single block will be resident on each SM.

The total amount of shared memory required by all blocks residing on an SM must be smaller than or equal to the size of shared memory provided by the SM.

### 2.3.2 Pipeline saturation

Other than occupancy, there are other possible reasons why no warp may be eligible in a given cycle. Pipeline saturation is one of such reasons. GPU hardware has several pipelines, each implementing a different part of the instruction set. As an example, for the RTX 2060 card, these include[13]:

- Load Store Unit (LSU),
- Arithmetic Logic Unit (ALU),
- Fused Multiply Add/Accumulate (FMA),
- Transcendental and Data Type Conversion Unit (XU).

Each instruction has a Compute Capability specific throughput. If exceeded, the pipeline implementing the instruction becomes saturated and is unable to execute additional instructions. This becomes a problem when, for example, many or all warps often execute the same low throughput instruction, such as sine, cosine, or inverse square root, which are implemented by the XU pipeline. Even for simpler operations implemented by the ALU or FMA, if all warps execute the same instruction, the pipelines may become saturated, and warps which are waiting to execute more of the given instruction will not be eligible to be issued.

High LSU utilization reflects that the program may be memory bound, waiting for data from global or shared memory, or that the program executes many warp shuffle instructions, which are also implemented by the LSU pipeline. Due to this, the usage of shared memory together with warp shuffles is not advisable, as they both utilize the same pipeline and compete for resources.

### 2.3.3 Global memory access

As shown in Figure 2.5, each access to the global memory is grouped into 128 B naturally aligned chunks, where any chunk accessed by any of the threads of a warp has to be transferred from the global memory. The maximum performance is achieved when access to memory is aligned and coalesced, i.e., all threads of a warp access elements in the same 128 B chunk, which is aligned to 128 B. Any other form of access introduces overhead in the form of unnecessary data being transferred from global memory.

When accessing data larger than 32 bits, the access is split into two half-warp transactions for 64-bit or four quarter-warp transactions for 128-bit values, which are then processed independently, again reading any 128 B chunk any of the accesses.

Access to global memory goes through at least one level of cache. On older architectures, global memory accesses are by default only cached in the L2 cache, with the L1 cache utilized only for local memory access to speed up register spills. Special instructions can be used to cache data in L1 explicitly. For Compute Capabilities 5.0 or newer, the compiler can generate an instruction to load read-only data, such as the two input matrices in cross-correlation, and cache it in the L1 cache. The L1 cache, with a cache line size of 128 B, is local to each SM and shares hardware with shared memory described in the following section. The L2 cache, with a cache line size of 32 B, is still on-chip but is shared by all SMs. Each 128 B memory transfer is either served by single L1 cache access or split into four 32 B L2 cache accesses.

### 2.3.4 Shared memory access

To achieve high bandwidth, shared memory is divided into 32 banks. The optimal access pattern the shared memory is designed for is for each thread of a warp to access a different bank. To enable this access pattern, successive 32-bit words are mapped to successive shared memory banks. The simplest pattern is that the 32 threads of a warp access 32 consecutive 32-bit items from an array in shared memory, shown in the left column of Figure 2.6. If multiple threads access different addresses mapped to the same bank, as shown in the middle col-

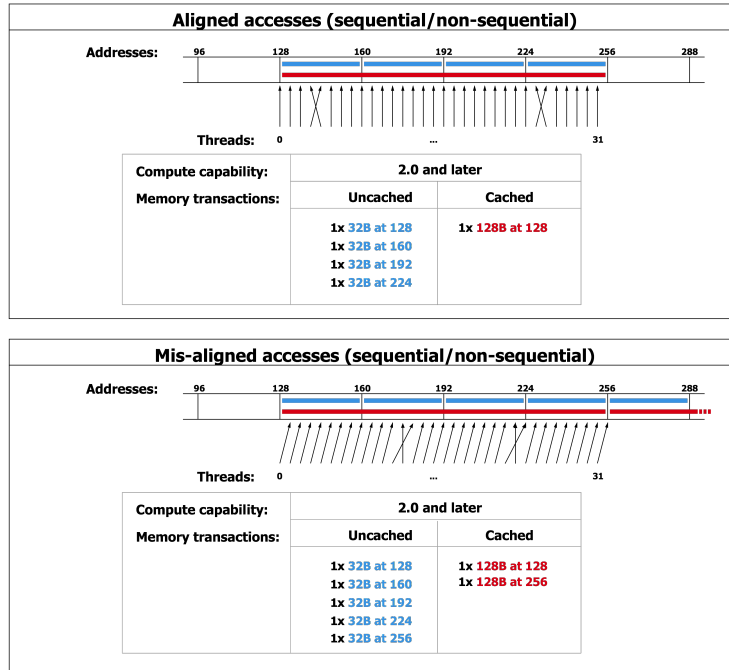


Figure 2.5: Global memory access [11].

umn of the figure, their accesses are serialized, the throughput of shared memory being divided by the maximum number of different addresses accessed in any of the banks. This is called a *bank conflict*. Read access of the same address by multiple threads does not lead to a bank conflict, resulting instead in a broadcast of the value between the threads. Writes to the same address by threads without synchronization result in a data race and an undefined behavior, as does unsynchronized read and write access.

### 2.3.5 General recommendations

We can summarize the information in previous subsections into a few simple rules [11]:

1. Maximize parallel execution by ensuring that the workload is distributed between a large enough number of threads, where each thread requires a low enough number of registers and each thread block requires a small enough part of shared memory so that enough thread blocks fit onto an SM;
2. Optimize memory usage by minimizing transfers from lower bandwidth memory by reusing data in hardware cache or manually moving data to shared memory. When accessing global memory, utilize coalesced accesses to minimize unnecessary data transferred. When accessing shared memory, minimize bank conflicts;
3. Optimize instruction usage by minimizing the use of low throughput instructions such as sine, cosine, or inverse square root. When working with

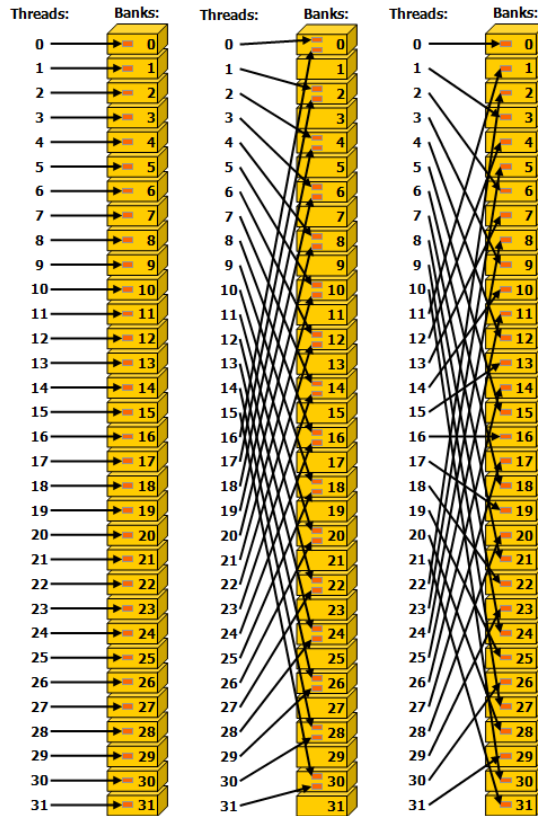


Figure 2.6: Shared memory access patterns [11].

floating point numbers, use 32-bit numbers if precision is not crucial. Minimize thread divergence to ensure all threads in a warp execute useful instructions.

These rules are used in the design of the optimized definition-based cross-correlation implementations described in the following chapter.





### 3. Implementation

In this chapter, we first give a high level overview of the possibilities for parallelization and data reuse in the implementation of the definition-based cross-correlation algorithm, introduced in section 1.1. We then describe a basic implementation of the definition-based algorithm with all its problems. Next, we try to mitigate these problems by introducing a simple implementation based on the warp shuffle instructions. We continue with several optimizations and create a family of implementations based on the warp shuffle instructions. Lastly we introduce a second family of optimizations designed to solve the problems with low occupancy, based on the assignment of the computation of a single job to a larger group of threads.

The definition-based algorithm has several properties which allow for parallelization, optimization through data reuse and distribution of work. Figure 3.1 depicts an output matrix with the corresponding relative shifts of the two input matrices for each output matrix element. This shift defines the overlap of the two input matrices which needs to be computed for given output matrix element. As described in Section 1.3, each element of the output matrix can be computed independently in parallel.

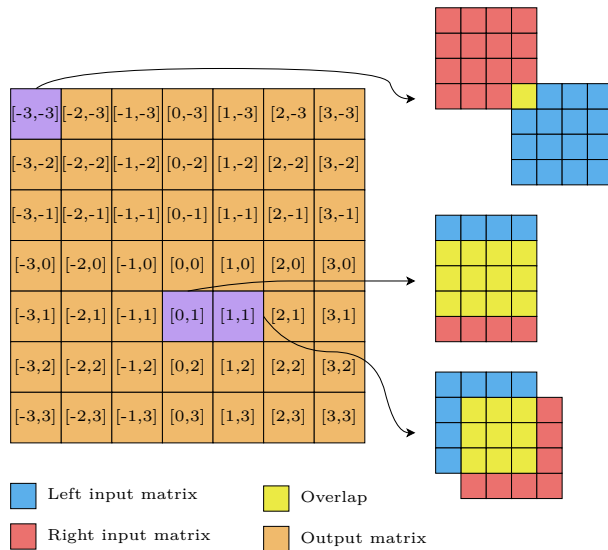


Figure 3.1: Result matrix with corresponding relative shifts.

Each overlap defines a unique set of element pairs which are to be multiplied. Each of these pairs of overlapping elements belongs to exactly one overlap of the two matrices.

#### 3.1 Parallelization

In this section, we highlight the independent parallel tasks in the definition-based cross-correlation algorithm.

The partitioning of the problem into tasks is inspired by Khalil [6], who distributes the computation of a one dimensional cross-correlation of two signals between nodes in a local network. The range of possible delays between the two

signals is split between nodes. In this thesis, we talk about shifts instead of delays as we are computing different ways two matrices overlap. We go further and instead of assigning ranges of shifts, we partition the problem into single shifts or even further, assigning part of a shift computation as a job.

The partitioning is also similar to the problem studied by Honzátko and Kruliš [4], as the problem of 2D cross-correlation is very close to the problem of block-matching in the type of independent parallel tasks it can be partitioned into. Block-matching takes a submatrix, called reference patch, and goes through all submatrices (patches) of the same size in a neighborhood around the reference patch, computing the distance between them and the reference patch using some distance function and giving as output patches with distance lower than some threshold. As described by Honzátko and Kruliš [4]: "The block-matching algorithm offers many opportunities for employing data parallelism. Multiple reference patches can be processed concurrently, distances between reference patch and patches in its neighborhood (the  $n \times n$  window) can be computed concurrently, and even the L2 distance function itself can be parallelized internally."

Definition-based computation of 2D cross-correlation provides similar possibilities for parallelization, where multiple pairs of input matrices can be processed concurrently, each possible overlap of two input matrices can be computed concurrently and even each pair of overlapping items in given overlap can be processed independently and in parallel.

### 3.1.1 Two matrices

When we focus on the computation of the cross-correlation between two matrices, called *one-to-one* in the rest of the thesis, we can reformulate the definition-based algorithm as a problem with two levels of independent parallel tasks, as shown in Figure 3.2. The top level represents the single output matrix, which with only two input matrices is the result of the whole computation. The second level of tasks, represented by orange boxes, contains one box for each relative shift of the two input matrices. In other words each orange box corresponds to a single element of the output matrix. Each shift defines an overlap of the two input matrices, which in turn defines a set of independent subtasks, each subtask representing an overlapping pair of elements of the two input matrices. In Figure 3.2, the subtasks representing pairs of overlapping elements are represented by yellow boxes. Every such subtask belongs to exactly one second level task, creating a tree structure. The set of subtasks which are the children of the same orange box defines a submatrix in both input matrices, as shown in Figure 3.1.

When we look at the operations, every yellow box represents a single multiplication and every orange box represents the sum of the results of all of its children.

The goal is to distribute these tasks between workers in such a way that we maximize parallelism, maximize data reuse and minimize the need for communication and synchronization between workers.

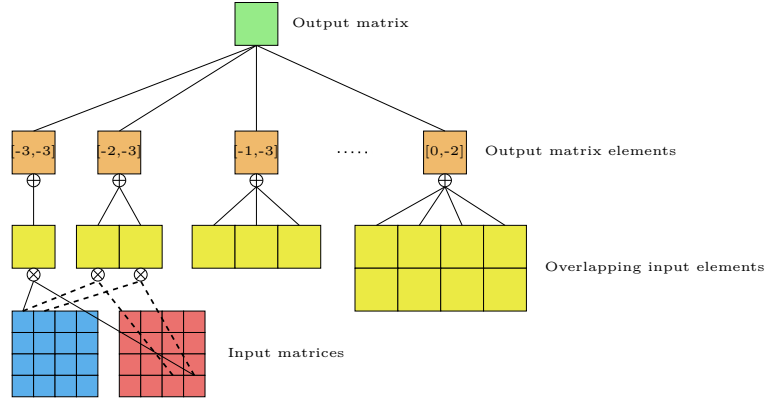


Figure 3.2: Tasks hierarchy in definition-based one-to-one cross-correlation.

### 3.1.2 Many matrices

With more than two matrices, we add additional tasks to the top level of the task hierarchy shown in Figure 3.2, creating a forest of trees. As described in Section 1.3.2, there are several forms of cross-correlation between multiple matrices. For us, the most important of these are:

1. *one-to-many* (Figure 3.3b, for example comparing deformation changes in images taken over time),
2. *n-to-mn* (Figure 3.3c, for example comparing deformations in time of multiple parts of a single large object),
3. *n-to-m* (Figure 3.3d, also called *all-to-all*).

The *one-to-many* type together with the *one-to-one* type, shown in Figures 3.3b and 3.3a respectively, are subtypes of the *n-to-mn* type and *n-to-m*, as the implementations of both of these general types can be used to compute the two simpler types. We separate the *one-to-one* and *one-to-many* types as they offer a greater possibility for caching the single left input matrix.

All of the described types can be partitioned into many *one-to-one* cross-correlations, as shown in Figure 3.4. For both *n-to-mn* and *n-to-m* types, the number of green top level tasks, corresponding to the number of result matrices, is equal to  $n * m$ . To reiterate, the difference between the *n-to-mn* and *n-to-m* types is that in the *n-to-mn* type, each of the  $n$  left input matrices is cross-correlated with a different set of  $m$  right input matrices, whereas in the *n-to-m* type, all  $n$  left input matrices are cross-correlated with the same  $m$  right input matrices. Based on this, the *n-to-m* type allows for greater data reuse, as each right input matrix is used multiple times compared to being used just once in the *n-to-mn* type.

As in the case of *one-to-one* type, the meaning of the boxes is as follows:

- Each green box represents a pair of input matrices, or equivalently a single output matrix;
- Each orange box represents an element in the output matrix, or equivalently a relative shift of the two input matrices;

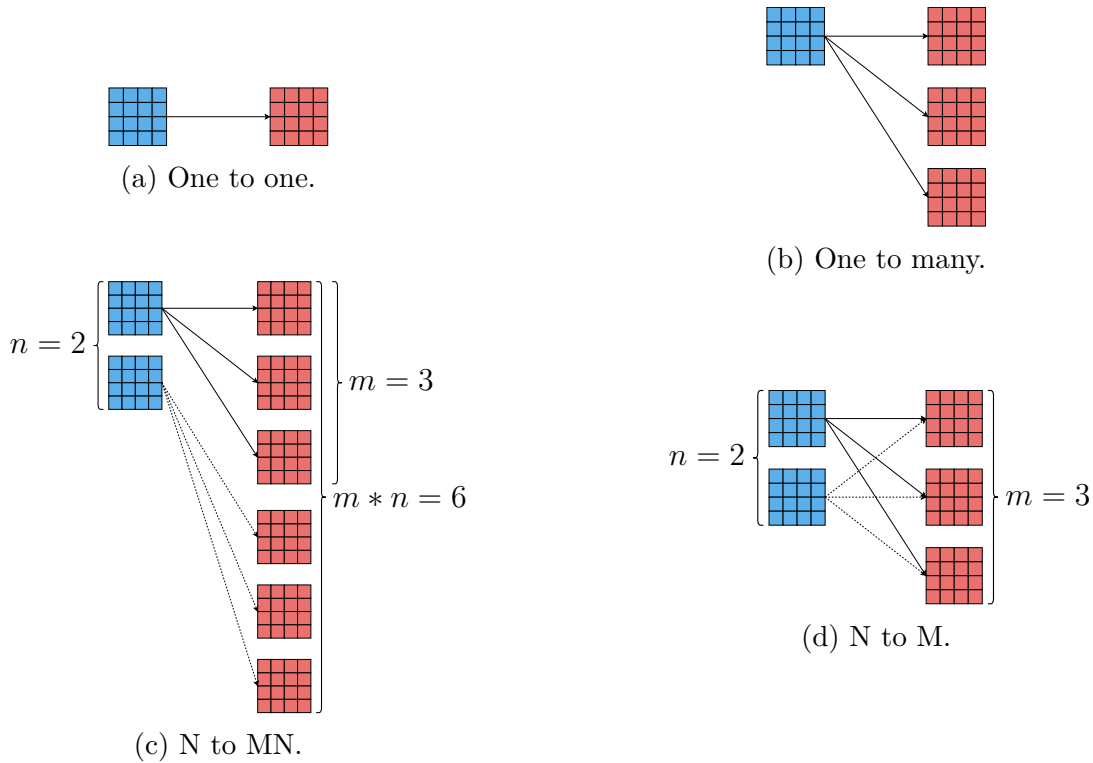


Figure 3.3: Forms of cross-correlation.

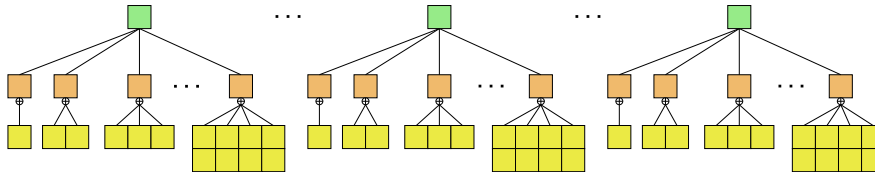


Figure 3.4: Task hierarchy of types with many matrices.

- Each yellow box represents a pair of overlapping elements from the two input matrices.

All boxes on a given level can be processed completely independently. Results of the orange boxes have to be written into the output matrix represented by their green box parent. Each orange box represents a different element of the parent matrix, which allows the writes corresponding to different orange box tasks to be executed without any collisions. All results of the yellow box children of an orange box have to be added together, corresponding to a reduce operation.

As the number of tasks cannot be reduced, the only directions for optimization are parallelization and data reuse. Even though tasks can be processed independently and in parallel, many of them can share and reuse data from other tasks. For example, orange boxes from different subtrees representing the same shift between input matrices and sharing the same left input matrix can be computed by reusing the data from the left matrix. Relationships such as this can be used to group tasks into **jobs** for workers. This grouping then allows each worker to reuse data for multiple computations, or pass data directly to other neighboring workers. Both of these optimizations reduce the required memory throughput and keep data closer to the execution units.

## 3.2 Data reuse

To fully utilize the GPU hardware, we cannot rely on parallelization alone, but must keep the data as close as possible to the execution units for fast access. To achieve this goal, we have to group tasks defined in Section 3.1 into cooperating groups, mostly for sharing input data. We call these groups **jobs**.

The two basic levels on which tasks are grouped into jobs in our implementations are:

- overlap, grouping one or more orange boxes (output matrix elements) into a single job;
- row group or column group, grouping the yellow boxes from a single overlap by rows or columns into jobs.

The following subsections describe groupings based on each of these units.

This grouping is inspired by Bednárek et al. [2], who implement the computation of Levenshtein edit distance on many parallel accelerators, including a GPU. They also solve a slightly different problem in terms of data reuse, as they share intermediate results between threads, whereas we try to reduce the overhead of fetching input data from device memory by passing them between threads to reduce the impact of low arithmetic intensity of each task described in Section 3.1, but the principles employed by Bednárek et al. [2] can be utilized for both.

### 3.2.1 Overlap

When tasks are grouped on the level of overlaps, i.e. orange boxes in the task hierarchy in Figure 3.4, into jobs, we call that the *overlap* basic job size. With this job size, each job computes one or more elements of the output matrix. The job contains all tasks in the subtree with the assigned orange box as its root, or in all subtrees of all assigned orange boxes if multiple overlaps are grouped into a single job.

Multiple overlaps can be grouped into a single job in several ways. First is the **multimat overlap** job size, where multiple overlaps (orange boxes) from different output matrices (green boxes) are grouped into a single job. To enable data reuse, overlaps representing the same shift between different matrices are grouped, as shown in Figure 3.5. There are two versions of this optimization:

- multimat-right, designed for the  $n$ -to- $mn$  computation type, where each job contains overlaps with the same shift between a single left input matrix and multiple right input matrices, shown in Figure 3.5a;
- multimat-both, designed for the  $n$ -to- $m$  computation type, where each job contains overlaps with the same shift between multiple left input matrices and multiple right input matrices, shown in Figure 3.5b.

Another way to reuse data is to compute multiple overlaps which are close to each other in a single output matrix. We call this the **multirow overlap** job size. As neighboring elements of the output matrix correspond to similar shifts between the input matrices, they share most of the input matrix required for their computation, as shown in Figure 3.6. This grouping is also shown in

Figure 3.5. Our implementation groups overlaps from multiple consecutive rows of a single column of the output matrix into a single job. The reasons for this grouping choice are further expanded on in Section 3.4.4. The *multimat* and *multirow* optimizations can be combined as shown in Figure 3.5.

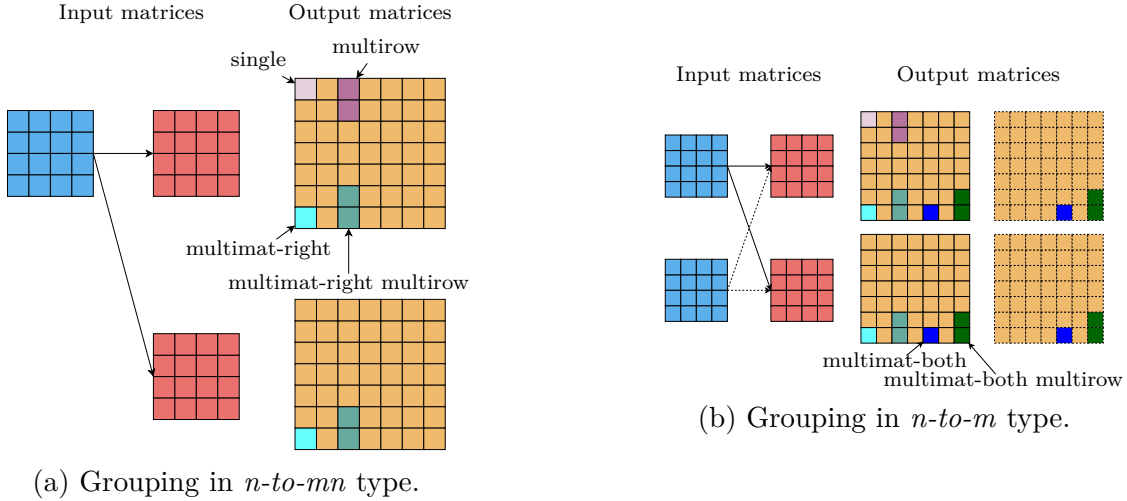


Figure 3.5: Grouping of overlaps into jobs.

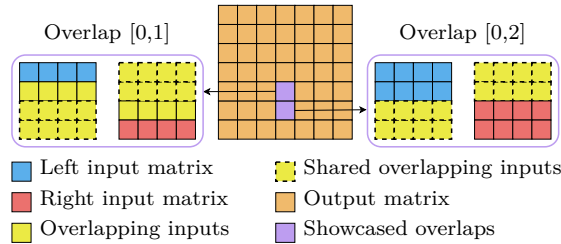


Figure 3.6: Input data shared between neighboring overlaps.

### 3.2.2 Row group and column group

With overlaps as the tasks grouped into jobs, load balancing becomes a problem. The amount of work required by each job may differ massively, as illustrated by the two overlaps in Figure 3.7. This leads to problems with occupancy once jobs with small amount of work are finished.

We implement an alternative where instead of grouping overlaps into jobs, we go one step lower in the task hierarchy and group the individual tasks representing multiplication of one overlapping pair of input elements (yellow box) into jobs. This change results in the computation of a single overlap being split into several smaller jobs, improving load balancing between jobs while also increasing parallelism. A disadvantage of this change is the required final reduce operation to consolidate the results of all the jobs which are computing parts of the same overlap.

To enable additional optimizations described in the following sections of this chapter, we choose to group the yellow box tasks into jobs by whole rows of the overlap. The number of rows grouped into a single job is configurable through an

algorithm argument. This grouping is illustrated in Figure 3.7, where *Max job rows* is the argument of the algorithm. Each overlap with  $r$  overlapping rows of the two input matrices is split into  $\lceil \frac{r}{\text{max\_job\_rows}} \rceil$  jobs, with each job containing at most *max\_job\_rows* consecutive rows. With this distribution of tasks into jobs, the tasks assigned into a single job form a submatrix of the overlap. As we are assigning whole rows, the submatrix has the same number of columns as the original overlap. This distribution also ensures that all overlaps with the same number of rows will be split into the same number of jobs.

For data reuse, one important observation is that jobs from the same overlap do not share any input data, but jobs with the same ID from overlaps neighboring in the same row of the output matrix will share most of the input data, as shown in Figure 3.8. If they are direct neighbors, the difference will be a single column of the overlap.

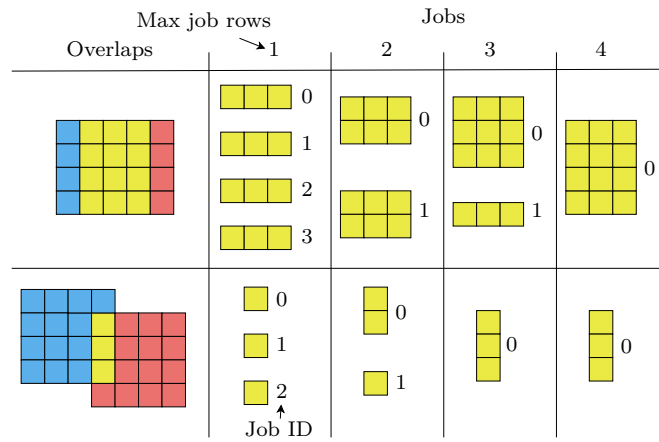


Figure 3.7: Grouping of rows of tasks into jobs.

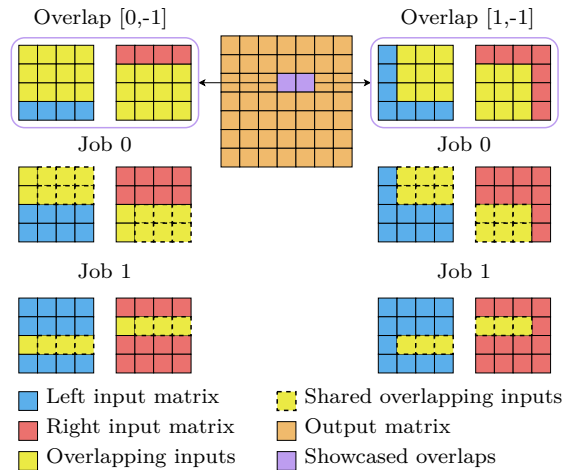


Figure 3.8: Data shared between jobs with the same ID from neighboring overlaps.

For some optimizations, it is better to group tasks by columns instead of rows. From the data reuse point of view, it is symmetrical to the grouping by rows. Again, column groups from the same shift do not share any input data, but column groups with the same ID from two neighboring overlaps in the same column of the output matrix share most of their input data.

The *multimat* optimization introduced in Section 3.2.1, which groups overlaps from multiple output matrices into a single job, can also be used with both row group and column group task grouping. The *multirow* optimization, which groups multiple overlaps from a single output matrix into a single job, is unfortunately incompatible with both row group and column group task grouping.

### 3.2.3 Workers

Jobs defined in the previous section are assigned to one level of the CUDA thread hierarchy, described in Section 2.2.2. From the CUDA thread hierarchy we utilize the following groups of threads as workers:

1. thread,
2. warp,
3. thread block.

As we will see in Section 3.6, a thread block is already too large to properly utilize the GPU threads our job sizes, which is the reason grid is not utilized here. We call each member of the chosen thread hierarchy level, i.e. the thread, warp, or thread block, a **worker**. Each worker is assigned at most one job, with some workers possibly unused as the number of jobs may not be multiple of warp size or thread block size. Based on the choice of worker size, we can utilize smaller groups in the hierarchy to compute tasks in the assigned job, and primitives provided by larger groups to exchange input data or combine results with other workers.

Similar choice is done by Bednárek et al. [2], who provide two implementations of the Levenshtein edit distance, one assigning stripes (their unit of job size) to warps and one assigning stripes to thread blocks. The warp version utilizes warp shuffle instructions to exchange intermediate results between threads, whereas the thread block version exchanges data through shared memory. Even though we are not exchanging intermediate results but instead trying to reuse input data loaded from device memory, we will see that these principles can also be used for this purpose.

### 3.2.4 List of implementations

Different implementations of the definition-based cross-correlation utilize different job sizes, worker types, and different ways of assigning jobs to workers. The chosen parameters then lead to different ways of cooperation, communication, synchronization, work distribution, and load balancing. Following is the list of algorithms implemented in this thesis with their choice of job size and worker type. Each algorithm is described in more detail in the following sections of this chapter.



Algorithm	Job size	Worker type
Basic	overlap	thread
Warp shuffle	overlap multimat overlap multirow overlap multimat multirow overlap row group multimat row group	thread
Warp per shift	overlap row group	warp
Warp per shift with shared memory	overlap column group multimat column group	warp
Block per shift	overlap	thread block

Algorithms with multiple job sizes are provided in multiple implementations, each implementing different optimization for data reuse.

### 3.3 Basic algorithm

A basic implementation of the definition-based cross-correlation of two input matrices, in our naming scheme corresponding to the *one-to-one* type, utilizes a two dimensional grid of two dimensional thread blocks to start one thread for each element of the output matrix. The overlap to be computed by a given thread is derived from the position of the output matrix element, as shown in Figure 3.9. The thread then iterates over the overlapping parts of the two input matrices, multiplying the pairs of overlapped elements and accumulating the result of these multiplications which is then written to the assigned output matrix element. The code for this implementation can be found in the attachments of this thesis as the `cross_corr_naive_original` kernel.

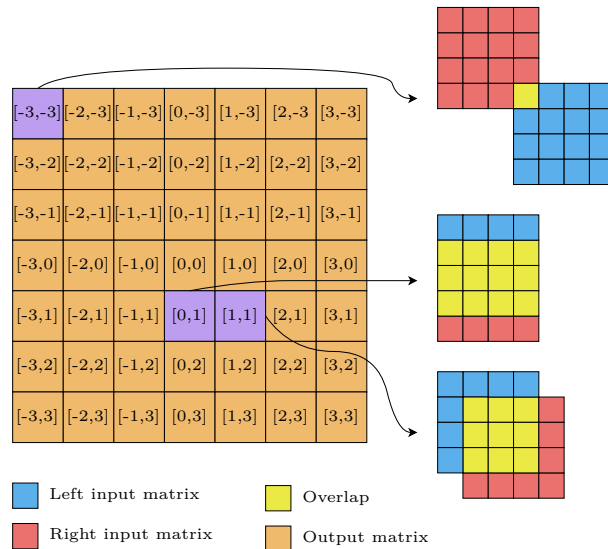


Figure 3.9: Examples of overlaps corresponding to output matrix elements.

This implementation allows for a great amount of parallelism, as each element of the output matrix is computed independently. The disadvantages, on the other hand, are no data reuse, thread divergence, and a large difference between workloads assigned to each thread.

The problem with no data reuse is illustrated in Figure 3.10. The figure shows elements of the left input matrix (in blue) and right input matrix (in red) accessed by thread 0 and thread 1 in iterations 0 to 11. As memory accesses are done in units of 32 threads, also known as the warp, when we extrapolate this example, the 32 values loaded from the left input matrix in global memory will contain 31 values read in the previous iteration by the threads of this warp. In other words, we are moving a window of 32 elements across each row of the left matrix 1 element per iteration and reading the window from global memory in each iteration. Even though these global memory accesses will most likely be served from L2 or L1 cache, the cache access still carries with it additional latency compared to accessing registers, even though 31 of the 32 items are already in registers of threads of the warp. This problem is exacerbated when the  $x$  component of the thread block size is not a multiple of warp size. In this situation, the threads of a warp are assigned overlaps from different rows of the output matrix. These overlaps differ in the number of rows they contain, and consequently in the rows of the input matrices which are read in the given iteration. This means that the threads of a single warp access two or more different rows of the left input matrix in each iteration, leading to non-coalesced loads.

In the right input matrix, all threads of the warp will read the same value from global memory in each iteration, resulting in 32 reads of the same block of global memory when reading 32 bit values.

The exact pattern of reads from global memory differs based on the overlaps processed by the threads of the warp, but will always result in repeated reads of the same block of global memory.

The problem of thread divergence is illustrated in Figure 3.10 with iterations 3, 7 and 11. The basic implementation of looping over a two dimensional matrix with two nested for loops results in thread 0 reading an element from each input matrix, computing multiplication and accumulating the result in these iterations, while thread 1 has no data to process on this row and as such is masked during the execution of the inner for loop due to the range condition being false. While we show only two threads in Figure 3.10, the situation is much worse, as 31 of the 32 threads of the warp will be masked and not doing anything in the last iteration. All threads of the warp will go through both for loops based on the size of the largest overlap in the given axis processed by any thread of the warp.

Last significant problem of the Basic algorithm, largely connected with the previous problem, is that overlaps differ in size. From overlaps containing one element from each input matrix to the overlap of the whole input matrices, this difference in workload size means that some threads will finish rather quickly, while a small number of threads computing the largest overlaps will keep executing much longer. For example, warps of threads assigned overlaps in the first or last row of the output matrix will only read a single row of each input matrix, and finish quickly, while warps assigned overlaps in the middle of the output matrix will read most elements of each input matrix and run for much longer. This results in problems with occupancy of the GPU.

A slight modification of this algorithm to allow for an  $n$ -to- $mn$  computation is implemented by the original thesis by Bali [1].

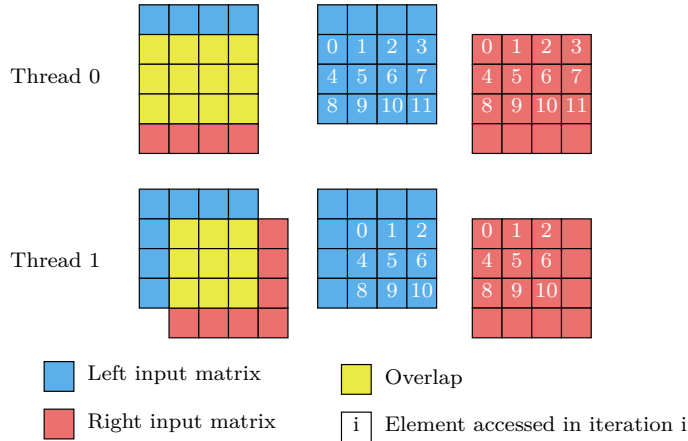


Figure 3.10: The iteration in which each input matrix element is accessed by two neighboring threads.

### 3.4 Warp shuffle algorithm family

This section describes the implementation of definition-based cross-correlation utilizing warp shuffle instructions, which tries to fix the problems of the Basic algorithms described in the previous section. We first introduce a simple version of the implementation, later improving it step by step with optimizations evaluated in Section 4.2.

This implementation is based on the warp based implementation of Levenshtein distance by Bednársek et al. [2], which utilizes the warp shuffle instructions to exchange intermediate results between threads of a warp. In our implementation, we do not share intermediate results, instead utilizing registers as L0 cache to keep input data loaded from the global memory as close to the execution units as possible.

In the simplified implementation, warp shuffle instructions are utilized to shuffle data loaded from the left input matrix and broadcast data loaded from the right input matrix between the threads of a warp. As shown in Section 3.2.4, each CUDA thread is assigned a single overlap to compute, which is exactly as was done in the Basic algorithm. The difference from the Basic algorithm is only in the reuse of input data once it is loaded into registers. The code for this implementation can be found in the attachments of this thesis as the `ccn_shuffle` kernel.

The main idea behind this algorithm is illustrated in Figure 3.10. The two threads computing overlaps with shifts  $[0, 1]$  and  $[1, 1]$  process elements of the two input matrices in the indicated iterations of a *for loop* in the code.

The element from the left matrix read by the thread processing shift  $[x, y]$  in iteration  $i$  is required by the thread processing shift  $[x + 1, y]$  in iteration  $i + 1$ . This fact holds for any two neighboring shifts and maps exactly onto the *warp shuffle down* function, described in Section 2.2.3. When looking at the right matrix in any given iteration, both shifts require the exact same element from the

right matrix. This broadcast can be implemented using the general warp shuffle function with direct source lane indexing. Iterations 3, 7, and 11 are skipped by thread 1 to preserve this property.

To utilize this relationship, threads of a single warp process 32 consecutive elements in a row of the output matrix, as shown in Figure 3.11. The number of warps per thread block is configurable using a run-time algorithm argument. The grid size is set so that there is at least one thread started for each element of the output matrix. Any unused threads do not write to the output matrix and during computations are handled by the bound checked reads described next.

The problem of iterations 3, 7, and 11 in Figure 3.10, in which thread 1 does not have any value to compute, can be solved in several ways. If we were creating a program to run on a CPU, we would give the two for loops implementing the two worker threads different bounds so that the second worker would stop earlier. A more GPU friendly implementation needs to prevent thread divergence. This is achieved by executing the range check only once when loading the data from the left matrix into a register of the thread. If the thread is loading a value outside the matrix, it loads 0 instead. This makes the result of the multiplication performed in each step 0, which is then added to the sum, effectively skipping the iteration while preventing thread divergence and allowing further optimizations such as loop unrolling. There will most often be additional work introduced by loading 0 and executing all iterations instead of doing checks in the for loop and utilizing thread divergence. This additional work is balanced out by the ability to unroll the loop, as it has fixed number of iterations. This also handles any extra threads introduced due to the fixed size of a thread block and overlap sizes not divisible by warp size.

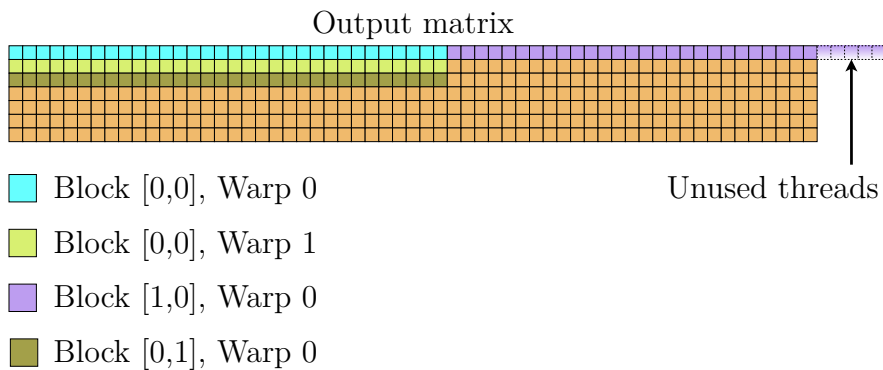


Figure 3.11: Distribution of overlaps in a 7 by 59 output matrix between threads of thread blocks and warps.

### 3.4.1 Algorithm steps

The following description assumes *warp size* to be 32, as is the case for all currently existing Nvidia GPUs. The actual value of this constant is not important for our algorithms and is defined as a constant in our code. To utilize coalesced loading from global memory, the buffer that is shuffled between the threads of a warp, containing data from the left input matrix, is split into two parts of 32 items each, which together function as a single 64 item ring buffer. We call the

parts the *top* and the *bottom*, where new data is always loaded to the top part and then shuffled towards the bottom part, as shown in Figure 3.12. As described above, any out of bounds loads are range checked and instead of trying to load from the global memory return value 0. This is done by the following code:

```
template<typename T>
__device__ T load_with_bounds_check(const T* source, int idx,
    size_t size) {
    return (idx >= 0 && idx < size) ? source[idx] : 0;
}
```

When loading a buffer, bound checked load shown above is used to load 32 consecutive values (or load 0 if out of bounds), storing one item per thread into a register. This is implemented by the following code:

```
T thread_left_bottom = load_with_bounds_check(
    left_row,
    warp_x_left + warp.thread_rank(),
    matrix_size.x
);
```

The values of the buffer are held in two variables in each thread. The bottom part of the buffer is held in the variable `thread_left_bottom` and the top part in the variable `thread_left_top`. This creates a 64 item ring buffer distributed between threads of a warp, which is shuffled using the warp shuffle instructions as shown in Figure 3.12.

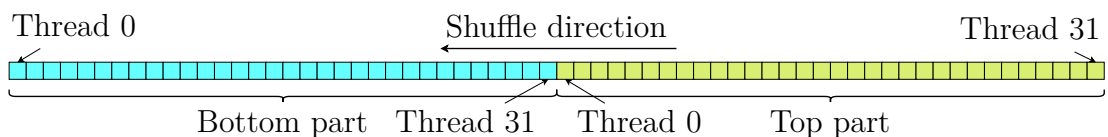


Figure 3.12: Shuffling of the left buffer.

For the data loaded from the right matrix, which we use for broadcasting, we require only a single value per thread. In the 32 iterations of the innermost loop, we will broadcast only these 32 values, whereas we need 64 from the left matrix as the 32 values loaded into the top part will be shifted all the way to the bottom part.

The core of the implementation is illustrated in Listing 3.1. The 32 threads of a warp are assigned 32 consecutive overlaps in a row of the output matrix. Each overlap is defined by the shift between the two input matrices, with the overlap assigned to thread 0 of the warp having shift `warp_min_shift` and overlap assigned to thread 31 (or the last used thread if some of the threads have no jobs assigned to them) having shift `warp_max_shift`. Overlap assigned to thread  $i$  then has shift  $[warp\_min\_shift.x + i, warp\_min\_shift.y]$ , with `warp_max_shift` equal to  $[warp\_min\_shift.x + 31, warp\_max\_shift.y]$  if there are no unused threads, otherwise the  $x$  component is clamped to the maximum shift defined by the output matrix. The `warp_min_shift` and `warp_max_shift` define a submatrix of both input matrices which contain elements required by any thread in the warp, shown in Figure 3.13. We call this the *warp submatrix*.

The outer and middle loop then iterate over the warp submatrix in the right input matrix, outer loop iterating over rows of the submatrix with the `warp_y_right` variable and the inner loop iterating in buffer load size steps over the columns of the submatrix with the `warp_x_right` variable. Bounds of the for loops are computed using the `warp_min_shift` and `warp_max_shift` variables defining the warp submatrix. As described above, we have two buffers. The buffer holding data from the right matrix is made up of 32 registers, one per each thread represented by the variable `thread_right`. The buffer holding data from the left matrix is made up of 64 registers with 2 registers per thread, represented by the variables `thread_left_bottom` and `thread_left_top`. Both buffers are loaded 32 items at the time to allow for coalesced loads, with the left buffer loading into the top part.

The innermost loop then does 32 (warp size) iterations. In iteration  $i$  we broadcast the value stored in the part of the *right buffer* owned by the thread  $i$ . This value is then multiplied by each thread with the value from the *bottom left buffer* stored by given the thread. We then shuffle the whole *left buffer* one step towards the index 0 of the bottom part of the buffer using two warp shuffle instructions. After the 32 steps, the top part of the *left buffer* is now in the bottom part of the *left buffer* and all the values from *right buffer* have been broadcast.

The next iteration of the middle loop then loads 32 values to the top part of the *left buffer* and 32 values to the *right buffer* which are then processed by the *main loop*. This is repeated until the whole row of the warp submatrix is processed, where we continue to next iteration of the outer loop and process the next row. This is repeated until the whole warp submatrix is processed.

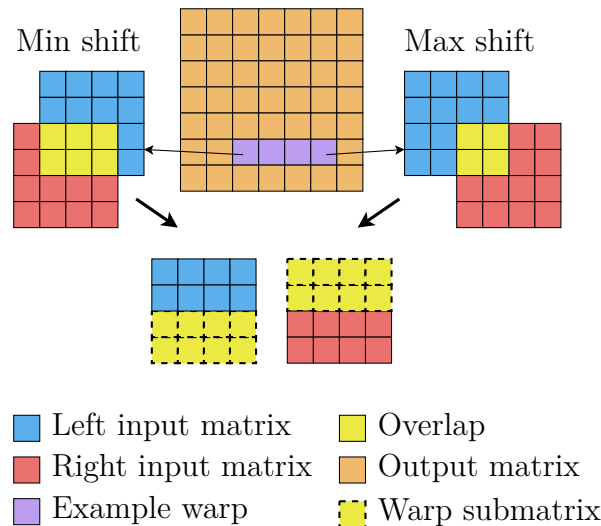


Figure 3.13: Submatrix of input data used by any thread in the warp.

### 3.4.2 Work distribution

The work distribution optimization changes job size from a whole overlap used by the simplified implementation to a row group, as described in Section 3.2.2. Each job is still assigned to a single thread, with jobs of the same ID from

```

// Compute bounds of the overlaps processed by warp
// Comput thread output position

T sum = 0;
/* for each overlapping row in the right input matrix */
for (size_t warp_y_right ... ) {

    // Corresponding row in the left input matrix
    int warp_y_left = warp_y_right + warp_min_shift.y;

    // First column in the left input matrix
    // corresponding to the first column in the right input matrix
    int warp_x_left = warp_x_right_start + warp_min_shift.x;

    // Preload 1 value to each thread from the input left matrix
    T thread_left_bottom = load_with_bounds_check(left_matrix, ...);

    for (size_t warp_x_right ...; warp_x_right += warp.size()) {
        int warp_x_left = warp_x_right + warp_min_shift.x;

        T thread_left_top = load_with_bounds_check(left_matrix, ...);
        T thread_right = load_with_bounds_check(right_matrix, ...);

        for (size_t i = 0; i < warp.size(); ++i) {
            // Broadcast right buffer
            auto right_val = warp.shfl(thread_right, i);
            sum += thread_left_bottom * right_val;

            // Shift left buffer
            // General shuffle does module on source lane argument
            // Thread 0 needs to connect the top buffer to the bottom
            // buffer
            thread_left_bottom = warp.shfl(
                warp.thread_rank() != 0 ? thread_left_bottom :
                thread_left_top,
                warp.thread_rank() + 1
            );
            thread_left_top = warp.shfl_down(thread_left_top, 1);
        }
    }
}

if (/* thread output not out of bounds */) {
    out_matrix[output_offset] = sum;
}

```

Listing 3.1: Core of the Simple warp shuffle based implementation

32 consecutive overlaps in a row of the output matrix assigned to threads of a single warp. This enables us to again compute the warp submatrix of the right input matrix containing elements used by all threads of the warp and reuse the core computation code of the simplified implementation described in the previous section without any change by just providing different bounds to the outer and middle for loops. The code of this implementation can be found in the attachments as the `ccn_shuffle_work_distribution`.

As there are multiple workers computing single element of the output matrix, we need to add all their results together. Because it is only a single write of a single value per worker, utilizing the `atomicAdd` [9] operation on the output matrix in global memory is sufficient. It also allows us greater freedom of assigning tasks to workers across the whole grid compared to grouping workers for the given overlap into a thread block, which would be required to utilize shared memory for communication. The maximum number of rows in a task is provided as a runtime argument to the algorithm, and influences the number of workers created.

In the simplified algorithm, the output matrix was covered by a two dimensional grid of two dimensional thread blocks. With this optimization, we cover the output matrix multiple times by increasing the number of thread blocks in the grid, assigning each overlap to multiple threads. Each of the threads assigned to the given overlap is then assigned a single row group as a job. The number of blocks is increased in the  $y$  axis of the grid size. The overlap is then assigned using the  $x$  axis of thread rank the same way it is done in Simplified algorithm and  $y$  axis thread rank is used to assign both the overlap and the job within the overlap jobs. In the simplest work distribution we call *Rectangle* the  $y$  axis of thread rank modulo output matrix size gives us the overlap and divided by output matrix size gives us the Job ID. Thanks to the unchanged use of the  $x$  axis rank, all threads of a warp will be mapped to 32 consecutive overlaps in a row of the output matrix same as in the simplified algorithm, but also to the job with the same ID in each of the overlaps as they all share the same  $y$  axis thread rank.

We provide several algorithms to derive the number of workers started (how much to increase the number of thread blocks started) for given total number of jobs and the mapping from worker ID to the overlap and the job ID. The provided algorithms are:

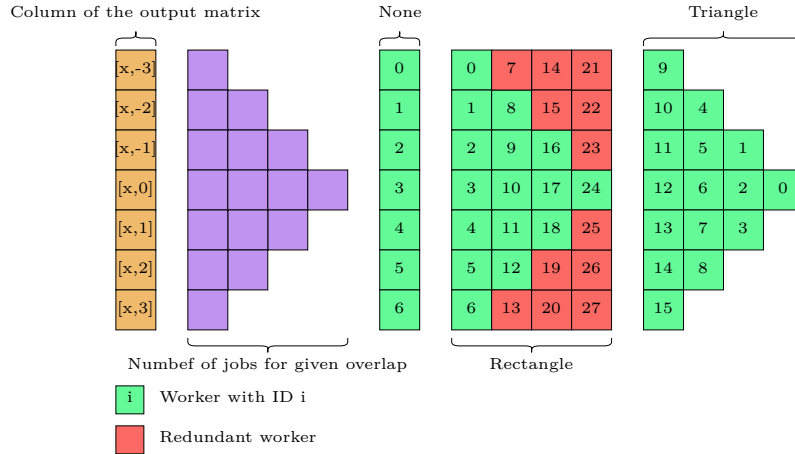
- None,
- Rectangle,
- Triangle.

The algorithms are illustrated in Figure 3.14. The purple boxes represent number of jobs for each overlap in the given row of the output matrix. As row groups are made up of rows and all overlaps in a given row of the output matrix have the same number of rows, they will also have the same number of jobs.

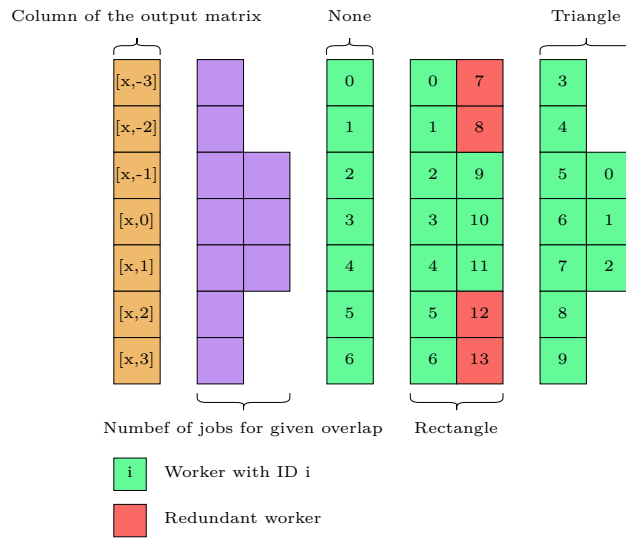
### None distribution

The *None* distribution behaves exactly the same as simplified implementation introduced in Section 3.4.1. Each overlap is assigned only to a single thread





(a) Mapping with maximum of 1 row per job.



(b) Mapping with maximum of 2 rows per job.

Figure 3.14: Mapping of a column of workers onto a column of the output matrix.

which then has to compute the whole overlap alone. Grid covers the whole output matrix to start one thread per output matrix element and the  $y$  axis of the thread rank is used to assign the row of the output matrix, as is done in the simplified implementation. This distribution is provided mainly to measure the overhead of the code changes required to implement work distribution.

### Rectangle distribution

The *Rectangle* distribution computes  $m$ , the maximum number of jobs any overlap will be split into. The maximum number of jobs is always required for the overlap in which both matrices are exactly aligned over each other in the  $y$  axis, covering all rows. We increase the number of thread blocks so that there are at least  $m$  times as many threads as there are elements in the output matrix. Each element is then assigned  $m$  workers which are then further assigned one of the at most  $m$  jobs the given overlap is split into. As  $m$  is maximum, in Figure 3.14a equal to 4, we see that most overlaps will not be split into that many jobs. The unused workers are then stopped. The number of thread blocks is increased in the  $y$  axis

of the grid size, with the  $y$  axis of thread index used to assign row of the output matrix using thread index modulo number of rows in the output matrix and job ID using thread index divided by the number of rows in the output matrix. As it is all done based on the  $y$  axis of the thread index, the threads of a single warp are again assigned consecutive overlaps in the output matrix, with all threads being assigned the job with the same ID from the given overlap. This enables us to stop the whole warp, as either all threads will be assigned work or no threads will be assigned work, leading to no thread divergence.

### Triangle distribution

The *Triangle* distribution extends the grid by increasing the number of thread blocks to start the exact number of threads required for the total number of jobs in all overlaps. Due to the user configured size of thread block, there will most often still be some unused workers, but always less than one row of thread blocks worth of workers.

The  $y$  axis of the thread rank is then used to assign row of the output matrix and job ID as seen in the 3.14. The values of the  $y$  axis of the thread index are mapped to the triangle we see in the figures from left to right, in each column from top to bottom. The output matrix row is then derived from the vertical position and job ID from the horizontal position.

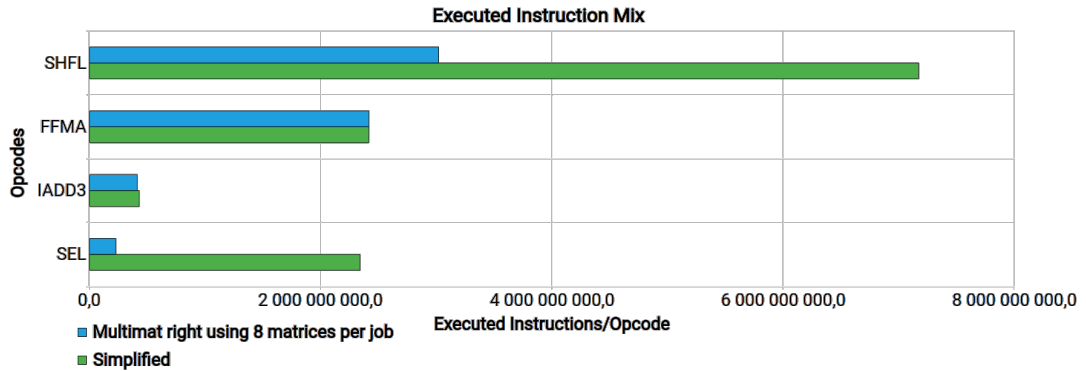
The computation of row and column in the triangle is based on Triangular numbers [21], which we extended to work with triangles growing by more than one item per row. The disadvantage of this distribution is the complex computation required to assign overlaps and job IDs to workers. This computation includes many multiplications, divisions and most importantly a low throughput square root instruction. For small job sizes the overhead of triangle distribution may be greater than any gains provided by better load balancing and increased occupancy.

As with the rectangle distribution, output matrix row and job ID are derived only from the  $y$  component of the thread rank, so all threads of a warp will again be assigned consecutive overlaps on a single row of the output matrix, with each thread of the warp assigned the same job ID within its overlap. This again enables us to stop any unused worker right after job assignments, as only whole warps may be unused, and reuse the simple warp shuffle implementation code with only changes being the different bounds of the outer and the middle loop.

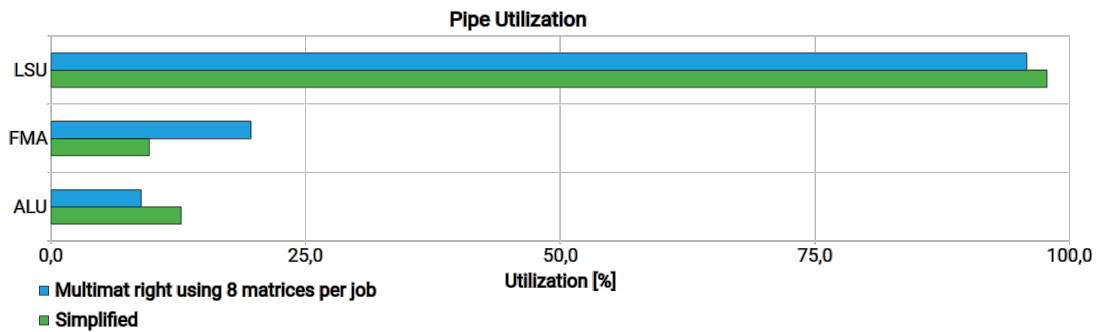
### 3.4.3 Utilizing multiple right matrices

Another problem of the simplified implementation not solved by work distribution described in Section 3.4.2, is the ratio of warp shuffle instructions to arithmetic instructions. In the simplified algorithm, for each multiplication and addition represented by a single yellow box, we must execute three warp shuffle instructions. This makes warp shuffle instructions the bottleneck in the simplified implementation, as shown in Figure 3.15a. The warp shuffle instructions (SHFL) dominate the executed instruction mix, which results in 97% utilization of the *LSU* pipeline implementing the shuffle instructions, as shown in Figure 3.15b. Compare this to the fused multiply-add instructions (FFMA) implementing the multiplication and

addition, which are executed by the *FMA* pipeline with less than 10% utilization for the simplified algorithm.



(a) Executed instruction mix.



(b) Pipeline utilization.

Figure 3.15: Comparison of *one-to-many* simplified algorithm with the multiple right matrix optimization.

There are several ways to improve the ratio of SHFL instructions to FFMA instructions. The one with easiest changes to the code of the Simple warp shuffle implementation is to utilize the *one-to-many* type of computation, and let each worker compute cross-correlation between one left matrix and many right matrices at once, as described in section 3.2.1 under the name *multimat*. We call this exact implementation usable for *one-to-many* and *n-to-mn* types the *multimat\_right* optimization, as each job contains multiple overlaps of a single left matrix with multiple right matrices. The obvious advantage is data reuse, as the data from the left matrix is used to compute multiple results. The main advantage is that each additional right matrix only adds a single SHFL instruction, while also adding one FFMA instruction. The ratio of SHFL to FFMA instructions can then be expressed as  $2 + r : r$ , where  $r$  is the number of overlaps (from  $r$  right matrices) computed by each worker, which for larger values of  $r$  significantly improves the 3 : 1 ratio of the simplified warp shuffle algorithm.

The code changes required to implement this are very straightforward, and can be found in the attachments of this thesis in the `ccn_shuffle_multimat_right` kernel. The kernel `ccn_shuffle_multimat_right_work_distribution` then implements a combination of this optimization and the *work distribution* optimization described in Section 3.4.2.

As each job contains the same overlap between one left matrix and multiple right matrices, the three for loops and their bounds described in Section 3.4.1

```

template<size_t NUM_RIGHTS, typename T>
__device__ void warp_shuffle_multimat_right_impl(...) {
    ...
    T sum[NUM_RIGHTS];
    for (size_t r = 0; r < NUM_RIGHTS; ++r) {
        sum[r] = 0;
    }
    ...
    T thread_right[NUM_RIGHTS];
    for (size_t r = 0; r < NUM_RIGHTS; ++r) {
        thread_right[r] = load_with_bounds_check(...);
    }
    ...
    for (dsize_t r = 0; r < NUM_RIGHTS; ++r) {
        // Broadcast right buffer
        auto right_val = warp.shfl(thread_right[r], i);
        sum[r] += thread_left_bottom * right_val;
    }
}

```

Listing 3.2: Changes for multimat right implementation

are left unchanged. The main difference is that the *sum* and the *thread\_right* variables in each thread are changed into arrays, utilizing the CUDA local array optimization described in Appendix A. This increases the amount of data present in registers and allows us to reuse data loaded from the left matrix with data from multiple right matrices. The code changes are illustrated in Listing 3.2.

We introduce the term *matrix group*, describing the right input matrices from which overlaps are grouped into a single job. As the size of the matrix group must be known at compile time to utilize the CUDA local array optimization, the *device* function implementing the algorithm needs to be compiled for each supported matrix group size in the `NUM_RIGHTS` template argument. This introduces a trade-off between compilation time, generated code size and the number of required registers on one hand and possible gains during run-time on the other. The actual matrix group size used during run-time is specified as run-time argument for the algorithm, which then chooses the correct implementation. If the number of matrices is not divisible by the matrix group size, the last few matrices will form a smaller matrix group which will choose the implementation based on its size. The maximum supported matrix group size is configurable during compile-time.

The number of thread blocks is increased to start enough workers to process all jobs. Threads of each thread block are assigned jobs from a single matrix group, again assigning jobs containing 32 consecutive overlaps in each output matrix of the matrix group to threads of a single warp. This allows us to reuse most of the Simple warp shuffle algorithm code.

The effects of this optimization shown in Figure 3.15, which compares the simplified algorithm against the optimized algorithm using 8 right matrices grouped into a single job (which is a default maximum group size to keep compile times and executable size manageable) with input of size 256x256 with 1 left matrix and

16 right matrices, which are enough to saturate the RTX 2060 used for profiling. In this profiling, the LSU pipeline is still a bottleneck even for the optimized algorithm, but the utilization of the FMA pipeline, which does the useful part of the computation, has increased from 9% to 20%. The most visible change is in the mix of the executed instructions, where we see a very noticeable improvement in the ratio of shuffle instructions (SHFL) to the floating point fused multiply-add instructions (FFMA). As expected, the ratio improves from 3 : 1 to 10 : 8, with 3019898880 : 2415919104 SHFL to FFMA instructions. The relatively small improvement in the LSU pipeline utilization can be explained by the low throughput of the SHFL instructions compared to the FFMA instructions. This is exacerbated by our use of Compute Capability 7.5 card for profiling, which has half the warp shuffle throughput of all other Compute Capabilities.

### 3.4.4 Multiple rows from the right matrix

Another way to improve the instruction ratio is to process multiple overlaps from the same output matrix, which can be used even for the *one-to-one* type of computation. We call this the *multirow\_right* optimization, as we compute overlaps from multiple consecutive rows of a single column of the output matrix as shown in Figure 3.16, where we see two different jobs, each containing 4 overlaps, i.e. *job\_size* is 4. We call it *multirow\_right* as it loads multiple rows from the right matrix at once to compute the assigned overlaps. This optimization provides us a different way to improve the ratio of warp shuffle to fused multiply-add instructions, independent of the changes in *multimat\_right*. Thanks to this it can be combined with *multimat\_right*. It is not however able to be combined with the *work distribution* optimization. The code of this optimization can be found in the attachments of this thesis as the `ccn_shuffle_multirow_right` kernel.

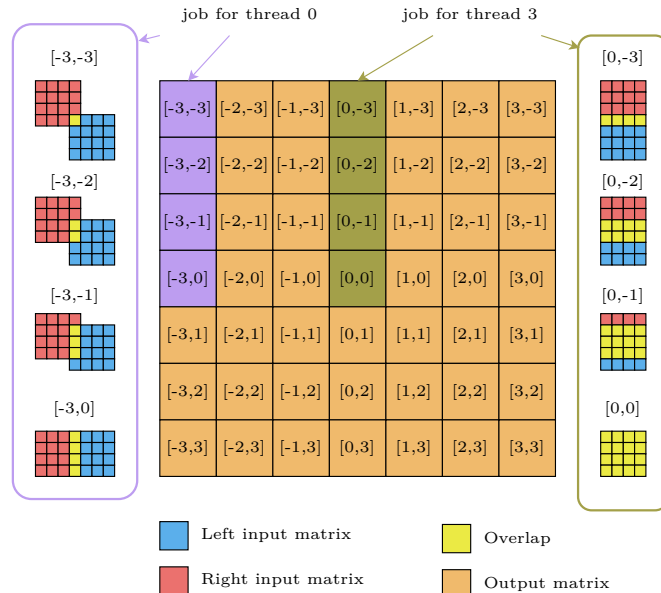


Figure 3.16: Overlaps grouped into two different jobs by the *multirow\_right* algorithm with 4 overlaps per job.

The core of the implementation is similar to the simplified algorithm. We compute the warp submatrix of the right input matrix containing all elements

used by any of the overlaps in jobs assigned to the threads in the given warp. We then iterate over this submatrix, computing all *job\_size* overlaps in a single pass. This reduces parallelism, as simplified algorithm would have split these overlaps into different jobs and computed them in parallel, but allows for data reuse, which is advantageous when the GPU is already saturated.

As each overlap in a given job has different shift in the  $y$  axis, each overlap will contain different number of rows as shown in Figure 3.16, but thanks to the column-wise grouping of overlaps, corresponding overlaps in each job assigned to threads of a single warp will contain the same group of rows. This again allows us to reuse much of the simplified implementation code, which expects a warp to process overlaps with the same number of rows.

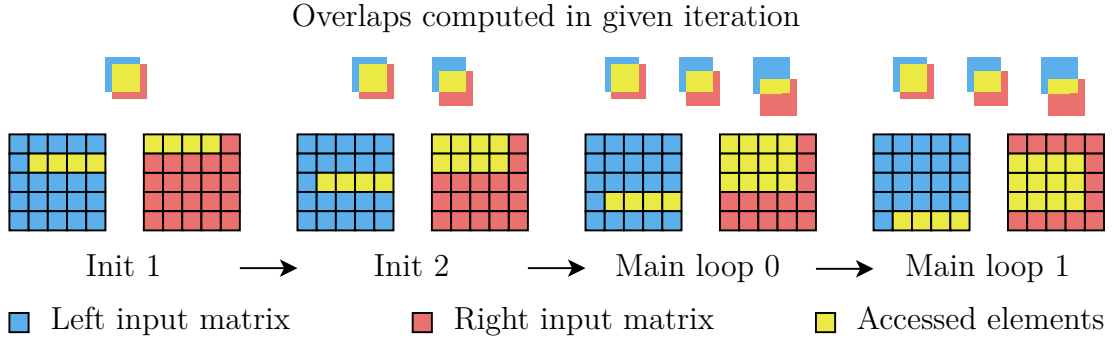
The problem experienced by this optimization is in its nature similar to the one shown in the Simple warp shuffle implementation, where some of the threads need to execute the first few and the last few iterations of the innermost loop by adding zero to their sum thanks to bound checked loads. This is caused by the different shifts of the overlaps assigned to threads of a single warp, where some of the overlaps do not use whole warp submatrix, which contains input data used by any of the overlaps assigned to the threads of the warp.

As we now group several overlaps into a single job computed by a single thread, the same problem arises where only a subset of the overlaps has the first few rows and last few rows of the warp submatrix as inputs. More precisely, some of the first 0 to  $job\_size - 1$  and the last 0 to  $job\_size - 1$  rows are only required by some of the overlaps assigned to the given thread, and as all threads of a warp are assigned overlaps from the same rows of the output matrix in 32 consecutive columns, the subset of overlaps to which each row of warp submatrix is an input is the same for all threads of a warp.

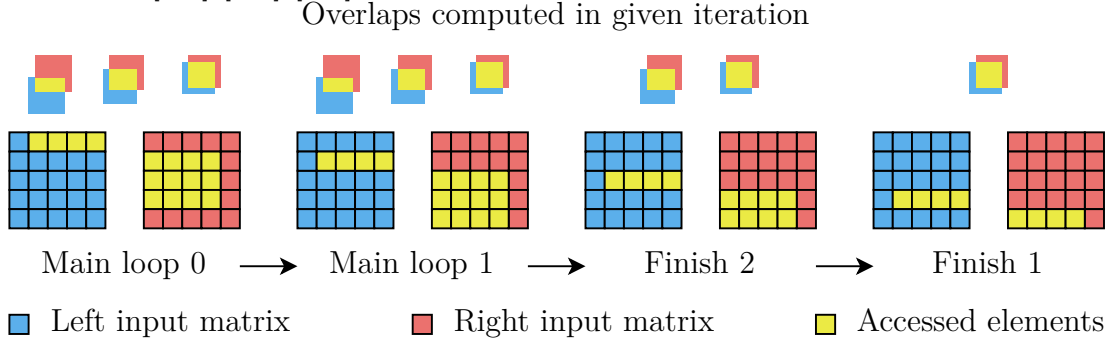
To solve this problem, we split the outermost loop going over the rows of the warp submatrix into three parts. First few iterations are separated into *Init* iterations, which compute only the subset of overlaps which actually require the rows of the warp submatrix as input. Then we have the *Main loop*, which computes all overlaps assigned to the thread. Lastly we have several *Finish* iterations, which again compute only the subset of overlap which require the given warp submatrix row as input. This partitioning is illustrated in Figure 3.17. The number of *Init* and *Finish* steps depends on the exact shift of the overlaps grouped into a job.

Code changes for this implementations are similar to the changes for the *multimat\_right* from Section 3.4.3, again using Local array optimization described in Appendix A. We again compute multiple results in each thread, iterating over multiple rows from a single right matrix where *multimat\_right* loaded the different rows from multiple separate right matrices. The only other major change is the partitioning of the outermost loop as described above. The similarity of the changes is utilized when combining *multirow\_right* and *multimat* optimizations.

One of the disadvantages of this algorithm is the repeated reading of right input matrix rows by each worker. As warp shuffle is already utilized for data reuse in the given row, there is no simple mechanism to reuse data between rows as we traverse the warp submatrix from top to bottom. With 3 overlaps grouped into a job, each row of the right input matrix processed by the main loop is read 3 times by the worker, once for each of the overlaps assigned to the worker. Each



(a) Complete computation of the *multirow\_right* algorithm with *job\_size* 3 for overlaps with shifts  $[1, 1]$ ,  $[1, 2]$ ,  $[1, 3]$  showcasing Init steps.



(b) Complete computation of the *multirow\_right* algorithm with *job\_size* 3 for overlaps with shifts  $[1, -3]$ ,  $[1, -2]$ ,  $[1, -1]$  showcasing Finish steps

Figure 3.17: Illustration of Init and Finish steps of the *multirow\_right* algorithm with overlaps processed in each step displayed above the step.

time, it is used with different left row. This can be improved by also utilizing multiple rows from the left input matrix, computing multiple iterations of the current main loop at once. This implementation, named *multirow\_both* as we read multiple rows in each iteration from both input matrices, is described in Section 3.4.6.

When profiling this optimization, as shown in Figure 3.18, we see similar improvements as with the previous *multimat\_right* optimization. We have to keep in mind that the *multirow\_right* algorithm improves the *one-to-one* type of computation, which cannot be improved by the previous optimization. These two optimizations can also be combined, which is described in Section 3.4.7. As before, the *LSU* pipeline remains a bottleneck, but the utilization of *FMA* pipeline is improved from 9% to 17%. With 4 overlaps per job, the ratio improves from 3 : 1 to 6 : 4 as expected from the  $2+r : r$  theoretical ratio with 227367936 : 150994944 SHFL to FFMA instructions. As this optimization improves the *one-to-one* computation, it is more sensitive to occupancy reduction when workers process more than one overlap, mainly due to the smaller input size compared to the *one-to-many* computation.

### 3.4.5 Multiple left matrices

This optimization is an extension of the *multimat\_right* aiming at the reuse of data from the right input matrix to compute cross-correlation with multiple left input matrices. As we now reuse data from both left and right input matrices,

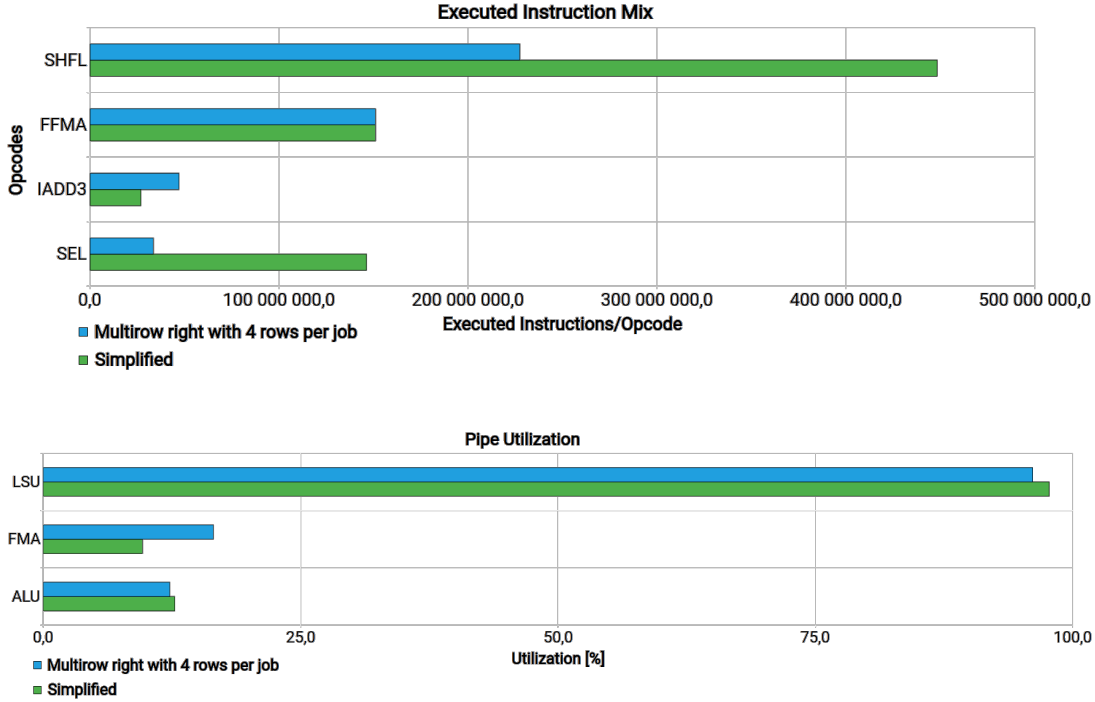


Figure 3.18: Comparison of *one-to-one* simplified algorithm with the *multi-row-right* optimization.

we call this the *multimat\_both* optimization. This optimization is only usable for the *n-to-m* computation type, as the *one-to-one*, *one-to-many*, and *n-to-mn* types correlate each left matrix with a different set of right matrices.

Similarly to the *multimat\_right* optimization, we group overlaps represented by elements at the same index in multiple output matrices into a single job. These overlaps represent the same shift between the input matrices, with each representing an overlap of a different pair of input matrices. Whereas the *multimat\_right* output matrices represented cross-correlation between a single left input matrix and multiple right matrices, with *multimat\_both* the output matrices represent cross-correlations of the *n-to-m* (*all-to-all*) type between multiple left and multiple right matrices, as explained in Section 3.2.1

The implementation of this optimization can be found in the attachments of this thesis as the `ccn_shuffle_n_to_m_multimat_both_work_distribution` kernel. As the name suggests, this optimization can be combined with the *work distribution* optimization. To measure the performance without work distribution, we use the *None* distribution type described in Section 3.4.2.

The changes to the *multimat\_right* optimization code to implement *multimat\_both* again utilize the Local array optimization described in Appendix A, changing the variable representing the left buffer in each thread into an array representing multiple buffers.

Similarly to the *multimat\_right* optimization, we group input matrices into matrix groups, this time separately grouping left matrices into *left\_matrix\_groups* and right matrices into *right\_matrix\_groups*. Each pairing of  $l$  left matrix group with  $r$  right matrix group defines a set of  $l * r$  output matrices due to the *n-to-m* computation type. Elements in column  $x$  and row  $y$  from all of these  $l * r$  matrices



are grouped into a single job, computed by a single thread.

The number of matrices in a left matrix group is configured independently of the number of matrices in a right matrix groups. The maximum size of left matrix group and right matrix group has to be known at compile time so that we can generate the implementing device function for all combinations of these values from 1 to the configured maximum, as the arrays must have a size known at compile time. At run-time, the implementation chooses the correct method. The last matrix groups from both left and right input matrices may be smaller as the number of left or right matrices may not be divisible by the value of the run-time argument. The implementation then chooses the function with the correct matrix group size, which is why we must generate the implementing function for possible matrix group sizes.

For each pairing of left matrix group and right matrix group, we start enough thread blocks to process all jobs defined by this pair of thread groups. Threads of a single thread block process jobs from a single pairing of left matrix group and right matrix group. This again allows us to minimize the required changes to the code of *multimat\_right* optimization when implementing *multimat\_both*.

The *multimat\_both* optimization can be combined with either *work distribution* or *multirow\_right* optimizations. It can also be combined with *multirow\_both* optimization introduced in the following section.

This optimization improves the ratio of warp shuffle (SHFL) to fused multiply-add (FFMA) instructions to  $2 * l + r : l * r$ , where  $l$  is the number of left matrices in the left matrix group and  $r$  the number of right matrices in the right matrix group. This is to be compared to the 3 : 1 ratio of the Simple warp shuffle implementation,  $2 + r : r$  of the *multimat\_right* optimization, and slightly worse than  $2 + r : r$  *multirow\_right* with  $r$  representing number of rows instead of matrices grouped into a single job. As with these previous optimizations, this improvement comes at the cost of parallelism, as all overlaps grouped into a single job would be executed in parallel without this optimization. For larger input matrices and larger numbers of input matrices, this reduction in parallelism is more than compensated by the improved throughput of each thread thanks to the improved instruction ration. For smaller input sizes, the reduction in parallelism can be compensated for by combining this optimization with *work distribution* optimization.

The ratio of SHFL to FFMA instructions is shown in Figure 3.19. The profiling was executed with both matrix group sizes set to 4 on input of 4 left matrices and 16 right matrices of size 256x256 elements. The expected ratio is 12 : 16, which is exactly what we see in the measurements with 7247757312 : 9663676416 SHFL to FFMA instructions. This improved ratio also results in improved utilization of the FMA pipeline, which is now utilized to 31.2% of its maximum throughput. Comparison of the effects on execution time is provided in Section 4.2.

### 3.4.6 Multiple rows from both matrices

When improving the *one-to-one* computation using the *multirow\_right* optimization described in Section 3.4.4, which processes multiple overlaps from consecutive rows of a single column of the output matrix, we hinted at a further improvement

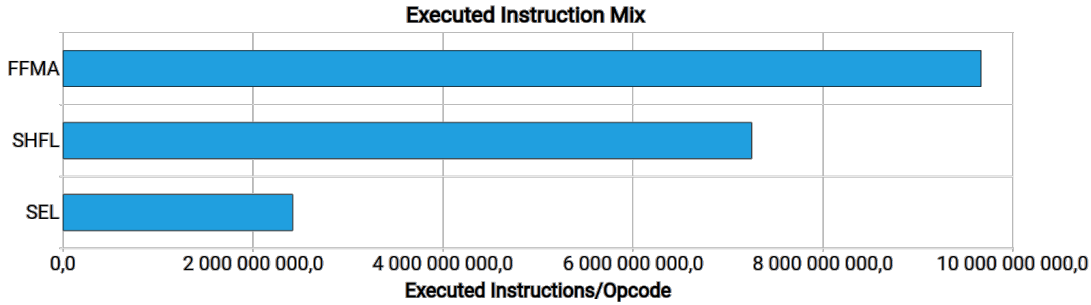


Figure 3.19: Three most often executed instructions by the Warp shuffle algorithm with *multimat\_both* optimization.

using multiple rows from the left matrix in the main loop. This not only improves the ratio of warp shuffle to fused multiply-add instructions, but also reduces the number of times every row from the right input matrix is read.

The main change to the code of *multirow\_right* optimization is that the main loop now advances by multiple left input matrix rows instead of a single row. This new implementation can be found in the attachments of this thesis as the `ccn_shuffle_multirow_both` kernel.

The exact number of left rows to advance by in each iteration is configured by an algorithm argument. An additional stage between this multistep main loop and Finish is also needed to compute the remaining rows from the left input matrix when the total number of left input matrix rows is not divisible by the main loop step. This stage utilizes the original single step main loop. The Init and Finish parts are left unchanged.

The ratio of warp shuffle instructions (SHFL) to fused multiply-add instructions (FFMA) for this optimization is  $l + (o - 1 + l) : l * o$  in the main loop, where  $l$  is the number of left rows processed by each iteration of the main loop and  $o$  is the number of overlaps grouped into a single job. The Init, single step main loop and Finish parts share the original ratio of the *multirow\_right* implementation, which is  $2 + o : o$ . This ratio is also apparent in Figure 3.20. The profiling is done for cross-correlation of two 256x256 matrices with both number of left rows per iteration  $l$  and number of overlaps grouped into a job  $o$  set to 4. The expected ratio of SHFL to FFMA instructions is 11 : 12, which is almost exactly what we see with 140006752 : 150994994 total SHFL to FFMA instructions. This improved ratio also results in additional utilization of the FMA pipeline, which utilizes 23.9% of its total throughput, compared to 10% utilization by the Simple warp shuffle implementation and 17% by *multirow\_right* optimization.

### 3.4.7 Summary

In this section, we have implemented a family of Warp shuffle based implementations with the following optimizations:

- *work distribution* (Section 3.4.2),
- *multimat\_right* (Section 3.4.3),
- *multirow\_right* (Section 3.4.4),

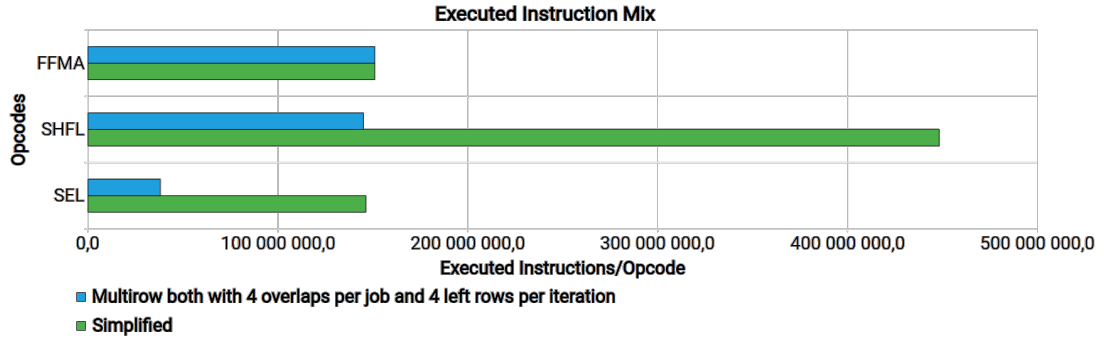


Figure 3.20: Three most often executed instructions by the Warp shuffle algorithm with *multirow\_both* optimization.

- *multimat\_both* (Section 3.4.5),
- *multirow\_both* (Section 3.4.6).

The Warp shuffle family utilizes warp shuffle instructions to reuse data already loaded into registers by multiple threads of a warp, reducing the required number of load operations from global memory. The optimizations then improve occupancy through splitting work into smaller jobs, improve ratio of warp shuffle instructions to fused multiply-add instructions or improve data reuse once loaded into registers.

The *work distribution*, *multimat\_right*, and *multirow\_right* are implemented by improving the Simple warp shuffle implementation. The *multimat\_both* and *multirow\_both* optimizations are implemented as extensions to the *multimat\_right* and *multirow\_right* optimizations respectively.

All of the optimizations listed above can be combined with the following restrictions:

1. *multirow* optimizations cannot be combined with work distribution,
2. *multimat\_both* can only be used to optimize the *n\_to\_m* computation.

With the *multirow* optimization, each job contains several different overlaps of the two input matrices, where each overlap has different number of rows. As our work distribution optimization is based on the number of rows of the overlap, the current implementation cannot be easily reused. This is not a problem with the *multimat* optimizations, in which each thread computes the same overlap in multiple output matrices.

The *n\_to\_m* computation type is the only type where multiple left matrices share the same right matrix, which makes it possible to reuse the data from the left matrices.

With these restrictions in mind, we have implemented the following versions of the warp shuffle algorithm:

- *multimat\_right*,
- *multimat\_right\_work\_distribution*,
- *multimat\_both\_work\_distribution*,

- `multirow_right`,
- `multirow_right_multimat_right`,
- `multirow_both`,
- `multirow_both_multimat_right`,
- `multirow_both_multimat_both`.

Both *multimat* optimizations were already prepared for combination with work distribution, as hinted at in their respective sections. The core computation code does not change, the only difference is that we split the original warp submatrix the same way we did when implementing work distribution for simplified warp shuffle algorithm, described in Section 3.4.2.

Combination of *multimat* and *multirow* optimizations takes the implementation of *multimat* optimization, separates the middle and inner loop as is done to the simplified implementation in the implementation of *multirow* and splits the outer loop iterations into Init, multistep main loop, single step main loop, and Finish parts.

The measurement and comparison of these implementations is presented in Section 4.2.

### 3.5 Warp per shift algorithm family

For small inputs, processing a single overlap or a row group per thread may not split the computation into enough jobs to saturate the whole GPU, leading to low occupancy. As described in Section 2.3.1, low occupancy prevents the full utilization of the throughput of the GPU hardware, while also preventing the GPU from hiding the high latency of each instruction, resulting in poor performance. To increase the number of threads started for smaller inputs, we increase the size of each worker from a single thread to a whole warp. This increase in number of threads in combination with the small input data size leads to a need of balancing the overhead of each thread, which consists mainly of scheduling, repeated data reads, and computation of array indexes for each access, with the reduced workload.

In this section, we first introduce a base implementation of the *warp per shift* algorithm utilizing whole warps as workers with each job containing a single overlap, also called shift. We then introduce several improvements of this algorithm, first by using shared memory and then by further increasing the number of jobs using work distribution optimization

This algorithm family is inspired by Bednárek et al. [2], who also choose to assign their unit of work to larger groups in the CUDA thread hierarchy. The work presents two implementations, first one where each stripe (their unit of work) is processed by a single warp which exchange data through warp shuffle instructions, which inspired our Warp shuffle algorithm family presented in Section 3.4. The warp per shift algorithm family described in this section is based on the second implementation where each strip is processed by a whole thread block with threads exchanging data using shared memory.

In this section, we first introduce a base implementation assigning each element of the output matrix to a separate warp without any cooperation between warps. We then take inspiration from Bednárek et al. [2] and use shared memory to cache input data used by warps of each thread block. We then further increase the number of jobs using work distribution optimization, adapted from the implementation described in Section 3.4.2.

### 3.5.1 Base implementation

Implementation of the *Warp per shift* algorithm is very simple compared to the warp shuffle-based algorithm described in Section 3.4. The basic implementation utilizes whole warps as workers and assigns each worker a job consisting of a single overlap. Each overlap is uniquely identified by the shift of the two input matrices, and the shift is what is stored and propagated throughout the code. This is why we call this the *warp per shift* algorithm family.

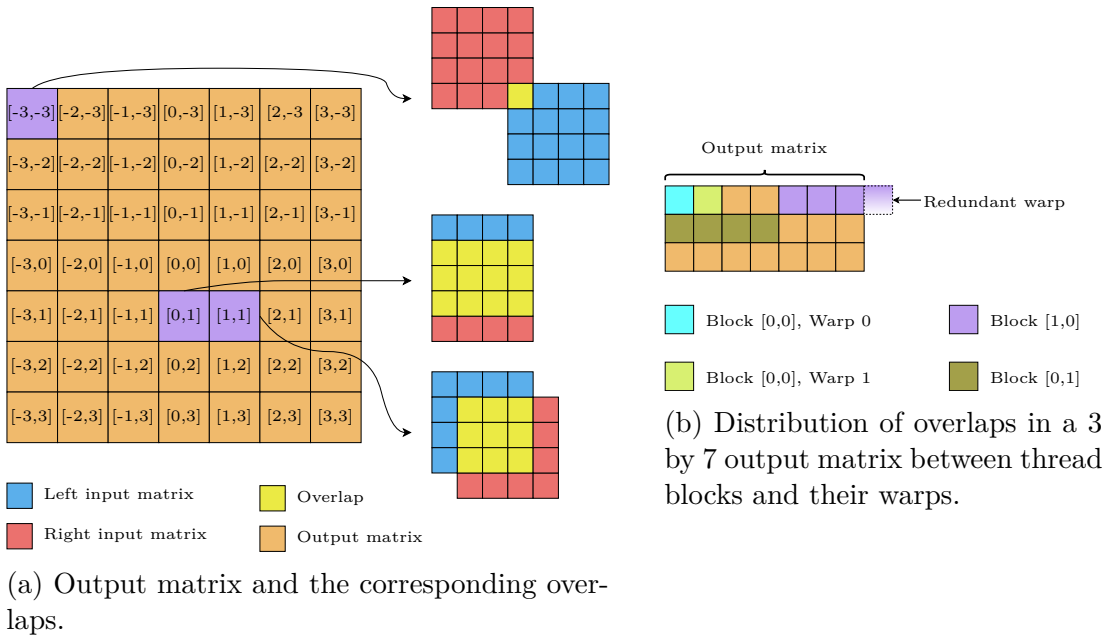


Figure 3.21: Output matrix and its distribution between warps.

As in the Basic cross-correlation algorithm, introduced in Section 3.3, this implementation uses two dimensional grid of two dimensional thread blocks to assign elements of the output matrix to workers. The difference is in how we use each dimension to map threads to overlaps, this time based on which warp and thread block they are part of. All threads of a warp are assigned the same overlap and they cooperate to compute all the tasks (yellow boxes) which belong to this overlap. The mapping from thread blocks and warps to overlaps of the output matrix is illustrated by Figure 3.21b. Warps of each thread block are assigned consecutive overlaps in a row of the output matrix. The number of warps per thread block is configurable by algorithm argument.

Each thread of a warp is assigned subset of the multiplication tasks (yellow boxes), as shown in Figure 3.22, which it computes and holds the sum in local variable. This distribution is done using the code in Listing 3.3, which is a snippet of the kernel `ccn_warp_per_shift` found in thesis attachments.

```

for (
  size_t i = warp.thread_rank();
  i < total_items;
  i += warp.size()
) {
  size_t overlap_row = i / overlap_size.x;
  size_t overlap_row_offset = i % overlap_size.x;

  size_t right_idx = ...;
  size_t left_idx = ...;

  sum += left[left_idx] * right[right_idx];
}

```

Listing 3.3: Main loop of the Base warp per shift implementation

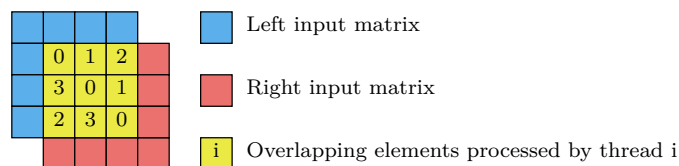


Figure 3.22: Thread computing given task with basic indexing (example warp size 4).

This distribution of tasks minimizes thread divergence but may lead to uncoalesced global memory access. Another possible disadvantage of this implementation is the division and the modulo instruction in each loop iteration, which is used to determine the position in the overlapping submatrix to be computed by the current thread.

The distribution is based on the cooperative distance calculations by Honzátko and Kruliš [4]. In their work, warps of a thread cooperate to compute distance between neighboring overlapping patches of an image. Each thread computes a subset of columns and stores the results to shared memory. After all threads compute their assigned columns, each thread picks the results corresponding to its assigned patch.

Our base warp per shift implementation utilizes slightly easier approach. Instead of assigning columns, the whole overlapping part of the input matrices is serialized in row major order and iterated over using the for loop illustrated above.

The sums computed by each thread of the warp are then combined using the `cooperative_groups::reduce` function, which may even be hardware accelerated if running on the newest Ampere GPUs. The final result is then written by thread with warp rank 0 to the output matrix.

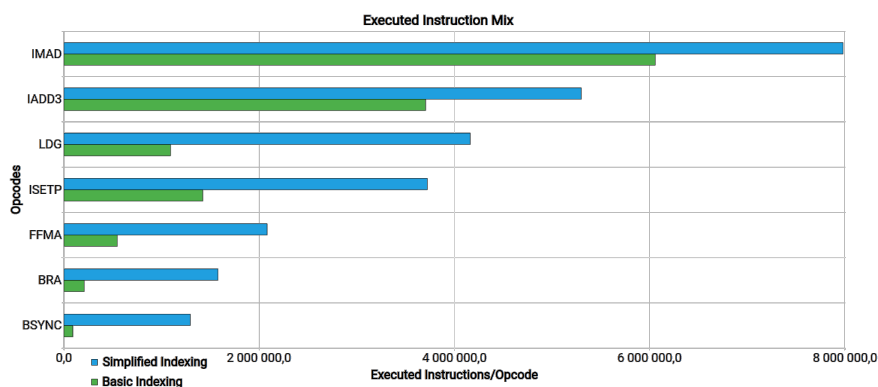
### 3.5.2 Simplified indexing

The Simplified indexing is an attempt to solve the problems highlighted in the previous section, namely the uncoalesced global memory access and the low throughput division instruction in the main loop. To fix these problems, we change the

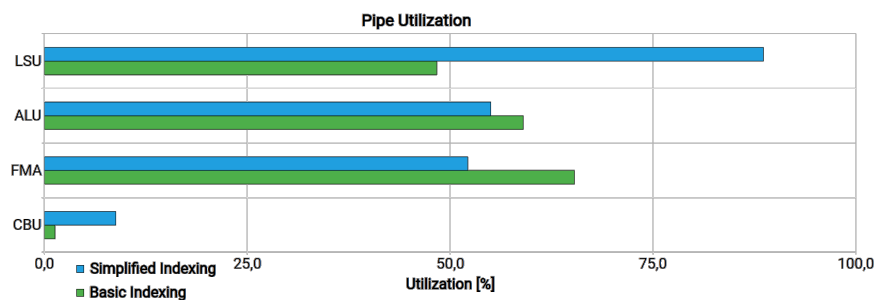


lead to better coalescing of global memory access, the opposite seems to be the case as illustrated by Figure 3.25a. This may be highly dependent on Compute Capability of the underlying hardware, but on CC 7.5 of RTX 2060, we observe a 47% increase in the number of global memory requests when using simplified indexing. This corresponds to high *LSU* pipeline usage of 88% visible in Figure 3.25b, which becomes a bottleneck. The profiling was done on input matrices of size 64 by 64 containing 32bit floating point numbers. In these matrices, each row is 256B long. In many overlaps, the last item of each row will be less than 128B (global memory transaction size) from the first item in the next row. This leads to coalescing of the global memory read with basic indexing but results in 2 separate accesses with simplified indexing, which may explain the 47% difference in global memory requests.

Another visible difference in Figure 3.25a is the increase in number of instructions across the board, most visible with branching (BRA) and barrier synchronization (BSYNC) instructions. This is caused by the increase in number of iterations each warp executes to process the same data. Even with the increase in number of instructions, the *ALU* and *FMA* pipelines are less utilized than with basic indexing. This is caused by warps waiting for warp recombination on the barrier synchronization points and loads from global memory.



(a) Executed instruction mix.



(b) Pipeline utilization.

Figure 3.25: Comparison of basic and simplified indexing.

The effects of different pipeline utilization can also be seen in Figure 3.26. Warps of basic indexing algorithm are mostly stalled due to not being selected, i.e. there are multiple eligible warps and only one of them can be issued. This indicates that there may be too many warps for the size of the GPU. As these benchmarks were run on a RTX 2060 mobile, which is a rather small GPU, this



was to be expected. The other main reason of warp stall is **Stall Math Pipe Throttle**, which is caused by the high utilization of *ALU* and *FMA* pipelines. These pipelines are responsible for computing the indices and the actual results of cross-correlation, which represents the useful work done by the GPU.

Simple indexing warps on the other hand are more often stalled on the **Stall Wait**, which represents warps waiting for a fixed latency execution dependency, i.e. a data dependency between two instructions or an instruction dependency on predicate computation. We can also see noticeable increase in stalls due to access to global memory (**Stall Long Scoreboard** and **Stall LG Throttle**) together with stalls due to branching. This is consistent with the properties of simple indexing described above.

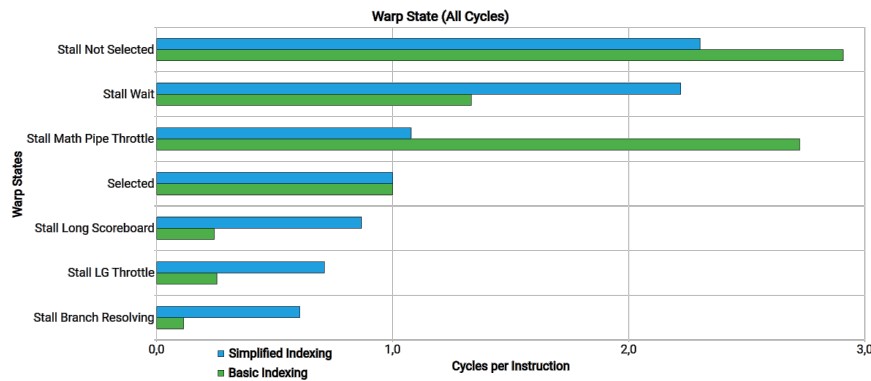


Figure 3.26: Comparison of warp stall reasons between the basic and simplified indexing.

### 3.5.3 Shared memory

This optimization of the Base warp per shift implementation is based on the work by Tomiyama and Suda [14], who evaluate the impact of global memory access, occupancy and other parameters on execution time of a CUDA implementation of Levenshtein edit distance. Their implementation loads input data into shared memory to reduce the number of accesses to global memory, which is exactly what we want to achieve here.

We also take inspiration from the warp shuffle algorithm and its *multirow* optimization. Instead of sharing input values by shuffling and broadcasting across threads of a warp, we load input values into shared memory and reuse them by all warps of the thread block.

Similarly to the warp shuffle algorithm, we utilize two alternating parts forming a ring buffer for data from the left input matrix and a single buffer for data from the right input matrix. Compared to the warp shuffle algorithm, the buffers are placed in the shared memory and are shared by all warps of each thread block. The data is not shuffled across threads as was done by warp shuffle, instead staying in place until overwritten by next load of the buffer, with each warp accessing the subset of the buffer it requires. The windows of the input data loaded into buffers are not moved along the rows of the input matrices, but along a group of columns from top to bottom, processing the whole columns group before moving onto the next column group, as shown in Figure 3.27a. This access pattern is

based on the work of Honzátko and Kruliš [4], who access the columns between overlapping patches in similar way.

With appropriately sized column groups, this enables us to maximize the throughput when loading data from global memory using coalesced loads. The appropriate size here is a multiple of 32, i.e., warp size. We call the variable holding the width of the column group the *shared\_mem\_row\_size*, as it also determines the size of each row of the shared memory buffers. The number of rows in each of the three shared memory buffers (two for data from the left matrix and one for data from the right matrix) is a run-time algorithm argument and stored in variable *shared\_mem\_num\_rows*. Another reason we choose column groups instead of row groups is because of the way we assign overlaps to warps of a thread block. To prevent bank conflicts when accessing shared memory, we assign consecutive overlaps from a single column of the output matrix to the warps of a single thread block. This is explained in more detail further in this section.

As warp shuffle algorithm had warp submatrix, i.e. submatrix of each of the input matrices containing elements required by any of the threads of the given warp, this algorithm computes thread block submatrix containing elements of the input matrices required by overlaps assigned to any of the warps of the given thread block. This thread block submatrix is what we partition into column groups and what we iterate over and load into the shared memory buffers.

The implementation is again made up of three nested for loops, which can be found in the attachments of this thesis as the `ccn.warp_per_shift_shared_mem` kernel. The outer loop iterates over column groups while the middle loop iterates over rows of the column group in *shared\_mem\_num\_rows* sized steps. These loops are shown in Listing 3.4. Threads of the whole thread block go through these two loops synchronously to allow cooperation when loading data to the shared memory buffers.

When loading the bottom part of the left shared memory buffer in the outer loop, we need to limit which rows are loaded to the buffer and offset the loaded rows, as shown in Figure 3.27a. If we were to just load the full buffer as shown in Figure 3.27b, we would encounter a situation where rows loaded in the second iteration of the middle loop into the right buffer overlap rows which were loaded during the first load of bottom left buffer, which at that point is already overwritten.

In each iteration, we compute the rows in the right buffer which overlap with rows in the given part of the left buffer in the overlap assigned to the current warp. The reason we have two parts of the left buffer is that different warps of a thread block will be computing different overlaps, as shown in the right column in Figure 3.27a. For  $r$  rows loaded into right buffer,  $w$  warps of a thread block will access  $r + w - 1$  different rows from the left buffer based on the shift each warp is computing. The  $w - 1$  rows will then be accessed by different warps in the following iteration as they compute shifts which overlap these rows of the left input matrix with rows of the right input matrix loaded into the right buffer in the following iteration.

This innermost loop, shown in Listing 3.5, iterates over the rows from the two shared memory buffers which are overlapped in the overlap assigned to the current warp. Shared memory accesses in this loop are without bank conflicts thanks to way we assign overlaps between warps of a thread block. If we were

```

T thread_sum = 0;
for (
    size_t column_group_start_x = block_matrix_start.x;
    column_group_start_x < block_matrix_end.x;
    column_group_start_x += shared_mem_row_size
) {
    // Bottom part of the left shared memory buffer
    left_bottom_s.load_submatrix(...);

    for (
        size_t right_buffer_start_row = block_matrix_start.y;
        right_buffer_start_row < block_matrix_end.y;
        right_buffer_start_row += shared_mem_num_rows
    ) {
        left_top_s.load_submatrix(...);
        right_s.load_submatrix(...);

        __syncthreads();
        compute_from_shared_mem_buffers(left_bottom_s, right_s, ...);
        compute_from_shared_mem_buffers(left_top_s, right_s, ...);
        swap(left_bottom_s, left_top_s);
        __syncthreads();
    }
}

```

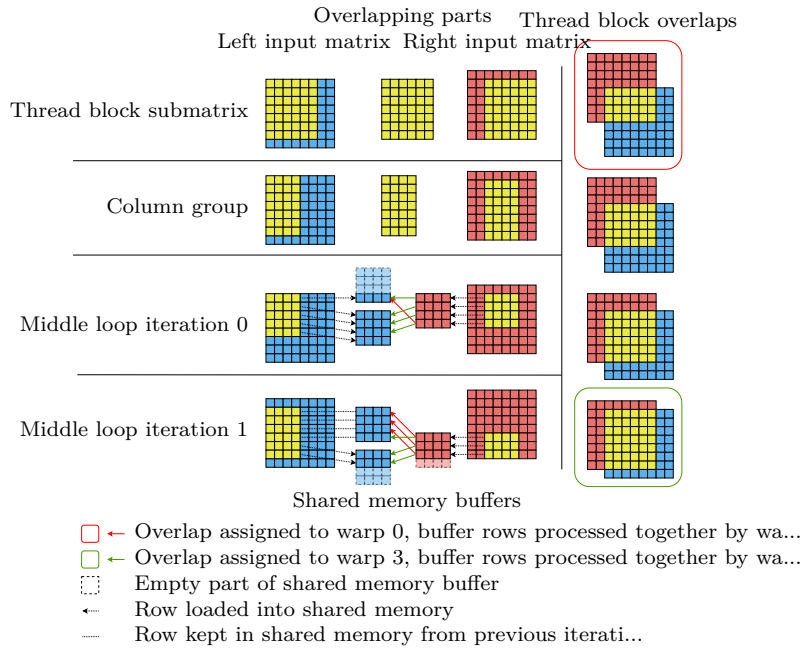
Listing 3.4: Outer and middle loop of the Warp per shift with shared memory optimizations

```

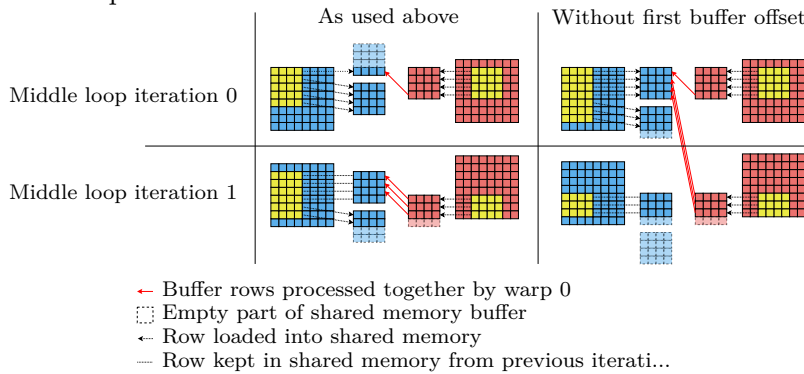
__device__ void compute_from_shared_mem_buffers(...) {
    // Offset in shared memory buffer
    int warp_right_start_offset = ...;
    int warp_right_end_offset = ...;
    // Offset between buffers
    int buffer_offset = ...;
    for (
        int right_idx = warp_right_start_offset + warp.thread_rank();
        right_idx < warp_right_end_offset;
        right_idx += warp.size()
    ) {
        l = left_buffer[right_idx + buffer_offset];
        r = right_buffer[right_idx];
        thread_sum += l * r;
    }
}

```

Listing 3.5: Inner loop of the Warp per shift with shared memory optimizations accessing the shared memory buffers



(a) Computation of a single column group showcasing different warp offsets and left bottom buffer preload offset.



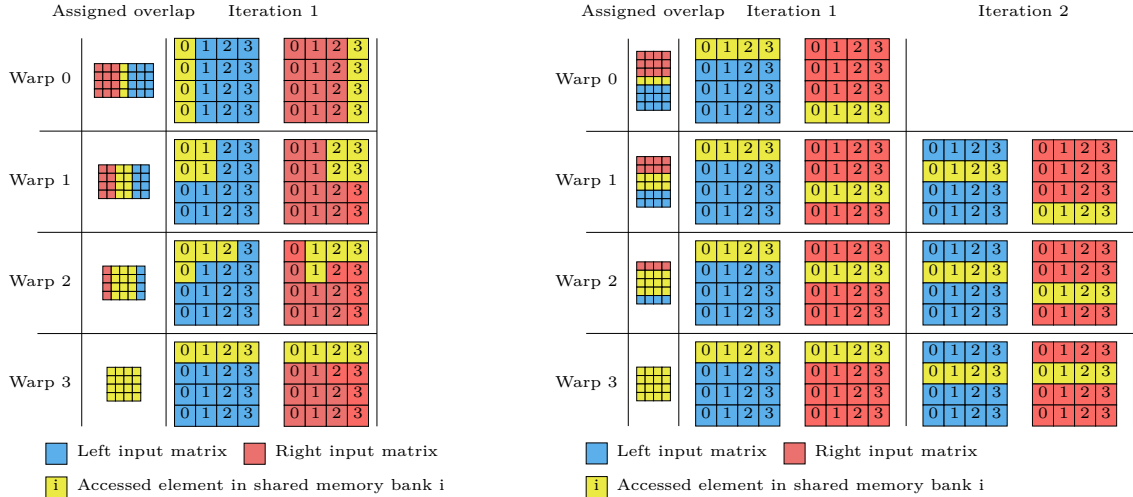
(b) Cross-iteration dependency when the bottom part of the left buffer is not loaded with an offset during the first load.

Figure 3.27: Processing of a column group by the Warp per shift algorithm with shared memory optimization.

to assign overlaps from a single row of the output matrix to warps of a thread block, as is done by the basic implementation of *warp per shift* algorithm, we would encounter a problem illustrated in Figure 3.28a. For the purposes of this example, we work with warps of 4 threads, shared memory with 4 banks and assume each input matrix fits into one shared memory buffer. The figure shows the left and right input matrix and how their elements map into banks of shared memory when loaded by the thread block. For simplicity, we have chosen a thread block whose thread block submatrix contains whole input matrices as one of the overlaps computed by the thread block is the overlap with shift  $[0, 0]$ . When warps of a given thread block are assigned overlaps along a row of the output matrix, the overlaps differ in the number of columns. This leads to an access pattern with different stride in each warp. The strides for warps 1 and 2 result in 2-way bank conflicts, the stride for warp 0 results in 4-way bank conflict. With

32 threads per warp, this type of access would cause up to 32-way bank conflict, which would severely limit the shared memory throughput.

Due to this, we choose to assign overlaps from a single column to warps of a thread block. This assignment leads to access illustrated in Figure 3.28b. This figure depicts two iterations of the innermost loop, with the same simplifications as the previous figure. As the overlaps differ in the number of rows, not columns, the access to shared memory has different starting and ending offset, but between these the access is perfectly linear and coalesced, each thread accessing different bank. Left buffer is accessed independently of the right buffer, so sharing banks between these buffers does not lead to bank conflicts.



(a) Iteration 1 when job contains overlaps from a row of the output matrix.

(b) The first two iterations when job contains overlaps from a column of the output matrix.

Figure 3.28: Input matrices with numbers designating their mapping to shared memory banks and how they are accessed by 4 different warps of a single thread block.

Even with the throughput of shared memory, the load from shared memory *LDS* instructions become a bottleneck, as shown in Figure 3.29. The memory input/output stall is caused by the memory input/output queue being full. This queue handles special math instructions, dynamic branches and most importantly for us the shared memory access instructions. Even with this bottleneck, the reduction in number of global memory accesses allows the warp per shift algorithm with shared memory optimization to be usable even for larger inputs, as will be shown in Section 4.2.

### 3.5.4 Shared memory with multiple right matrices

Similarly to the warp shuffle algorithm, we can increase the ratio of arithmetic instructions to shared memory loads by computing the same shift between a single left matrix and multiple right matrices. This improvement of the shared memory optimization is limited by the size of shared memory, as we need to fit multiple right shared memory buffers described in the previous section into shared memory at once. The code changes are very similar to the warp shuffle changes.

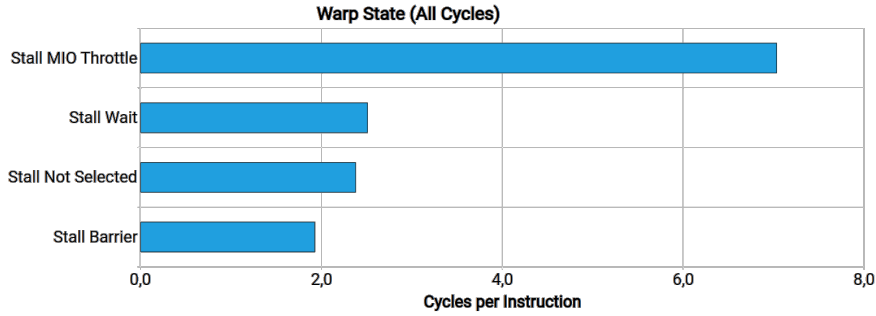


Figure 3.29: Memory input/output (MIO) stall caused by excessive shared memory access.

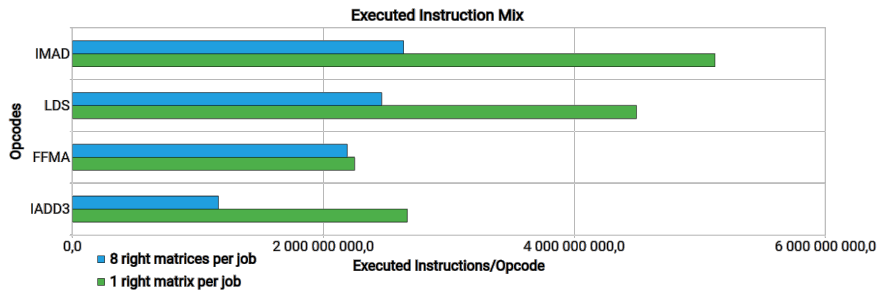
We again utilize the Local array optimization described in Appendix A, caching data in registers for reuse. We are computing overlaps with the same shift from different output matrices, as is done by the *multimat\_right* optimization of the Warp shuffle family in Section 3.4.3. Thanks to the same shift of all overlaps computed by given worker, any loop bounds computed hold for all the overlaps.

The effects of this optimization are shown in Figure 3.30. The profiling shows the difference between running the original shared memory optimization and running the shared memory optimization computing overlaps from multiple matrices at once. The profiling was done on  $256 \times 256$  matrices, with one left input matrix and 16 right input matrices. The original shared memory optimization computes one overlap per warp, whereas the optimized version was run computing overlaps from eight matrices at once. The total number of shared memory load instructions (LDS) and memory access index computations using the integer multiply-add (IMAD) is significantly reduced, as the data from the left matrix once loaded into register is reused with data from eight right input matrices. Even with this reduction in the number of LDS instructions, the utilization of the *LSU* pipeline is still a bottleneck, most likely due to the reduced throughput of shared memory in the Compute Capability 7.5 we use for profiling. The higher utilization of *FMA* pipeline hints at better performance, which will be shown in Section 4.2.5.

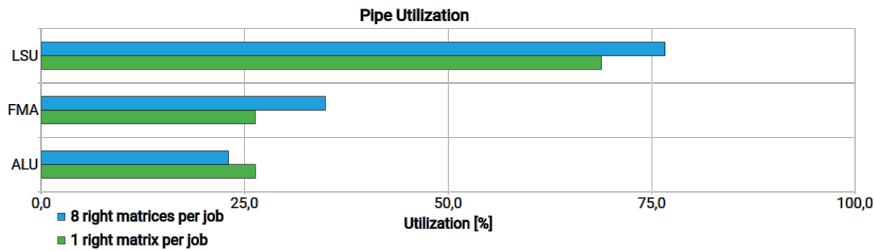
### 3.5.5 Shared memory with single column group per block

As described in Section 3.5.3, the thread block matrix is split into column groups. Each of these column groups can be processed independently, with the partial result added to the final result using *atomicAdd* instruction as was done for the Work distribution optimization of the Warp shuffle algorithm family, introduced in Section 3.4.2. This improves the occupancy of the Warp per shift with shared memory optimization, possibly offsetting the reduced occupancy caused by overlaps from multiple overlaps grouped into each job introduced in Section 3.5.4. The optimization further borrows from the rectangle work distribution, first computing the maximum number of column groups  $m$  any overlap can be split into, and then starting  $m$  workers for each overlap. As  $m$  is the maximum number of column groups an overlap can be split into, most overlaps will be split into fewer column groups.

This change should allow for additional parallelization as each column group



(a) Executed instructions.



(b) Pipeline utilization.

Figure 3.30: Profiling of the effects of multiple right matrices on shared memory optimization.

is processed independently. The only change in terms of code of the CUDA kernel is the different computation of loop bounds and final store of the result using *atomicAdd*, otherwise the code of the original implementation of the shared memory optimization can be reused without any changes. The effects of this change are evaluated in Section 4.2.5.

### 3.5.6 Work distribution

As described in Section 3.4.2 with the warp shuffle algorithm, there are massive differences between work done by different workers in the basic algorithm. This optimization can only be applied to the base Warp per shift algorithm, as the use of Column groups by the shared memory optimization cannot be combined with Row groups used with work distribution. The implementation shares much of the code with the warp shuffle algorithm, only difference being the size of workers. We can choose from the `triangle` or `rectangle` distributions and set the maximum number of rows processed by a worker. The code of this optimization can be found in the attachments as the `ccn_warp_per_shift_work_distribution` kernel.

This optimizations improves occupancy, further improving the main benefit of the Warp per shift family of algorithms. As described above, it also improves load balancing by reducing the differences between workloads of different workers. The disadvantage of this optimization is the reduced workload of each worker, which has to be balanced with the overhead of each worker such as scheduling, index calculations, atomic instructions to combine results from multiple workers etc. The optimization should provide improvements until the GPU is saturated. Additionally, without the use of shared memory described in Section 3.5.3, the added strain onto global memory due to no data reuse between workers limits the performance of this optimization.

## 3.6 Further increasing worker size

Another possible way to further increase occupancy is to switch from warps as workers to whole thread blocks as workers. This can massively increase the number of threads started for given size of input, saturating the GPU even for smaller inputs. This optimization is again inspired by the work of Bednárek et al. [2], who assign stride, which is their unit of work, to be processed by a whole thread block. In our case, the implementation is rather simple. The thread block index directly maps to the position in the output matrix and consequently to the overlap computed by given thread block. This is why we call this the *Block per shift* optimization. We then compute the bounds of the overlapping submatrix and iterate over the overlapping elements using block stride loop. We then utilize `reduce` function provided by Cooperative Groups API to sum results in each warp, which are then stored into shared memory and reduced again by warp [9]. The final result is then stored into the output matrix.

This implementation should further improve occupancy, but at the cost of lower workload per thread, unbalanced workloads between workers and no data reuse. Based on our measurements presented in Section 4.2.5, this implementation does not improve run time over the Base warp per shift algorithm even for small input matrices. This is most likely caused by the simple warp per shift algorithm already saturating the GPU. Even for more powerful GPUs, the improved occupancy does not offset the problems listed above.

### 3.6.1 Summary

In this section, we have introduced the Warp per shift algorithm family and presented the following optimizations of this family:

- simplified indexing (Section 3.5.2),
- shared memory (Section 3.5.3),
- shared memory with multiple right matrices (Section 3.5.4),
- shared memory with column group per worker (Section 3.5.5),
- work distribution (Section 3.5.6).

The Warp per shift algorithm increases the worker size, utilizing whole warp to compute each job. The main goal of this family is to improve occupancy, saturating the GPU and utilizing its full throughput even for smaller inputs. The optimizations listed above then try to reduce overhead of the code caused by array indexing, introduce data reuse by loading data into shared memory and using them from multiple workers or further improve occupancy.

Using these optimizations, we have implemented the following versions of the Warp per shift algorithm:

- base Warp per shift,
- Warp per shift with work distribution,
- Warp per shift with shared memory (combining all three optimizations).



We have also introduced one additional algorithm further optimizing for occupancy, the *Block per shift* algorithm. Measurements and comparison of these algorithms and their implementations is presented in Section 4.2.5.



# 4. Results

In this chapter, we first describe our setup for measurement and validation of the implementations described in the previous chapter. We then compare the definition-based cross-correlation implementations against each other before comparing them with an FFT-based CUDA implementation. Finally, we compare the definition-based implementations with existing real-world cross-correlation implementations in the Python SciPy library and in Matlab.

## 4.1 Experiments

As the main aim of this thesis is to compare implementations of an algorithm, the code is heavily instrumented to enable measurements and comparisons of different parts of the implementation. This instrumentation is designed to limit its impact and to allow measurements that minimize background noise and imprecision of the time measurement tools provided by the CUDA C++ language.

As part of this thesis, we have also developed a benchmarking tool that allows the use of a declarative description of the set of benchmarks to be executed. The tool generates input and validation data, runs the benchmarks for all inputs and with all argument combinations specified, and records the times and validation results. As such, the tool is used both for measurements and for validation of the implementation.

To simplify the implementation of the definition-based algorithm optimizations, we have placed several restrictions on the input matrices and the computation:

- both input matrices are of the same size,
- whole output matrix is computed.

Both restrictions are used to simplify the implementation and reduce the number of variables when measuring. Both restrictions could be removed in production-grade implementation but would make the optimizations unnecessarily harder to implement.

### 4.1.1 Code instrumentation

All implementations, including definition-based, FFT-based, and CPU-based, are split into the following steps:

- *Load* loads the input matrices into host memory,
- *Prepare* allocates device memory and precomputes things derived from the input data size,
- *Transfer* moves data from host to device memory,
- *Run* executes the computation,
- *Finalize* moves data from device to host memory,

- *Free* releases resources allocated in the *Prepare* step,
- *Store* stores results from host memory.

Each of these steps can be individually measured and compared. The main focus of this thesis is the *Run* step, but to properly compare the behavior of the FFT-based implementations with definition-based implementations, we will have to compare other steps as well.

We also provide simple CPU-based single-threaded definition-based implementation, for which most of these steps are empty. This implementation is provided for the basic validation of results and of the benchmarking infrastructure.

The code instrumentation allows us to measure the algorithms with three different levels of granularity:

- *Compute* measuring the duration of the Prepare, Transfer, Run, Finalize, and Free steps together;
- *CommonSteps* measuring every step separately;
- *Algorithm* measuring algorithm-specific parts such as individual kernels or library calls.

For parts that can be executed repeatedly, such as computations and data transfers, we utilize measurement with an adaptive iteration count. The number of iterations is automatically increased until the measured duration is longer than a configured minimum, most often a second. This type of measurement should mitigate background noise and get around problems with minimum clock resolution for very short steps. It is used for the *Compute* measurement, for measuring the *Run* step, and for measuring kernel and function call durations in each algorithm.

For timing the SciPy implementation, we use the `perf_counter_ns` function provided by the Python standard library. For Matlab, the pair of functions named `tic` and `toc` is used to measure the execution time. For both implementations, we also utilize the adaptive iteration count. For both, we measure with only the *Compute* granularity.

### 4.1.2 Experiment setup

Experiments were run on two systems:

- Intel Xeon Silver 4110 with 256GB of RAM and NVIDIA Tesla V100 PCIe 16 GB (gpulab), running Rocky Linux 8.5, gcc 11.2, CUDA 11.6, and nvidia driver 510.47.03;
- AMD Ryzen 5 4600H with 16GB of RAM and NVIDIA GeForce RTX 2060 (laptop), running Ubuntu 20.04, gcc 9.4.0, CUDA 11.4, and nvidia driver 470.129.06.

The two systems allow us to evaluate our implementations on two different classes of GPU hardware, gpulab representing the enterprise server systems with

Tesla GPU and Xeon CPU, and laptop representing consumer hardware with gaming GeForce card and Ryzen CPU. The two systems also allow us to compare two different GPU generations, Compute Capability 7.0 for the V100 and Compute capability 7.5 for the RTX 2060. Unless stated otherwise, the results showcased in this text are measured on gpulab. Laptop results will be added only when the behavior significantly differs from that of gpulab, as the algorithms are in no way optimized for any of the two cards and should run similarly in both cases.

Most showcased results are collected using the adaptive iteration count. The timing is done using CUDA events when measuring the run time of CUDA kernels or the high-resolution clock provided by the C++ standard library for all other measurements. The resulting value shown is the total measured time divided by the number of iterations. To further remove noise, all measurements are repeated 20 times, and the mean of these measurements is taken as the final result, as there are no significant outliers that would skew the mean.

### 4.1.3 Result validation

When validating the results of a computation, we compare them to valid results computed using SciPy, Matlab, or our simple CPU definition-based implementation. The output matrix is compared element by element with the valid result, computing a matrix of differences using formula 4.1 [20].

$$\text{Relative\_difference}(a, b) = \frac{|a - b|}{\max(|a|, |b|)} \quad (4.1)$$

The maximum element in the matrix of differences is then taken as the error of the output matrix.

## 4.2 Comparing definition-based algorithms

In this section, we first measure and compare the members of the Warp shuffle algorithm family, described in Section 3.4, against each other. Next, we compare the members of the Warp per shift algorithm family, introduced in Section 3.5. Lastly, we compare the best optimizations from both algorithm families with the Basic definition-based implementation.

Each of the *one-to-one*, *one-to-many*, *n-to-mn*, and *n-to-m* input types is compared separately, as it allows for different optimizations and may benefit certain implementations better than others. In the following sections, we list and use only the best-performing arguments for each implementation. The benchmarks measuring behavior with different argument values which were used to choose these optimal arguments are available in the thesis attachments in the directory `code/benchmarking/args_test`. The results were left out of the text of the thesis for brevity, as they closely follow the descriptions of each optimization.

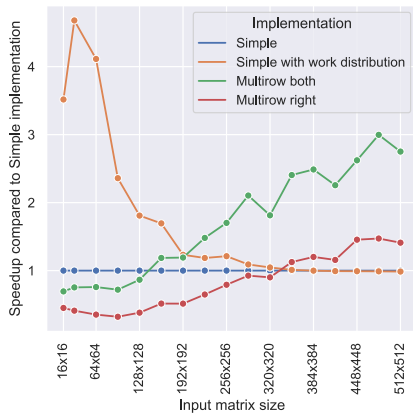
When comparing the definition-based algorithms, we measure only the kernels in the *Run* step, as the implementation of this step is the only difference between the algorithms. As such, the speedup reported in this section represents only the change in execution time of the *Run* step, i.e., the computation itself, not including allocations, loading from disk, transfers to GPU, etc.

Implementations utilizing warp shuffle instructions are usable across a range of input sizes. We measure their behavior for input matrix sizes ranging from 16x16 to 512x512 elements. These input matrix sizes were chosen as the larger input sizes are faster computed using the FFT-based implementation, and as such the speed of the optimizations of the definition-based implementation is irrelevant for the larger sizes. Based on the input type, we also measure with a different number of left and right input matrices to gauge the changes in the behavior of the implementations with a changing number of input matrices.

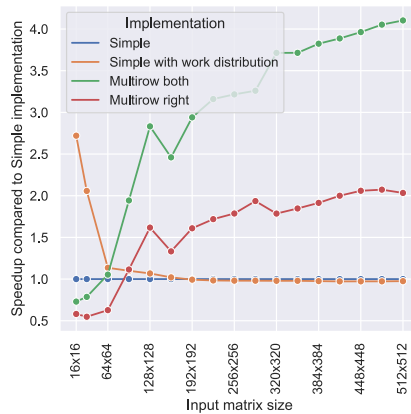
### 4.2.1 Warp shuffle optimizations with the one-to-one input

For this input type, we have the following four implementations with these arguments:

Implementation	Argument	Value
Simple	Warps per thread block	4
Simple with work distribution	Warps per thread block	8
	Rows per thread	1
	Distribution type	triangle
Multirow right	Warps per thread block	4
	Right rows per thread	8
Multirow both	Warps per thread block	4
	Shifts per thread	8
	Left rows per iteration	4



(a) gpulab



(b) laptop

Figure 4.1: Speedup of *one-to-one* warp shuffle optimizations.

The results displayed in Figure 4.1 show the speedup of each optimization compared to the Simple warp shuffle implementation. For smaller inputs on gpulab, the *multirow* optimizations are slower, up to 31% slower for the *multirow\_both* and up to 68% slower for the *multirow\_right* than the Simple implementation. This slowdown is caused by the reduction in the number of threads and correspondingly reduced occupancy of the GPU. Due to the smaller size of the laptop GPU,

the reduced number of threads has a much lower effect. For *multirow\_right*, this is combined with each thread reading each row of the right input matrix multiple times, adding global memory access latency, which the GPU is unable to hide due to the low occupancy. This problem is mitigated in the *multirow\_both* optimization, which is reflected here in better performance for all input sizes when compared with the *multirow\_right* optimization. For larger input sizes, the better ratio of warp shuffle to fused multiply-add instructions of these two optimizations allows them to overtake the Simple implementation. This is above 128x128 for *multirow\_both* and above 320x320 for *multirow\_right* on gpublab. For laptop, the lower performance of the GPU increases the effect of the optimizations, overtaking the Simple implementation sooner.

The behavior of work distribution optimization tells us that the gpublab GPU is not fully saturated by the Simple implementation up until the 320x320 input matrix size. Again due to the smaller size of the laptop GPU, it is saturated much sooner. Low occupancy is an expected problem with the *one-to-one* input type. On gpublab for inputs smaller than 320x320, the large number of additional threads allows us to fully utilize the GPU, making the work distribution optimization more than four times faster than the Simple implementation without work distribution for certain input matrix sizes. As we increase the input size, the benefit of additional threads diminishes, completely disappearing above 320x320 input size, where the overhead introduced by the additional threads negates the increased GPU saturation.

The maximum absolute time improvement is for the 512x512 input size, improving from 67.18 ms to 24.08 ms on gpublab and from 303 ms to 72 ms on laptop.

#### 4.2.2 Warp shuffle optimizations with the one-to-many input

This input type has six implementations with the following arguments:

Implementation	Argument	Value
Simple	Warps per thread block	4
Multimat right	Warps per thread block	4
	Right matrices per thread	8
Multimat right with work distribution	Warps per thread block	8
	Right matrices per thread	8
	Rows per thread	1
	Distribution type	triangle
Multirow right multimat right	Warps per thread block	4
	Right rows per thread	2
	Right matrices per thread	4
Multirow both multimat right	Warps per thread block	4
	Shifts per right matrix	4
	Right matrices per thread	4
	Left rows per iteration	4

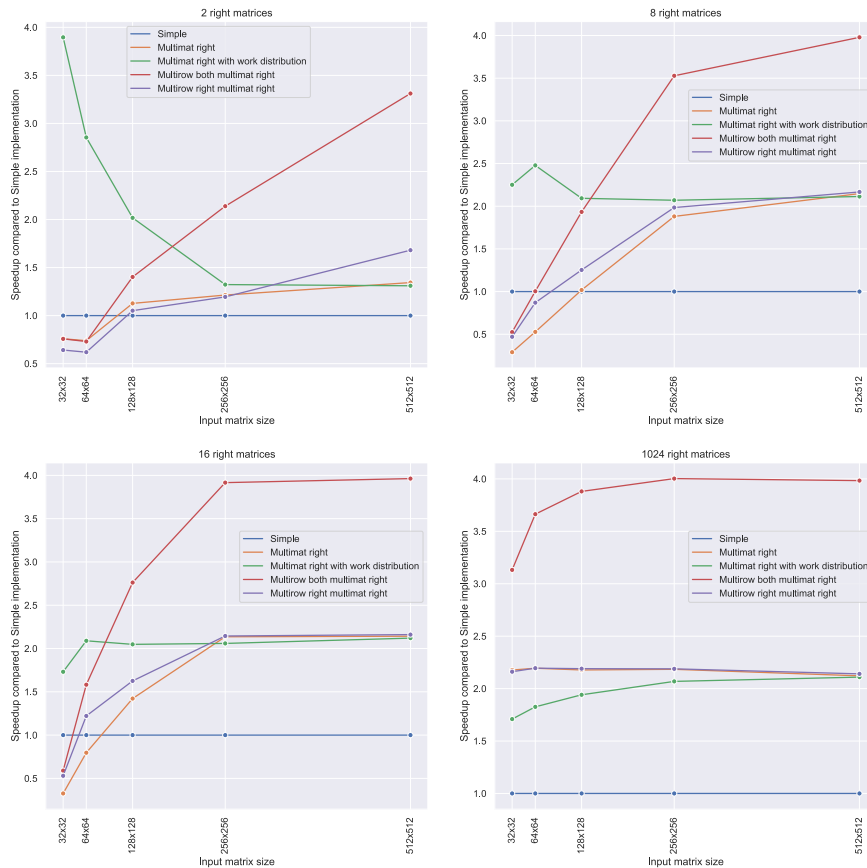


Figure 4.2: Speedup of *one-to-many* warp shuffle optimizations on gpublab.

From the results in Figure 4.2, we see that most optimizations are more than 50% slower than the Simple implementation for small input sizes and small numbers of matrices. This is caused by lower occupancy of the GPU, as both *multimat* and *multirow* group multiple overlaps into each job, reducing the total number of jobs and decreasing the total number of workers. The exception is *Multimat right with work distribution*, where the *work distribution* optimization is specifically designed to solve the problem of low occupancy by splitting each overlap into several jobs. This results in the 4 times speedup we see for the input 32x32 with two right input matrices. However, with increasing total input size, be it the size of each matrix or the total number of matrices, the need to increase occupancy diminishes, and the speedup provided by *work distribution* is lower.

For larger input sizes, the improved ratio of warp shuffle instructions to fused multiply-add instructions balances out the decreased occupancy. The combination of *multimat right* and *multirow right* is slightly better than the *multimat right* optimization alone but is hampered by the increased number of reads from global memory as each row from the right input matrix is reread two times by each worker. This is also the reason why the argument *right rows per thread* is best when set to 2, as increasing the value of this argument increases the number of times each row is read by the given worker. This is the reason why for larger inputs, the *multimat right* and its combination with *multirow right* provide similar speedup, as any improvement of the instruction ratio is balanced by the increased number of reads.



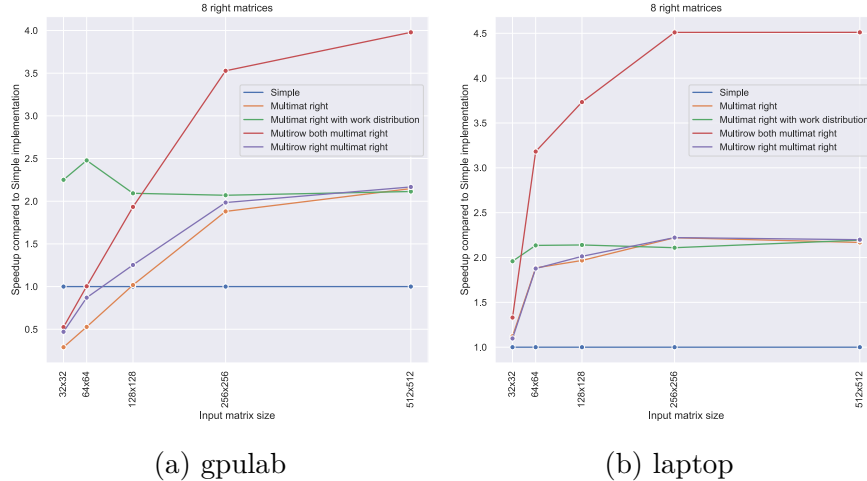


Figure 4.3: Comparison of the input with 8 right matrices on gpulab and laptop.

The best improvement for the input sizes we are interested in is provided by the combination of *multimat right* with *multirow both*. This combination removes the disadvantage of multiple reads of the *multirow right*, leaving just the improved instruction ratio.

When we compare behavior on gpulab and laptop in Figure 4.3, we see that the change is very similar to the one shown in Section 4.2.1. The optimizations improving occupancy are not as effective, while the optimizations reducing the number of warp shuffle instructions and global memory accesses significantly improve the performance. The measurement in Figure 4.3b, computing input with 8 right matrices, are very similar to the results from Figure 4.2 with 16 input matrices, i.e., with twice the input data size. This shows the effects of the lower performance and smaller size of the GPU.

The maximum absolute improvement is for the  $512 \times 512$  matrix size with 1024 right matrices, where we see a decrease from 67 s to 16.8 s on gpulab and from 308 s to 67 s on laptop.

### 4.2.3 Warp shuffle optimizations with the n-to-mn input

This input type shares implementations with the *one-to-many* type, as it does not provide any additional possibilities for data reuse because each left input matrix is cross-correlated with a different set of  $m$  right input matrices. This means that each implementation of *n-to-mn* type just executes the *one-to-many* implementation kernel  $n$  times in parallel, once for each left input matrix. Due to this, the main factor here is how many of the *one-to-many* kernels can we run in parallel, or more precisely, how many thread blocks from these kernels can fit on a single SM.

The arguments differ slightly due to the higher GPU utilization:

Implementation	Argument	Value
Simple	Warps per thread block	4
	Warps per thread block	4
Simple with work distribution	Rows per thread	1
	Distribution type	triangle
Multimat right	Warps per thread block	4
	Right matrices per thread	8
Multimat right with work distribution	Warps per thread block	4
	Right matrices per thread	8
	Rows per thread	1
Multirow right multimat right	Warps per thread block	4
	Right rows per thread	2
	Right matrices per thread	4
	Number of CUDA streams	16
Multirow both multimat right	Warps per thread block	4
	Shifts per right matrix	4
	Right matrices per thread	4
	Left rows per iteration	4
	Number of CUDA streams	16

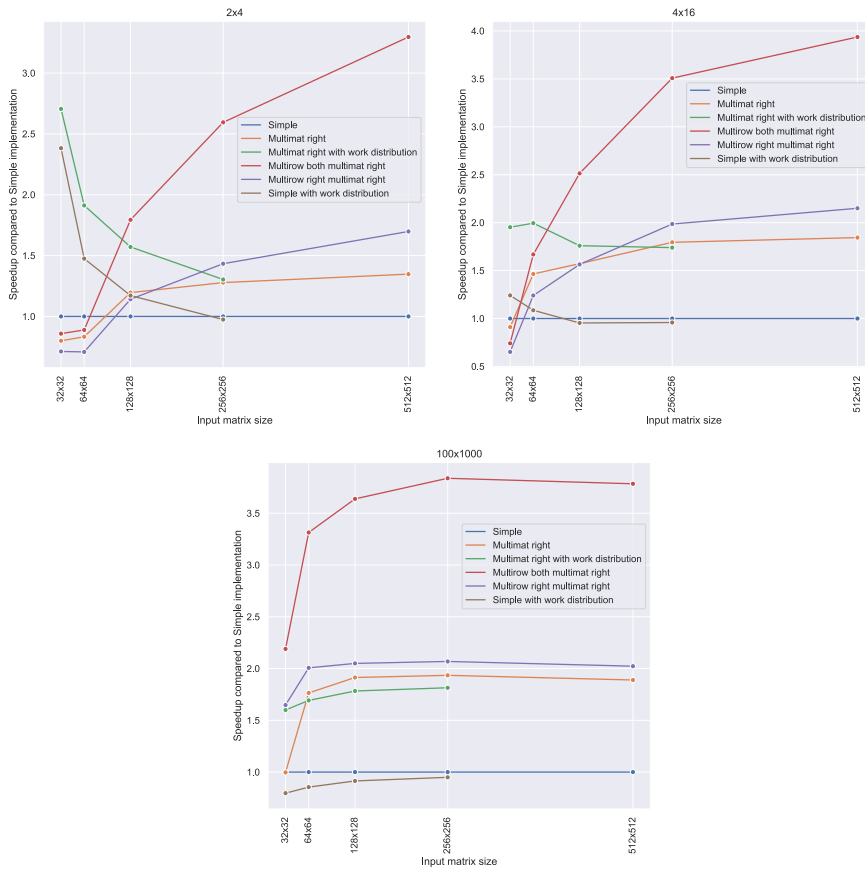


Figure 4.4: Speedup of  $n$ -to- $mn$  warp shuffle optimizations on gpulab.

These measurements are very similar to the measurements for the *one-to-many* type. The differences in measurements between the same implementation

used in these two input types reflect the total resources required by the kernel, i.e., how many kernels can run in parallel.

The results in Figure 4.4 show that for a small number of small input matrices, the *work distribution* optimization is still necessary to balance out the occupancy reduced by other optimizations. The arguments of the implementations using *work distribution* are optimized for the smallest input sizes. To run with the same arguments for input matrices of size 512x512 would require the CUDA grid size of 65536 in the  $y$  axis, which is just above the 65535 maximum limit. The same implementations did run for the 512x512 input size in *one-to-many* as they were run with eight warps per thread block, which reduces the required grid size, and for *one-to-many* was faster than four warps per thread block. In the measurements for *n-to-mn* type, the version with four warps per thread block came out faster. As work distribution is only faster for the smaller input sizes, we choose to use the four warps per thread even if it cannot run the whole range of input sizes, as we try to optimize the speedup for each size separately.

The explanation of the performance of the *multimat right*, the *multirow right multimat right* and the *multirow both multimat right* optimizations is the same as for the *one-to-many* type, as is the effect of running the benchmarks on gpulab when compared to laptop. The occupancy improving optimizations are less effective, while the efficiency improving optimizations are more effective. The maximum absolute improvement is for the  $512 \times 512$  matrix size with 100 left matrices to 1000 right matrices, where we see decrease from 65.43 s to 17.29 s on gpulab and from 303 s to 69.49 s on laptop.

#### 4.2.4 Warp shuffle optimizations with the n-to-m input

The final input type has a group of implementations specifically optimized for this type, the *multimat\_both* optimization and its combinations with other optimizations. We also reuse some *one-to-many* implementations, running them  $n$  times in parallel, once for each left input matrix, this time all with the same set of right input matrices.

Again, Figure 4.5 shows that *work distribution* is advantageous for smaller inputs, but is not required for larger inputs. As expected, the *multimat\_both* optimization specifically designed for this input type gives the best performance. For smaller inputs, it is best when combined with *work distribution*. For medium and large inputs, it is best when combined with *multirow\_both* optimization. As *multimat right* improvement does not reuse data from the left input matrices, it falls behind the *multimat\_both*.

The maximum absolute improvement is for the  $512 \times 512$  matrix size with 50 left matrices to 50 right matrices, where we see a decrease from 163.95 s to 31.66 s on gpulab. For laptop, the input with  $512 \times 512$  and 50 left matrices and 50 right matrices does not fit into GPU memory. As such, the maximum absolute improvement is for the size  $256 \times 256$  with 50 and 50 matrices, decreasing from 49 s to 14 s.

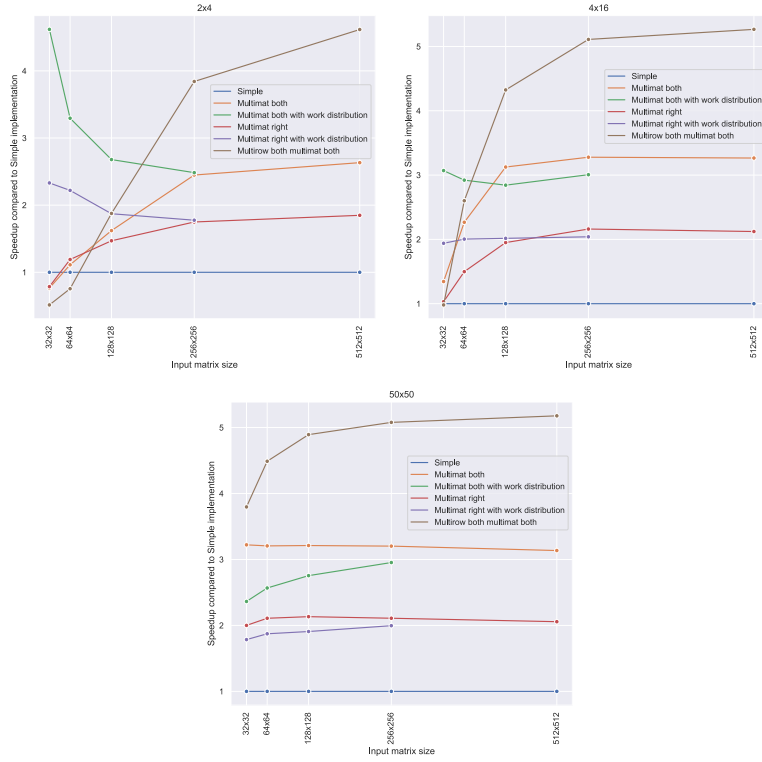


Figure 4.5: Speedup of  $n$ -to- $m$  warp shuffle optimizations on gpulab.

Implementation	Argument	Value
Simple	Warps per thread block	4
	Number of CUDA streams	8
Multimat right	Warps per thread block	4
	Right matrices per thread	8
Multimat right with work distribution	Warps per thread block	4
	Right matrices per thread	8
	Rows per thread	1
	Distribution type	triangle
Multimat both	Warps per thread block	4
	Left matrices per thread	4
	Right matrices per thread	4
Multimat both with work distribution	Warps per thread block	4
	Left matrices per thread	4
	Right matrices per thread	4
	Rows per thread	1
Multirow both multimat both	Distribution type	triangle
	Warps per thread block	4
	Left matrices per thread	4
	Right matrices per thread	4
	Shifts per right matrix	4
Multirow both multimat both	Left rows per iteration	4

## 4.2.5 Warp per shift optimizations with the one-to-one inputs

Occupancy is mainly a concern when working with the *one-to-one* input type and small input matrices. Because of this, we implement the algorithms from this family mostly for the *one-to-one* input type and will compare them only for this input type.

The following table lists the Warp per shift algorithm family implementations, together with the Block per shift algorithm implementation, with the arguments used for their measurement:

Implementation	Argument	Value
Warp per shift	Shifts per thread block	16
Warp per shift with work distribution	Shifts per thread block	8
	Rows per warp	10
	Distribution type	triangle
Warp per shift with shared memory	Shifts per thread block	16
	Shared memory row size	128
	Load with stride	True
	Column group per block	True
Block per shift	Block size	256

From the results in Figure 4.6, we see that the base Warp per shift implementation is enough to saturate the GPU. Due to this, the Block per shift algorithm and Work distribution optimization do not improve the run time. While still slower than the base Warp per shift implementation, the increasing speed of work distribution with increasing input size is most likely caused by the increasing size of each job and correspondingly decreasing proportion of the overhead caused by distributing the jobs and collecting the results.

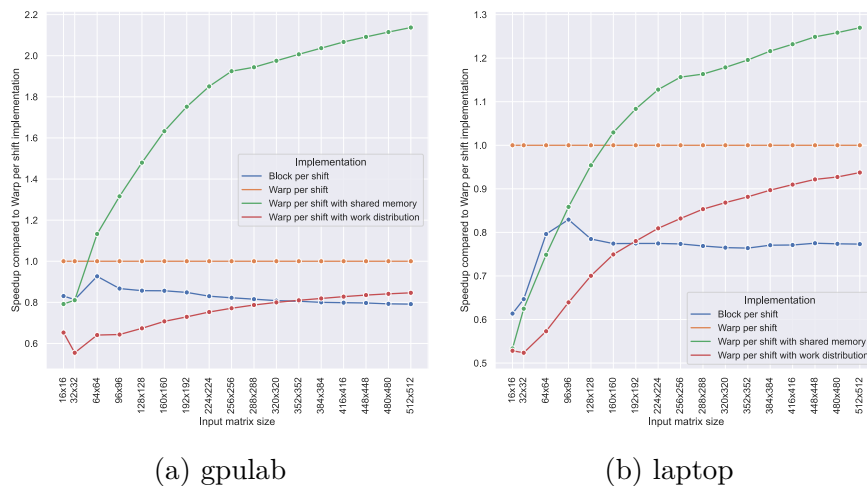


Figure 4.6: Relative speed of warp per shift optimizations.

The shared memory optimization is not beneficial for inputs smaller than 64x64, mostly due to adding synchronization overhead between warps of a thread block when loading data into shared memory. For larger input data sizes, the

reduced number of global memory accesses gives this optimization an advantage over the base Warp per shift implementation.

The largest absolute improvement in run time is for the  $512 \times 512$  input matrix size from 0.158 s to 0.074 s.

### 4.2.6 Comparison with Basic algorithm

Now that we have compared the optimizations of both families separately, we now compare the best of these optimizations against the Basic definition-based implementation described in Section 3.3. As the implementations still differ only in the GPU kernel, we again compare only the time taken by the Run step.

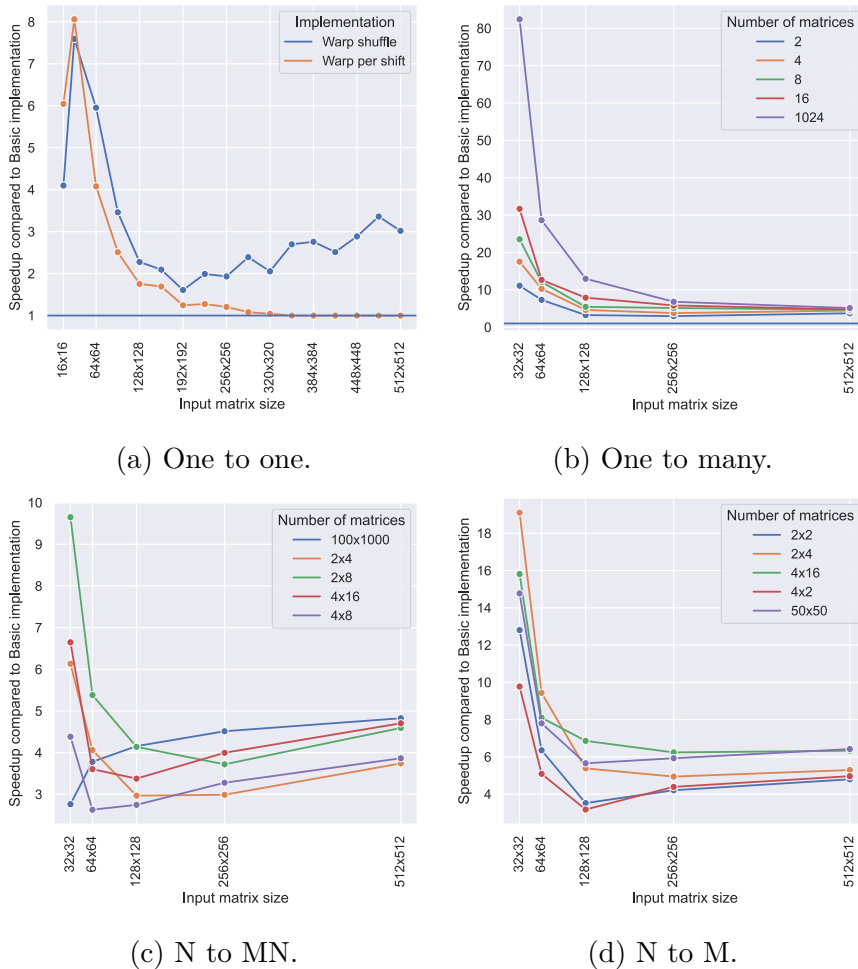


Figure 4.7: Speedup of the best optimized implementation compared to Basic implementation on gpulab.

Figure 4.7 shows the achieved speedup for each of the four input types by the best optimization when compared to the Basic implementation. We see inputs for which our implementations are up to 80 times faster. For large inputs, the speedup is around five times, i.e., the computation requires one-fifth of the time required by the Basic implementation.

For the *one-to-one* input type shown in Figure 4.7a, we separate the Warp shuffle and Warp per shift based optimizations. As Warp per shift optimizations

are designed to improve occupancy, they are generally only relevant for the *one-to-one* input type, as the total size of input data is not enough to saturate the GPU using Basic implementation and simple Warp shuffle implementation. But as we see in the results, Warp shuffle combined with the *work distribution* optimization is almost as fast as Warp per shift. For inputs larger than 200x200, we see that the occupancy is not a limiting factor and the data reuse provided by Warp shuffle optimizations becomes more relevant. The maximum absolute time improvement is from 0.072s to 0.024s. For all following input types, we use only Warp shuffle implementations as they are always better than Warp per shift implementations.

The *one-to-many* input type shown in Figure 4.7b of up to 80 times when computing one left matrix against 1024 right matrices of size 32x32, achieving the highest speedup. For smaller matrix sizes, increasing the number of right matrices improves speed, which indicates that the GPU is not fully utilized. For larger matrix sizes, the difference between speedups for the different number of matrices becomes negligible, with all converging around a speedup of 5. This seems to be the speedup of our best implementations when GPU is fully saturated. The maximum absolute time improvement is from 86.21s to 16.83s.

The *n-to-mn* input type shown in Figure 4.7c shows different behavior to the *one-to-many* type. The speedup spike for smaller matrix sizes caused by *work distribution* is also present, but now with the increasing number of matrices we get a smaller speedup. Above matrix size of 200x200, optimizations with improved data reuse become prominent, causing the improving speedup for larger matrix sizes. The maximum absolute time improvement is from 83.42s to 17.29s.

The *n-to-m* input type shown in Figure 4.7d shows similar characteristics to the *n-to-mn* type. We again see the *work distribution* spike for small matrix sizes, transitioning to optimizations providing better data reuse. The maximum absolute time improvement is from 203.28s to 31.66s.

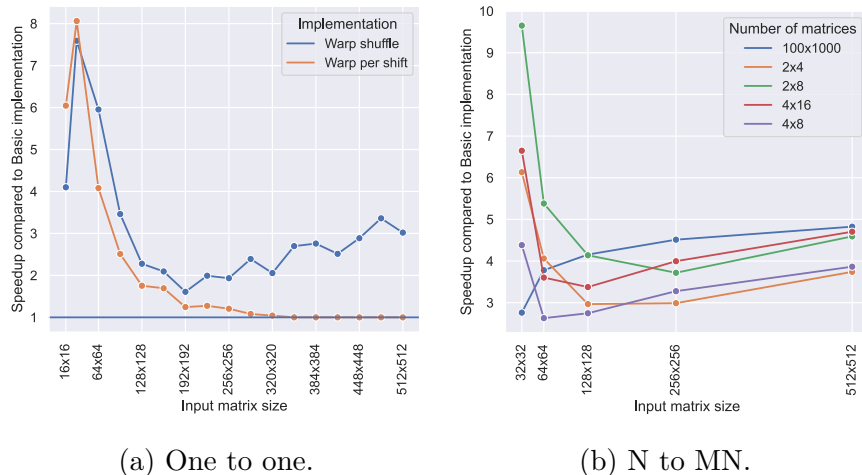


Figure 4.8: Speedup of the best optimized implementation compared to Basic implementation on laptop.

Two two input types that show a significant difference between gpulab and laptop are shown in Figure 4.8. The *one-to-one* type again shows the quick falloff of occupancy improving optimizations, which become slower than ones improving the instruction ratio or memory accesses with input matrix size 64x64.

We see a similar effect on the *n-to-mn* type, where the initial spike for small inputs caused by occupancy improving optimizations is completely gone. The maximum absolute time improvement is from 351s to 69s.

### 4.3 Comparison with existing implementations

In this section, we compare the best of our definition-based implementations as measured in Section 4.2, with existing 2D cross-correlation implementations. First, we make a comparison against the FFT-based CUDA implementation. Next, we take two existing tools/libraries in the form of Python SciPy Virtanen et al. [16] library and Matlab [7] which implement 2D cross-correlation, and compare them with our definition-based algorithms.

We have chosen the Python SciPy library as a generally used CPU implementation of 2D cross-correlation, and Matlab with Parallel Computing Toolbox for GPU accelerated 2D cross-correlation. Due to licensing limitations, Matlab will only be compared on the RTX 2060 system.

The methods for time measurement of all three implementations are described in Section 4.1.1. For each input size (combination of matrix size and the number of matrices), we choose the fastest implementation provided by this thesis. Generally, for smaller inputs, the implementations with work distribution optimization will be chosen, whereas for larger inputs, the implementations optimizing for efficiency through reduced global memory accesses, improved instruction ratios, etc., will be chosen. The comparison of the definition-based implementations and which of them are the fastest for a given input is presented in Section 4.2.

#### 4.3.1 FFT-based implementation

The FFT-based implementation used in this thesis is adapted from the one used by Bali [1]. It uses the cuFFT library for the Fast Fourier Transform and a custom kernel for Hadamard multiplication.

Before comparing this FFT-based implementation with the definition-based implementations, we first show a few properties of this implementation caused by the use of the Fast Fourier transform in general and of the cuFFT library in particular. First is the dependency between the precise size of the input matrix and computation time. As described in the cuFFT library documentation, cuFFT provides "Algorithms highly optimized for input sizes that can be written in the form  $2^a * 3^b * 5^c * 7^d$ . In general, the smaller the prime factor, the better the performance, i.e., powers of two are fastest." [12]. From our measurements, we see up to 30% slowdown between the power of two input sizes and input sizes one smaller.

Another feature is illustrated in Figure 4.9, where we show computation time for inputs smaller than 128x128. From these measurements, we see that the cuFFT library computes inputs with matrix size up to 96x96 faster in double precision than in single precision, even though the double precision version works with twice the amount of data and uses operations with lower throughput. The cause is the *Prepare* step, which allocates device memory and in this implementation runs the *cufftPlan\** functions. Based on our measurements, the *Prepare* step is slower for single precision computation than for double precision. Due to



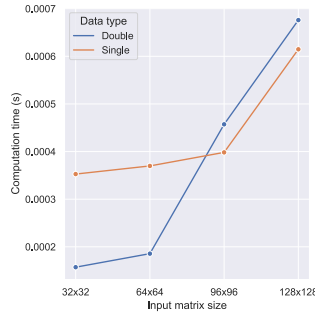


Figure 4.9: Comparison of FFT-based computation in single and double precision for small inputs.

the closed source of the cuFFT library, we can only speculate on the cause, but it is most likely due to some additional precomputation done for the single version.

When comparing the FFT-based implementation with the definition-based implementations, we are mostly interested in the input matrix size where the definition-based and FFT-based implementations are equal and how that size differs between the Basic algorithm and the best of our optimizations, which we now collectively call the *Optimized* algorithm. We call such matrix size the *equality point*, as it is represented by a point where the graphs of the implementations intersect in the diagram. The *Optimized* implementation is chosen for each input (i.e., a combination of input matrix size and number of input matrices) separately. In this section, we measure the whole computation, including allocation, transfer to the GPU, kernel execution, transfer from the GPU, and deallocation. This is because the FFT-based algorithm differs from the definition-based algorithm in all of these stages. Most importantly, we need to include the overhead of the Prepare step that has a major impact on the total run time as described in the previous paragraph.

First, we measure with the same matrix sizes as in previous sections, as shown in Figure 4.10. The figure shows the speedup of the Basic and Optimized definition-based algorithm compared to the FFT-based implementation, which is used as a baseline. As described above, cuFFT library used by the FFT-based implementation is optimized for certain input sizes, with powers of two being the fastest. As such, measurements in Figure 4.10 are optimal for the FFT-based implementation. The figure shows an improvement in the position of the equality point for all input types.

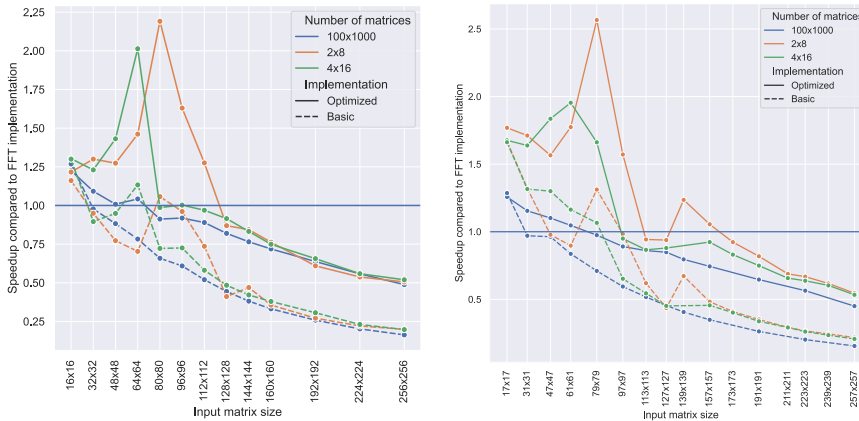
The most noticeable change between Basic and Optimized implementation is in the *one-to-one* type, shown in Figure 4.10a. Due to the small input data size, the GPU cannot be fully saturated by the FFT-based implementation. Even though this change is the most noticeable, it is the least important, as the total execution time is very low for all implementations of this input type.

For the *one-to-many* type in Figure 4.10b, the results again show great improvement for small input data sizes, here represented by small number of right input matrices. For these sizes, the Basic implementation often did not reach the speed of the FFT-based algorithm for any measured input matrix size, whereas the optimized implementation has its equality point above the matrix size of 100x100. For inputs with a large number of right input matrices, we see that the equality point moves to around 64x64 input matrices.



(a) One to one.

(b) One to many.



(c) N to MN.

(d) N to M.

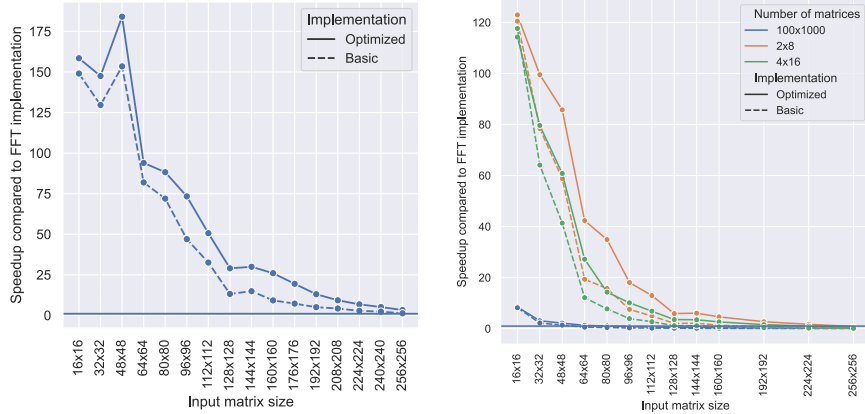
Figure 4.10: Speedup of the Basic definition-based implementation and best definition-based optimized implementation compared to FFT-based implementation on gpulab.

The  $n$ -to- $mn$  type in Figure 4.10c again displays great similarity to the  $one$ -to- $many$  type due to the way it is implemented. The equality points are at similar positions, being slightly below 64x64 for the largest input.

The  $n$ -to- $m$  type in Figure 4.10d shows surprisingly good performance even for the Basic implementation. For inputs with a small number of matrices, optimized equality points are all above 120x120 matrix size. For inputs with a large number of matrices, the equality point is just below 80x80.

When we compare the behavior between gpulab and laptop, as shown in Figure 4.11, we see that the FFT-based implementation suffers massively with low occupancy. For smaller input sizes, we see over 100 times improvement for both the  $one$ -to- $one$  type and for small number of matrices in the  $n$ -to- $mn$  type. Once the input size becomes large enough, as shown by the 100 to 1000 input for the  $n$ -to- $mn$  type, the behavior is very similar to that of gpulab, but with much bigger improvements for smaller input matrix sizes.

The second set of results, shown in Figure 4.12, changes the matrix sizes for which we measure the implementations. We take the matrix sizes used to measure the original results in Figure 4.10 and find the closest prime number. For example 64x64 becomes 61x61, 128x128 becomes 127x127 and 256x256 becomes



(a) One to one.

(b) N to MN.

Figure 4.11: Speedup of the Basic definition-based implementation and best definition-based optimized implementation compared to FFT-based implementation on laptop.

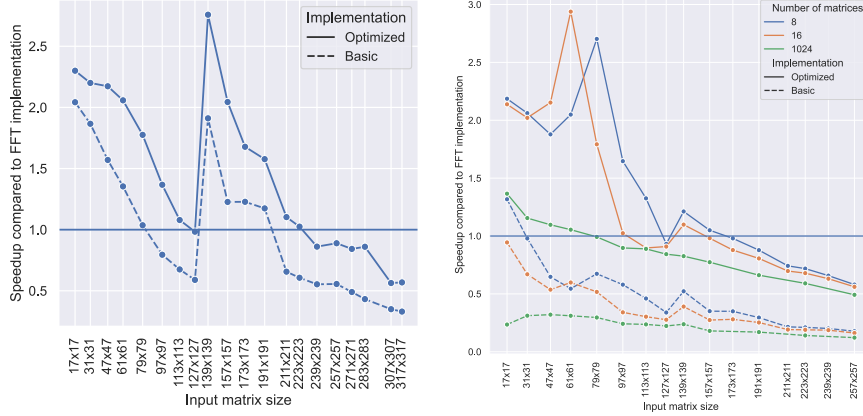
257x257. This should make the FFT-based implementation slower, making the improvements provided by our optimizations of definition-based implementation greater as the definition-based implementation is not that closely dependent on the precise size of the input matrices.

We see a major change in the behavior of *one-to-one* type, shown in Figure 4.12a. The equality point moves beyond the 256x256 matrix size, and we see two peaks in the improvement as the FFT-based implementation becomes faster for the 127x127 input before slowing down again for the 157x157 matrix size.

For other input types, we also see an improvement compared to the previous measurements, even if not as significant as for the *one-to-one* type. The speedup values are better across the board, with equality points moving to larger matrix sizes. A similar change is visible when comparing the two measurements on laptop.

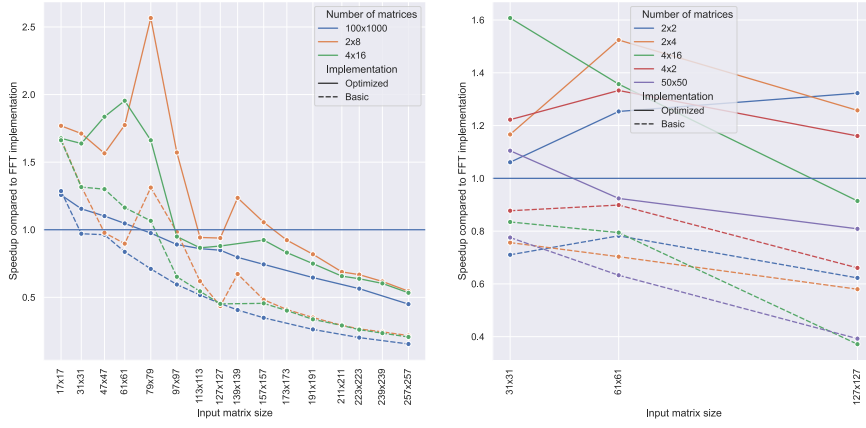
Due to the many iterations of the algorithm which are measured together, the measured time reflects many repeated computations on the same input data. This results in caches being fully populated and allows the cuFFT library possible internal caching. Figure 4.13 shows a measurement of a single iteration which limits or possibly even removes the ability for internal caching in the cuFFT library and populating of any caches, measuring *warm-up performance* instead of *sustainable performance*. This type of measurement better reflects the usual usage of a cross-correlation computing function, as it is not useful to compute cross-correlation for the same input multiple times.

This measurement can only be done for large input sizes, as the background noise when measuring smaller input sizes would make any measured results useless. In Figures 4.13a and 4.13b we see that the equality point is around 90x90, which is an improvement compared to previous measurements. This hints at some internal caching done by the cuFFT library between computations. The equality point in Figure 4.13c is also improved, now just below 60x60.



(a) One to one.

(b) One to many.



(c) N to MN.

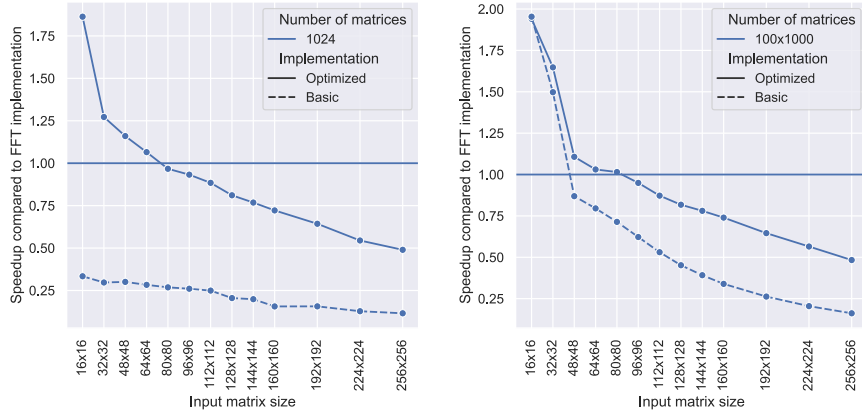
(d) N to M.

Figure 4.12: Speedup when measured in matrix sizes which are prime numbers.

### 4.3.2 SciPy

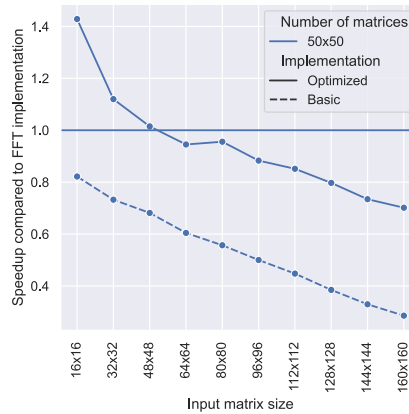
We compare the best of the implementations provided by this thesis with SciPy in Figure 4.14. Even though SciPy uses multithreaded FFT-based implementation, for any input with an input matrix size above  $8 \times 8$ , the definition-based CUDA C++ implementation is many times faster. We see the speedup increasing with increasing input size for all input types, showcasing the much higher throughput of the GPU. In terms of speedup, we see the *one-to-one* achieving the lowest speedup due to limited occupancy due to small input size, with all other input types achieving up to 3000 times speedup for the largest input sizes. In terms of absolute times, which range from 0.13 s for the *one-to-one* type to 2.03 s for the *n-to-m* type for SciPy, we see improvement to 0.32 ms and 0.66 ms respectively.

One figure that stands out is Figure 4.14d, where the maximum speedup is not achieved for the largest input in terms of the number of matrices but for a smaller with 4 to 4 matrices. We also see that the speedup does not increase linearly with increased input matrix size apart from the input with 4 to 4 input matrices. This is caused by the algorithm with *multimat\_both* and work distribution optimizations being the fastest for the small input sizes. Once the GPU is sufficiently saturated, another algorithm, this time with both *multimat\_both* and *multirow\_both* optimizations, achieves the highest speedup, which increases at a



(a) One to many.

(b) N to MN.



(c) N to M.

Figure 4.13: Speedup of the Basic definition-based implementation and best definition-based optimized implementation compared to FFT-based implementation.

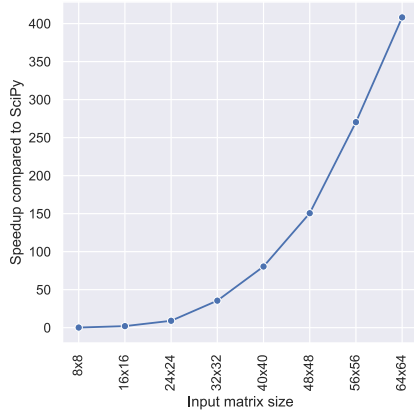
different rate than for the first algorithm.

For comparison, we show the  $n$ -to- $mn$  and  $n$ -to- $m$  input types measured on laptop in Figure 4.15. As expected, the behavior is generally the same as on gpulab, only with a smaller total speedup due to the lower performance of the laptop GPU.

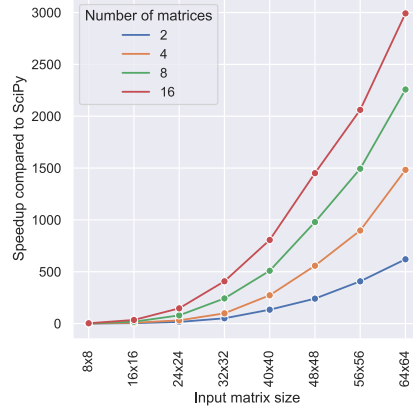
In summary, the results are as expected, with SciPy being faster for the smallest inputs as the latency of data transfer and kernel to and from the GPU and the overhead of kernel start are independent of the data size and will result in a slower total speed of the GPU implementation. For all larger inputs, the generally slow speed of Python and limited parallelism of the CPU results in the GPU CUDA C++ implementation being faster.

### 4.3.3 Matlab

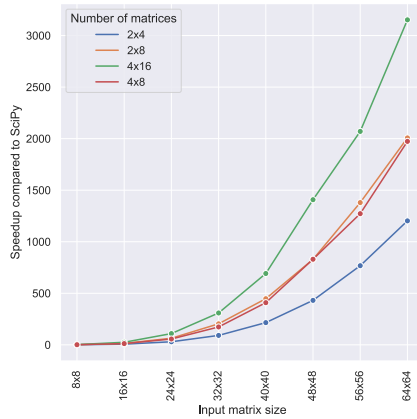
In this section, we compare the best of the implementations provided by this thesis with Matlab. The results of the comparison are shown in Figure 4.16. As the Matlab implementation of 2D cross-correlation we measure against utilizes a GPU, the total speedup compared to the speedup seen in the previous section is



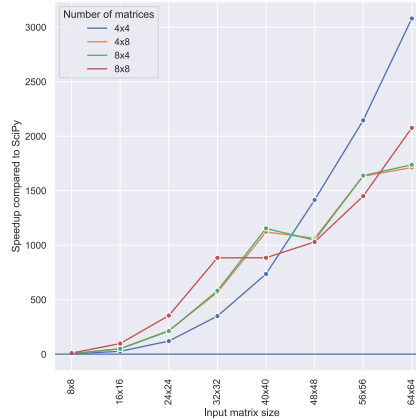
(a) One to one.



(b) One to many.



(c) N to MN.

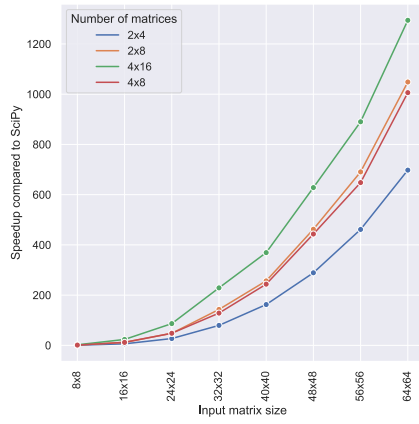


(d) N to M.

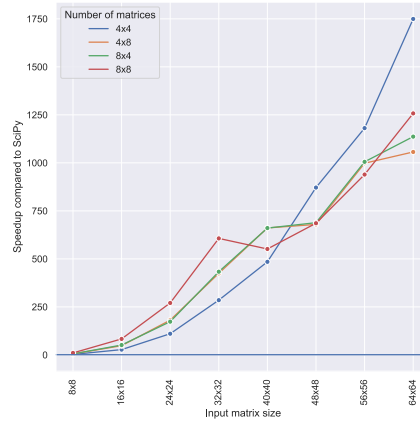
Figure 4.14: Speedup of the best definition-based implementation in this thesis compared to SciPy on gpublab.

much lower. As Matlab only implements the *one-to-one* type of cross-correlation, the best comparison between the implementations is in Figure 4.16a, where we see that our implementation gets progressively faster. As we expect Matlab to utilize FFT-based implementation, the speedup should decrease for larger input sizes. Unfortunately, due to time constraints, we were unable to measure where the equality point is.

For other input types, we sequentially execute the *one-to-one* input type for each pair of input matrices to be cross-correlated. As expected, this makes Matlab much slower for the smaller input matrix sizes, as it cannot saturate the GPU. For larger input sizes, the execution of each cross-correlation starts saturating the GPU, achieving almost parity with our implementation.

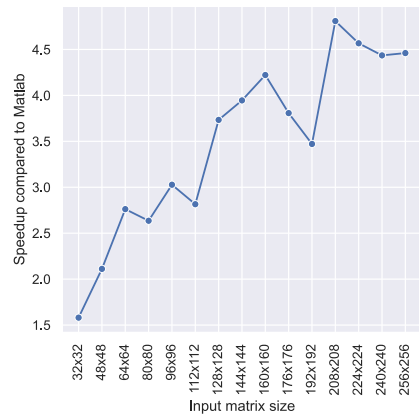


(a) N to MN.

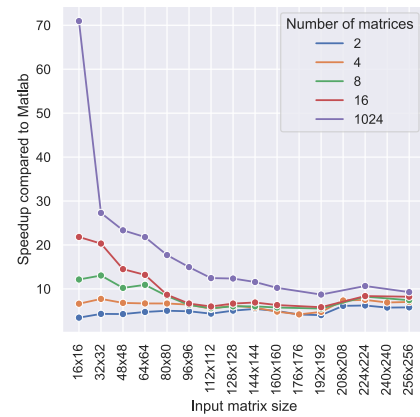


(b) N to M.

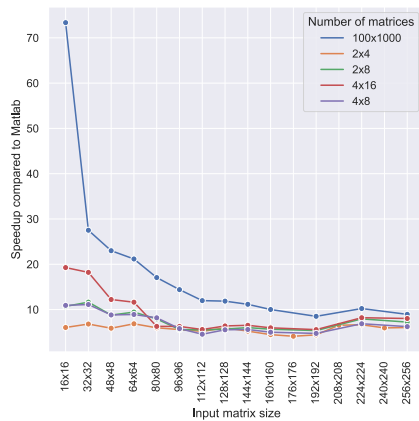
Figure 4.15: Speedup of the best definition-based implementation in this thesis compared to SciPy on laptop.



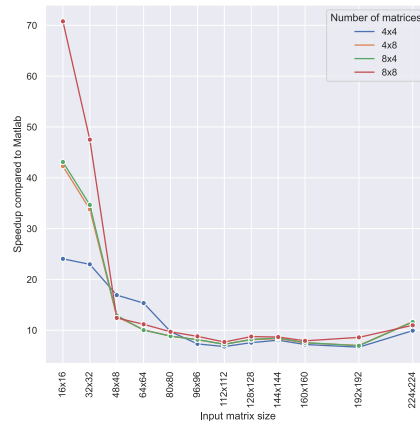
(a) One to one.



(b) One to many.



(c) N to MN.



(d) N to M.

Figure 4.16: Speedup of the best definition-based implementation in this thesis compared to Matlab on laptop.





# Conclusion

In this thesis, we have analyzed the definition-based cross-correlation algorithm, searching for parallelization and optimization possibilities based on the input matrix size and input type. Based on this analysis, we have implemented two algorithm families, each with many implementations employing different combinations of the optimization and parallelization strategies. The implementations are based on the CUDA framework.

The optimizations target many algorithm properties, from caching and data reuse with the goal of reducing the number of accesses to slower memory types, to the amount of parallelism available to fully saturate the GPU and utilize the full throughput provided by the hardware. Each optimization was rigorously profiled and measured for different input sizes and input types, some trying to optimize across all inputs and some targeting specific combinations of input sizes and types.

The first algorithm family presented by this thesis was the Warp shuffle family, which utilized warp shuffle instructions to share input data between threads of a warp, significantly reducing the number of accesses to global memory. The family includes further optimizations, which reduce the total number of warp shuffle instructions required. This is achieved by computing cross-correlation between one matrix and many other matrices at once or by computing multiple results from the same cross-correlation at once. Another optimization employed by this family improves parallelization and load balancing.

The second algorithm family was the Warp per shift family, which improved occupancy by utilizing a whole warp to compute a single element in the output matrix. This family includes optimizations for data reuse and cooperation of warps through shared memory, together with further improvements to occupancy by utilizing multiple warps per single output matrix element.

We then compared the implementations introduced in this thesis against several other cross-correlation implementations. First, we compared our optimized implementations against a Basic definition-based CUDA implementation. Next, we compared them against an implementation based on the Fast Fourier Transform algorithm also using CUDA. Lastly, we compared our implementations with cross-correlation from production-grade libraries and toolkits, namely with the CPU-based implementation provided by the Python Scipy library and the GPU implementation provided by Matlab.

When compared with the Basic definition-based CUDA implementation, our optimized implementation achieves at least 5 times speedup for most inputs and up to 10 to 80 times speedup for certain input sizes. When compared with the FFT-based implementation, we achieve speed parity for input matrix sizes over 100x100 for a smaller number of input matrices, decreasing down to 60x60 for a larger number of matrices. In comparison with the CPU-based SciPy library, our implementations achieve 50 times speedup for small input sizes and up to 3000 times speedup for larger input sizes. When compared with Matlab, we achieve around 5 times speedup for small input sizes.

## 4.4 Future work

Although the optimized implementations provided in this thesis are useful and achieve the speedups listed above, they are mostly designed for easy instrumentation and benchmarking. This results in several restrictions on the size and form of the input data, long build times, and a giant executable. In the future, the implementation could be streamlined and the limitations removed.

This thesis also focused heavily on utilizing the CUDA platform for the implementation of the optimized definition-based algorithms. Future work could be aimed at an implementation using other, currently less common tools such as OpenCL.

Next, the implementations in this thesis utilize only a single GPU. In the future, the implementation could be expanded to utilize more GPUs on a single system or even further to utilize GPUs over multiple systems. Based on the inherent parallelism in the definition-based cross-correlation described in this thesis, the implementation of a distributed version could build on the work provided in this thesis very easily.

To further speed up the definition-based cross-correlation, additional properties of the input data could be used. This includes utilizing non-negative input data and terminating the parts of the computation which cannot reach the current maximum or computing a submatrix of the full cross-correlation matrix.

# Bibliography

- [1] Michal Bali. Employing gpu to process data from electron microscope. Master's thesis, Charles University, 2020.
- [2] David Bednárek, Michal Brabec, and Martin Kruliš. Improving matrix-based dynamic programming on massively parallel accelerators. *Information Systems*, 64:175–193, mar 2017. doi: 10.1016/j.is.2016.06.001.
- [3] M. A. Clark, P. C. La Plante, and L. J. Greenhill. Accelerating radio astronomy cross-correlation with graphics processing units. July 2011.
- [4] David Honzátko and Martin Kruliš. Accelerating block-matching and 3d filtering method for image denoising on GPUs. *Journal of Real-Time Image Processing*, 16(6):2273–2287, nov 2017. doi: 10.1007/s11554-017-0737-9.
- [5] Konstantin Kapinchev, Adrian Bradu, Frederick Barnes, and Adrian Podoleanu. Gpu implementation of cross-correlation for image generation in real time. pages 1–6, Cairns, QLD, Australia, 2015. IEEE. ISBN 978-1-4673-8117-8. doi: 10.1109/ICSPCS.2015.7391783.
- [6] M.I. Khalil. Accelerating cross-correlation applications via parallel computing. *International Journal of Image, Graphics and Signal Processing*, 5(12): 26–31, oct 2013. doi: 10.5815/ijigsp.2013.12.04.
- [7] MATLAB. *9.10.0.1684407 (R2021a Update 3)*. The MathWorks Inc., Natick, Massachusetts. URL [https://www.mathworks.com/help/signal/ref/xcorr2.html?s\\_tid=mwa\\_osa\\_a](https://www.mathworks.com/help/signal/ref/xcorr2.html?s_tid=mwa_osa_a).
- [8] Maxim Milakov. GPU Pro Tip: Fast Dynamic Indexing of Private Arrays in CUDA. <https://developer.nvidia.com/blog/fast-dynamic-indexing-private-arrays-cuda/>, February 2015. URL <http://web.archive.org/web/20210724011254/https://developer.nvidia.com/blog/fast-dynamic-indexing-private-arrays-cuda/>.
- [9] NVIDIA. Faster Parallel Reductions on Kepler. <https://developer.nvidia.com/blog/faster-parallel-reductions-kepler/>, February 2014. URL <http://web.archive.org/web/20220406040954/https://developer.nvidia.com/blog/faster-parallel-reductions-kepler/>.
- [10] NVIDIA. Nvidia tesla v100 gpu architecture: The world's most advanced data center gpu. Technical report, NVIDIA, 2017.
- [11] Nvidia. CUDA C++ Programming Guide. <https://docs.nvidia.com/cuda/cuda-c-programming-guide/index.html>, 2022.
- [12] NVIDIA. cuFFT. <https://docs.nvidia.com/cuda/cufft/index.html>, 2022. URL <http://web.archive.org/web/20220624091956/https://docs.nvidia.com/cuda/cufft/index.html>.

- [13] NVIDIA. Kernel Profiling Guide. <https://docs.nvidia.com/nsight-compute/ProfilingGuide/index.html>, 2022. URL <https://web.archive.org/web/20220514025303/https://docs.nvidia.com/nsight-compute/ProfilingGuide/index.html>.
- [14] Ayumu Tomiyama and Reiji Suda. Automatic parameter optimization for edit distance algorithm on GPU. In *Lecture Notes in Computer Science*, pages 420–434. Springer Berlin Heidelberg, 2013. doi: 10.1007/978-3-642-38718-0\_38.
- [15] Sergi Ventosa, Martin Schimmel, and Eleonore Stutzmann. Towards the processing of large data volumes with phase cross-correlation. *Seismological Research Letters*, May 2019. doi: 10.1785/0220190022.
- [16] Pauli Virtanen, Ralf Gommers, Travis E. Oliphant, Matt Haberland, Tyler Reddy, David Cournapeau, Evgeni Burovski, Pearu Peterson, Warren Weckesser, Jonathan Bright, Stéfan J. van der Walt, Matthew Brett, Joshua Wilson, K. Jarrod Millman, Nikolay Mayorov, Andrew R. J. Nelson, Eric Jones, Robert Kern, Eric Larson, C J Carey, İlhan Polat, Yu Feng, Eric W. Moore, Jake VanderPlas, Denis Laxalde, Josef Perktold, Robert Cimrman, Ian Henriksen, E. A. Quintero, Charles R. Harris, Anne M. Archibald, Antônio H. Ribeiro, Fabian Pedregosa, Paul van Mulbregt, Aditya Vijaykumar, Alessandro Pietro Bardelli, Alex Rothberg, Andreas Hilboll, Andreas Kloeckner, Anthony Scopatz, Antony Lee, Ariel Rokem, C. Nathan Woods, Chad Fulton, Charles Masson, Christian Häggström, Clark Fitzgerald, David A. Nicholson, David R. Hagen, Dmitrii V. Pasechnik, Emanuele Olivetti, Eric Martin, Eric Wieser, Fabrice Silva, Felix Lenders, Florian Wilhelm, G. Young, Gavin A. Price, Gert-Ludwig Ingold, Gregory E. Allen, Gregory R. Lee, Hervé Audren, Irvin Probst, Jörg P. Dietrich, Jacob Silterra, James T Webber, Janko Slavič, Joel Nothman, Johannes Buchner, Johannes Kulick, Johannes L. Schönberger, José Vinícius de Miranda Cardoso, Joscha Reimer, Joseph Harrington, Juan Luis Cano Rodríguez, Juan Nunez-Iglesias, Justin Kuczynski, Kevin Tritz, Martin Thoma, Matthew Newville, Matthias Kümmerer, Maximilian Bolingbroke, Michael Tartre, Mikhail Pak, Nathaniel J. Smith, Nikolai Nowaczyk, Nikolay Shebanov, Oleksandr Pavlyk, Per A. Brodtkorb, Perry Lee, Robert T. McGibbon, Roman Feldbauer, Sam Lewis, Sam Tygier, Scott Sievert, Sebastiano Vigna, Stefan Peterson, Surhud More, Tadeusz Pudlik, Takuya Oshima, Thomas J. Pingel, Thomas P. Robitaille, Thomas Spura, Thouis R. Jones, Tim Cera, Tim Leslie, Tiziano Zito, Tom Krauss, Utkarsh Upadhyay, Yaroslav O. Halchenko, and Yoshiki Vázquez-Baeza and. SciPy 1.0: fundamental algorithms for scientific computing in python. *Nature Methods*, 17(3):261–272, feb 2020. doi: 10.1038/s41592-019-0686-2.
- [17] Chen Wang. *Kernel learning for visual perception*. PhD thesis, Technological University, Singapore, 2019.
- [18] Wikimedia Commons contributors. Visual comparison of convolution, cross-correlation and autocorrelation. [https://commons.wikimedia.org/w/index.php?title=File:Comparison\\_convolution\\_](https://commons.wikimedia.org/w/index.php?title=File:Comparison_convolution_)

correlation.svg&oldid=607616339, November 2021. URL [https://commons.wikimedia.org/w/index.php?title=File:Comparison\\_convolution\\_correlation.svg&oldid=607616339](https://commons.wikimedia.org/w/index.php?title=File:Comparison_convolution_correlation.svg&oldid=607616339).

- [19] Wikipedia contributors. Cross-correlation. <https://en.wikipedia.org/w/index.php?title=Cross-correlation&oldid=1065983922>, March 2022. URL <https://en.wikipedia.org/w/index.php?title=Cross-correlation&oldid=1065983922>.
- [20] Wikipedia contributors. Relative change and difference — Wikipedia, the free encyclopedia. [https://en.wikipedia.org/w/index.php?title=Relative\\_change\\_and\\_difference&oldid=1085142584](https://en.wikipedia.org/w/index.php?title=Relative_change_and_difference&oldid=1085142584), 2022. [Online; accessed 18-July-2022].
- [21] Wikipedia contributors. Triangular number — Wikipedia, the free encyclopedia. [https://en.wikipedia.org/w/index.php?title=Triangular\\_number&oldid=1098260469](https://en.wikipedia.org/w/index.php?title=Triangular_number&oldid=1098260469), 2022. URL [https://en.wikipedia.org/w/index.php?title=Triangular\\_number&oldid=1098260469](https://en.wikipedia.org/w/index.php?title=Triangular_number&oldid=1098260469). [Online; accessed 16-July-2022].
- [22] Lingqi Zhang, Tianyi Wang, Zhenyu Jiang, Qian Kemao, Yiping Liu, Zejia Liu, Liqun Tang, and Shoubin Dong. High accuracy digital image correlation powered by gpu-based parallel computing. *Optics and Lasers in Engineering*, 69:7–12, 2015. ISSN 0143-8166. doi: <https://doi.org/10.1016/j.optlaseng.2015.01.012>. URL <https://www.sciencedirect.com/science/article/pii/S0143816615000135>.



# A. Local array optimization

All *multimat* and *multirow* optimizations heavily rely on the ability of the CUDA compiler to place arrays such as the following into registers:

```
template<size_t LENGTH>
__device__ void foo(...) {
    ...
    float bar[LENGTH];
    for (size_t i = 0; i < LENGTH; ++i) {
        bar[i] = some_function(...);
    }
    ...
}
```

If an array is small and only accessed using static indexing, where all indices are known constants at compile time, the CUDA compiler places all elements of the array into registers [8]. The array can also be accessed in small for loops with known compile time bounds, which are unrolled by the compiler and again result in static indexing. If for any access the index cannot be computed during compile time, the whole array is placed into Local memory, described in Section 2.2.5. Local memory is part of the device memory, and as such is the slowest memory accessible from device code. Local memory access also utilizes the same pipeline as warp shuffle instructions, competing for the throughput of this pipeline.

## A.1 Advanced optimizations and local arrays

While implementing the *multimat\_both* and *multirow\_both* optimizations, which are described in Sections 3.4.5 and 3.4.6 respectively, we encountered a problem with the *nvcc* compiler not optimizing the local arrays into registers.

Using profiling and examining the SASS, we isolated the problem to the *thread\_left\_bottom* and *thread\_left\_top* arrays. We further isolated it to the part of the code, which in its original form shared by the simplified, *multimat\_right* and *multirow\_right* is shown in Listing A.1.

To process multiple values from left input matrices, which is the basis of both *multimat\_both* and *multirow\_both* optimizations, the code needs to be changed as shown in Listing A.2

The *nvcc* compiler should be able to unroll this loop, and thanks to static indexing, the *thread\_left\_bottom* and *thread\_left\_top* local arrays should be optimized

```
thread_left_bottom = warp.shfl(
    warp.thread_rank() != 0 ? thread_left_bottom : thread_left_top,
    warp.thread_rank() + 1
);
thread_left_top = warp.shfl_down(thread_left_top, 1);
```

Listing A.1: Base Warp shuffle implementation of left buffer shuffle

```

#pragma unroll
for (size_t l = 0; l < NUM_LEFTS; ++l) {
    thread_left_bottom[l] = warp.shfl(
        warp.thread_rank() != 0 ? thread_left_bottom[l] :
        thread_left_top[l],
        warp.thread_rank() + 1
    );
    thread_left_top[l] = warp.shfl_down(thread_left_top[l], 1);
}

```

Listing A.2: Multimat both and multirow both implementation of left buffer shuffle

```

LDL R0, [R63+0x4]
SHFL.IDX PT, R8, R0, R57, 0x1f
SHFL.DOWN PT, R0, R32, 0x1, 0x1f
STL [R62], R8
STL [R61], R0

```

Listing A.3: SASS instructions without local array optimization

into registers. Unfortunately, as shown in Listing A.3, the compiler behaves as if dynamic indexing was used and pushes the arrays into local memory. Due to the closed source nature of the *nvcc* compiler, we can only speculate on the reasons why the loop unrolling does not result in static indexing. One possibility, based on the generated SASS instructions seen in Listing A.3, is that the ternary operator is optimized into dynamic array indexing, which then prevents the local array optimization. As there is no visible branching in the unrolled loop, the base address of either the *thread\_left\_bottom* or the *thread\_left\_top* is loaded into register R63, which is then reused in all loads, resulting in dynamic indexing.

We experimented with several solutions, with version in Listing A.4 compiling into static indexing.

The only change is the expansion of the ternary operator into an equivalent if statement. As shown in Listing A.5, the body of the updated loop results in a single *SEL* instruction which selects the top or the bottom part of the buffer. This version of the loop is used by the *multimat\_both* and *multirow\_both* optimizations described in the following sections.

The difference is also noticeable when profiling, which shows additional local memory store (STL) and load (LDL) instructions in both the *multimat\_both* and *multirow\_both* without local array optimization. Apart from these additional instructions, the number of remaining instructions is generally the same, with some additional integer multiply-add instructions (IMAD) due to local memory address computations.

Based on this observation, the measured speedup in Figure A.1 is caused solely by the application of the local array optimization. The speedup for smaller inputs is limited due to low occupancy, but is still present. As an example, Figure A.1a shows that for input matrices of size 64 by 64, the solution without local memory access is already 2 times faster. Figure A.1b shows that there is slightly smaller



```

#pragma unroll
for (size_t l = 0; l < NUM_LEFTS; ++l) {
    T bottom_shift_val;
    if (warp.thread_rank() != 0) {
        bottom_shift_val = thread_left_bottom[l];
    } else {
        bottom_shift_val = thread_left_top[l];
    }

    thread_left_bottom[l] = warp.shfl(bottom_shift_val,
        warp.thread_rank() + 1);
    thread_left_top[l] = warp.shfl_down(thread_left_top[l], 1);
}

```

Listing A.4: Fixed *multimat* both and *multirow* both implementation of left buffer shuffle

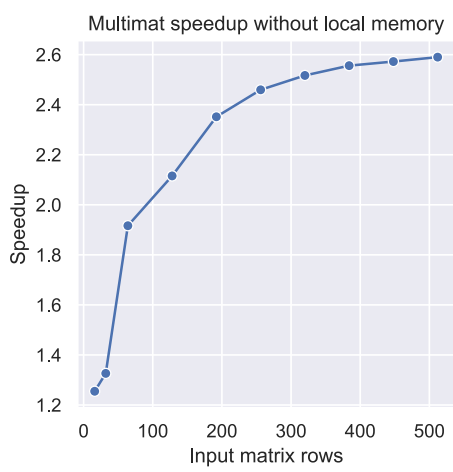
```

SEL R42, R52, R20, !P4
SHFL.IDX PT, R53, R48, R53, 0x1f
SHFL.DOWN PT, R52, R52, 0x1, 0x1f

```

Listing A.5: SASS instructions with local array optimization

improvement in the *multirow\_both* optimization compared to the *multimat\_both*. This is most likely caused by higher general overhead due to the greater overall complexity of the optimization.



(a) The *multimat\_both* optimization.



(b) The *multirow\_both* optimization.

Figure A.1: Improvement of the two optimizations without local memory access.

## B. Attachments

In the attachments to this thesis we include the source code of our CUDA C++ implementation and the benchmarking tool, together with the profiling and measurement results and the Jupyter Notebooks used for visualization of the measured results. The attachments contain the following directories:

- **src** - Source code of the CUDA C++ program implementing the definition-based and FFT-based algorithms for cross-correlation. Contains all the kernels referenced in Chapter 3.
- **benchmarking** - The Benchmarking tool described in Section 4.1.
- **existing** - Code allowing the use of cross-correlation implementations in Python SciPy and Matlab.
- **visualization** - Jupyter Notebooks and Python code used to process results generated by the Benchmarking tool and generate the diagrams shown in this text.
- **gpulab** - Helper scripts for building and running the CUDA C++ application and Benchmarking tool both locally and on the KSI Cluster gpulab.
- **profiling** - Results of profiling the CUDA C++ implementation using NVIDIA Nsight Compute tool.
- **sample\_app** - A sample application showcasing the steps required to utilize one of the implementations provided by this thesis in another application.

Detailed description is included in the attachments.

